

Master Degree course in Aerospace Engeneering

Master Degree Thesis

# Conceptual Design of a Box Wing Firefighting Aircraft

#### Supervisors

Prof. Giuseppe Palaia Prof. Karim Abu Salem Prof. Erasmo Carrera

Candidate
Andrea FASOLIS

# Acknowledgements

Desidero esprimere la mia sincera gratitudine al Prof. Karim Abu Salem, al Prof. Giuseppe Palaia e al Prof. Erasmo Carrera per la disponibilità, la guida e i preziosi suggerimenti che hanno reso possibile la realizzazione di questo lavoro di tesi.

Il ringraziamento più sentito va ad Andrea e ad Allison. Con il loro amore mi hanno sostenuto nei momenti difficili come in quelli sereni, mi hanno confortato quando stavo male e mi hanno sempre incoraggiato a proseguire. La loro presenza costante mi ha accompagnato lungo questi cinque anni fino a questo traguardo. Questo lavoro lo dedico a loro.

Un grazie speciale va infine a mamma e papà, a mio fratello e ai miei nonni Bruno, Margherita, Dino e Teresa, che hanno sempre creduto in me e nella mie capacità. Un pensiero riconoscente va anche ai miei amici, che in modi diversi mi sono stati vicini e che hanno reso questo percorso più leggero, sopportandomi anche quando parlavo troppo dell'università.

#### Abstract

Climate change, deforestation, and urbanization are contributing to a significant increase in the risk of wildfires, which are particularly critical in areas close to urban centers, where the potential damage to people and infrastructure is unacceptable. The use of aircraft in aerial firefighting is a well-established practice, involving both adapted aeronautical platforms and purpose-built aircraft. Among these, scoopers stand out for their ability to rapidly refill water from natural or artificial reservoirs. The box wing represents a disruptive innovation in the aeronautical field, capable of providing greater aerodynamic efficiency and load capacity thanks to its multiplane configuration. This work presents the conceptual design of a firefighting aircraft of the scooper category equipped with a box wing. The aerodynamic analysis has been carried out through numerical optimization software, while the weight estimation relies on a model specifically conceived for conceptual design but still physics-based. To this end, both models available in the literature and newly developed original models have been employed, with the aim of evaluating the performance of the proposed concept and comparing it with that of the main scooper aircraft currently in operation. The results highlight the potential of the box wing in the context of aerial firefighting and lay the groundwork for further design developments aimed at addressing the aspects not covered in this preliminary phase.

# Contents

1	Inti	roduction
	1.1	Aircraft Design
	1.2	Wildfire in the near future
	1.3	State of the art for aerial fire-fighting
		1.3.1 Firefighters Aircraft main Characteristics
		1.3.2 Use of the biplane for fire-fighting operations
		1.3.3 Classification of Water Bomber Aircraft
		1.3.4 Analysis on performance of fire-fighting aircraft
		1.3.5 Operating principles of water bomber aircraft
	1.4	Aircraft type selection
2	Ma	tching Chart
	2.1	Purpose and Meaning of the Matching Chart
	2.2	Cruise
	2.3	Climb
	2.4	Take Off
		2.4.1 Evaluation of the $C_{L,TO}$
		2.4.2 Regulations
	2.5	Stall
	2.6	Other Flight Condition
	2.7	Tank Refill
		2.7.1 Geometry of the planning hull
		2.7.2 Lift on the planning hull
		2.7.3 Drag for a planning surface
		2.7.4 Drag on the water intake
	2.8	Representation of the Matching Chart
		2.8.1 Results analysis
3	We	ights 35
	3.1	Wing/Lifting System
		3.1.1 Stick model for wing weight calculation
		3.1.2 Wing structural mass results
	3.2	Weight of the wing box computed with the stick model
		3.2.1 Sweep and Dihedral
	3.3	Other weights
	3.4	Fuel weight
		3.4.1 Airspeed
		3.4.2 Design-mission
		3.4.3 Simulation of the mission
	3.5	Results

4	Aer	rodynamics	63						
	4.1	AEROSTATE underlying theory	63						
	4.2	AVL functioning	63						
		4.2.1 Lift and drag on panels	66						
		4.2.2 Numerical optimization	67						
	4.3	Aerodynamics design method	68						
	4.4	Discussion on the assessment of the Design Weight							
	4.5	Constraints determination							
	4.6	Optimization starting point	71						
	4.7	Boundaries definition							
	4.8	Computation of the Mass Center							
5	Fuselage design								
		5.0.1 Transversal section considerations	77						
		5.0.2 Rounded fuselage option	79						
		5.0.3 Overall design of the squared fuselage	80						
	5.1	Design of the front and the rear sections of the fuselage	83						
6	Design of the plane and results 8								
	6.1	First Weight results	90						
	6.2	Aerodynamic optimization	94						
	6.3	Performances	98						
7	Conclusion								
	7.1	Conclusions	105						
List of Figures									
Bi	Bibliography								

## Chapter 1

# Introduction

#### 1.1 Aircraft Design

Aircraft design is a complex discipline that involves all areas of aerospace engineering. It consists of conceiving an aircraft either a completely new one or based on an existing design while taking into account the intended purpose, available technological solutions, performance, and costs, with the goal of identifying the most successful concept (configuration).

To gain a deeper understanding of the purpose of this process, it is essential to consider the vast number of parameters involved in the design of a large and complex system such as an aircraft, as well as the numerous perspectives from which its performance can be assessed.

In this work the goal is to deliver a brand-new concept for a firefighter aircraft exploiting the box-wing lifting system technology.

Aircraft design is a:

- Multi-Stage
- Multi-Disciplinary
- Multi-Fidelity

By Multi-Stage, we refer to a design process going on several years and divided into phases based on the level of detail being analyzed. In fact we can say that detailed design cannot even begin or be successful without a solid underlying concept. The various phases can be outlined as follows:

- Conceptual design (Our matter)
- Preliminary design of components systems specific features
- Detailed design which includes production testing and flying

Conceptual design is the first phase of this long process, and it is certainly a multidisciplinary effort that involves Aerodynamics, Structures, Flight Mechanics, Propulsion, Aeroelasticity, and Systems. In order to account for all these aspects, it is necessary to develop an algorithm capable of driving the design process in the most effective direction.

Conceptual design is also called "Multi-Fidelity". This idea can be explained with a practical example.

Imagine you're driving through dense fog. You can't rely only on seeing the center line of the road you look for any signs that might help, like one showing a turn ahead. Maybe you've driven on that road before, but you don't want to trust just your memory. What you need to do in that situation is gather as much information as possible to help you get home safely.

In conceptual design, it's the same: you try to collect as much useful data as you can from the internet, books, or research papers and put it together. The idea is to see if someone has done something similar before, so you can use their work as a reference or a benchmark for your own project.

The possible sources may be:

- Textbooks
- Statistical Data
- Analytical methods
- Numerical Simulations with different level of precision
- Experimental
- Flight test

This work represent a particular case: we are thinking of an aircraft that is not existing nowadays and more than this we are trying to use a new piece of technology called The boxwing lifting system. This lifting system, theorized by Prandtl itself, seem to be a very remarkable example of a disruptive innovation that may bring aviation in to the future in terms of size and fuel consumption of the airplanes, we will discuss this system in details in the next chapter [11].

#### 1.2 Wildfire in the near future

Wildfires are a common phenomenon that have always occurred in woods and forest all over the world. The main purpose while talking about Wildfires should be to understand and control the mechanism on which they are based. In the last years interactions between human and woods are changing. Since the first half of twentieth century nature was strictly under control of farmers and inhabitants who used to interact with the woods and forest keeping them clean and healthy. Times are changed, today the interactions between human and nature are reducing, people are moving in cities and progressively abandoning rural places. Another effect that represents a risk factor in terms of wildfires is the growing interface area between woods and towns. In this regions the start of wildfires is way more easy due to human activities going around near vegetation.

About wildfires is important to say that they are pretty "selective". Fuel is not all the same, and, some of the materials that humans used to burn or to eat, are the ones preferred by wildfires. We can say that the fire substitutes humans and give the possibility to the wood to get clean and regenerate. Wildfires are really important in the ecosystem of forest and woods.

On the other hand Wildfires are also dangerous, they can easily damage properties or human beings and it is fundamental to control them in order to save lives and money. To extinguish fires is really important but, according to this article [5], other ways have to be taken in to account.

### 1.3 State of the art for aerial fire-fighting

The idea of using aircraft for fire fighting activities was born in the US after WW2 when old bombers were converted into firefighters.

Aircraft are even more essential in firefighting operations today than they were back then, both in terms of dropping quantities of retardant on the affected area and for transporting firefighters to the scene. In this work, the focus is on water bombers, which are aircraft capable of storing large quantities of retardant that can be dropped on the burning area to cool it or on neighboring areas to prevent fires in new areas.

It's necessary to define some parameters to evaluate the effectiveness of this kinds of planes. An interesting method for properly designing the mission's drop phase is presented in [16].

Although this approach is not suitable for the present early stage of the design, it will be useful later. For the purposes of this work, however, the study provides valuable information on the flight parameters that characterize this crucial portion of the trajectory.

The first number to define is the coverage "C". Mathematically it is defined as:

$$C = \frac{Quantity}{Surface} \left[ \frac{l}{m^2} \right]$$
 (1.1)

Coverage is influenced by several factors:

- Hopper Pressure
- Airspeed
- Retardant Viscosity
- Retardant Density

It is necessary to have the correct coverage value depending on the type of vegetation, the purpose and the type/intensity of wildfire.

Sometimes additives are added to retardant for keeping the proper coverage value or for amplify the effects of the drop in general.

#### 1.3.1 Firefighters Aircraft main Characteristics

Fire fighting aircraft, as seen before can be divided in two main type: there are TACTICAL aircraft and WATER BOMBER aircraft.

The purposes of the tactical firefighter aircraft are:

- Reconnaissance of the fire area
- Operation coordination
- They can be airplanes or helicopters

The purposes of Water Bomber are:

- Throw retardant on the fire area
- They can be airplanes ore helicopters
- They are classified retardant tank capacity

The principal characteristics of fire-fighting aircraft are:

- Good Hopper capacity
- Fire-extinguishing agent must be released at a controlled rate in order to generate a coherent column of fluid
- Hopper filling system need to be the most quick and effective
- Good Cockpit visibility
- Minimal wing span to maintain the necessary clearance from ground
- The more versatility possible including, if possible, taking off from gravel field
- Strong, large diameter, low pressure tires

- Mild stall Characteristics, aircraft should loose altitude when at critical angles without stalling
- Big wing surface, preferring low aspect ratio for keeping wingspan as low as possible
- Stiff wing structure
- Good maneuverability also and especially at low speed
- Short take off and landing distance

These are, in general, the high level requirements for fire-fighting aircraft.

#### 1.3.2 Use of the biplane for fire-fighting operations

For the reasons told before designing fire fighting aircraft we should take in to account the possibility of designing a biplane aircraft [8].

Biplane aircraft can, maintaining the same span, carry lot more weight than monoplane aircraft because of the bigger wing surface at a reduced Aspect Ratio. This possibility is very interesting because, ideally, we can build an aircraft which, with the same span of, for example CL-415, can bring two times the retardant quantity.

Other advantages of a biplane configuration can be an increased aerodynamics efficiency at the same wingspan which alone is not enough to reduce fuel consumption because of the numerous parameters interacting in this complex systems but, in general, its a positive aspect. Fuel consumption can surely help mission last longer than the previous types of firefighters; having longer missions will help a lot in ensuring good overall firefighting performance as we will see after in this work.

In particular this work will focus on an idea of biplane called PrandtlPlane [11].

The idea is to eliminate the wingtip and the associated vortex formation increasing the aerodynamics efficiency of the lifting system.

For showing why the PrandtlPlane architecture may be an interesting option for this type of airplane two different planes are compared. The first one is the CeRAS-01 which, we can say, is very similar to the Airbus A320. The second one is the PrandtlPlane, a transportation aircraft with the following main characteristics. As we can see the PARSIFAL [?], with the same mission range and wingspan brings 308 passenger when Airbus a320 stops at 186 as its possible to see in figure 1.3. We can appreciate this also in terms of MTOW where the PARSIFAL plane reaches approx 125000 kg and the CeRAS just 76824 as shown in figure 1.2. We can say that these characteristics may be very useful on a firefighter aircraft. The PARSIFAL reaches, on the same mission at full passenger the stunning value of 0.01227 kg of fuel per km per pax, a reduction, in terms of CeRAS of 20%.

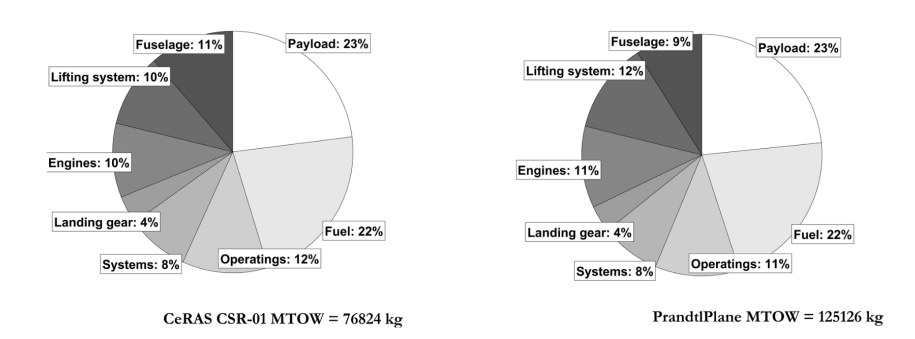


Figure 1.1: Image taken from [1]

	CeRAS CSR-01	PrandtlPlane
W <sub>oe</sub> (kg)	42,054	68,866
$W_{oe}/MTOW$	54.7%	55.0%
W <sub>fuel</sub> (kg)	17,100	27,000
$W_{fuel}/MTOW$	22.3%	21.6%
W <sub>pay</sub> (kg)	17,670	29,260
$W_{pay}/MTOW$	23.0%	23.4%
MTOW (kg)	76,824	12,5126

Figure 1.2: Image taken from [?]

	CeRAS CSR-01	PrandtlPlane
Number of passengers	186	308
Mission range	4790 km	4790 km
Mission fuel	13,670 kg	18,108 kg
Mission fuel per pax/km	0.01537 kg/km pax	0.01227 kg/km pax

Figure 1.3: Image taken from [1]

#### 1.3.3 Classification of Water Bomber Aircraft

The water-bomber aircraft are classified by the water-tank capacity:

• VLAT (Very Large Air Tanker): This type has tank capacity up to 19000 liters.



Figure 1.4: DC-10 SuperTanker



Figure 1.5: Boeing 747 SuperTanker

- Wide Body transport aircraft converted into water bombers

- Operational cost of this type of water bombers are lot higher then other kind of Water Bombers
- Ground filling on equipped track
- Type I LAT (Large Air Tanker): Tank capacity between 11500 and 19000 liters
  - Small Narrow Body transport aircraft converted into water bombers
  - Some of them can have a removable retardant tank which permits governments or organizations to buy a quantity of convertible water bombers that can be used on other purposes when wildfires doesn't occur
  - Same issues of VLAT because of these are converted transport aircraft
  - Ground filling on equipped track



Figure 1.6: AC-130 Tanker

- Type II: Tank capacity between 6000 and 11500 liters
  - This aircraft are also referred as scoopers for their ability to "scoop" water from a surface such as lakes, seas or even big rivers. The possibility for this machines to do in-air refill is an important characteristic that gives them a big capacity in terms of bombing rate
  - The CL-215 and CL-415 represent the best example of scoopers, this model achieved a huge success because of their low operational cost and high efficiency
  - On the other hand designing a scooper amphibious aircraft adds a big element of complexity. Designing the hull in a way the plane can do the in-air refilling planning on water, maintaining stability and controllability means lots of elements to design.
- Type III: Tank capacity between 380 and 6000 liters
  - Often one engine aircraft
  - Small retardant capacity means less efficiency in water bombing.

#### • Helicopters:

- Helicopters play a big role in firefighting activities. They offer the possibility to charge quite a big water quantity also from small, irregular sources that airplanes can't reach. It's possible to say that in some scenarios helicopters are a must have for effective operations
- Retardant can be stored in external tanks added to the machine or in internal tanks



Figure 1.7: CL-415



Figure 1.8: Grumann s2T

- Thanks to the small retardant quantity the refill time is short but, this operation, require to hover on the water source. This condition is very risky for helicopters
- Also Helicopters are divided in different size tank size categories

#### 1.3.4 Analysis on performance of fire-fighting aircraft

Once classified the firefighters aircraft we need to asses the performance in order to choose which is the best type of aircraft to think about while engaging this design process. We do this big choice now because different type of water bombers have big differences in operative features and so in the main design choice.

The study [14] provides an interesting amount of data on the operation of firefighter aircraft which are represented below in order to highlight the differences and the similarities between the various category.



Figure 1.9: Sikorsky s64 Tanker

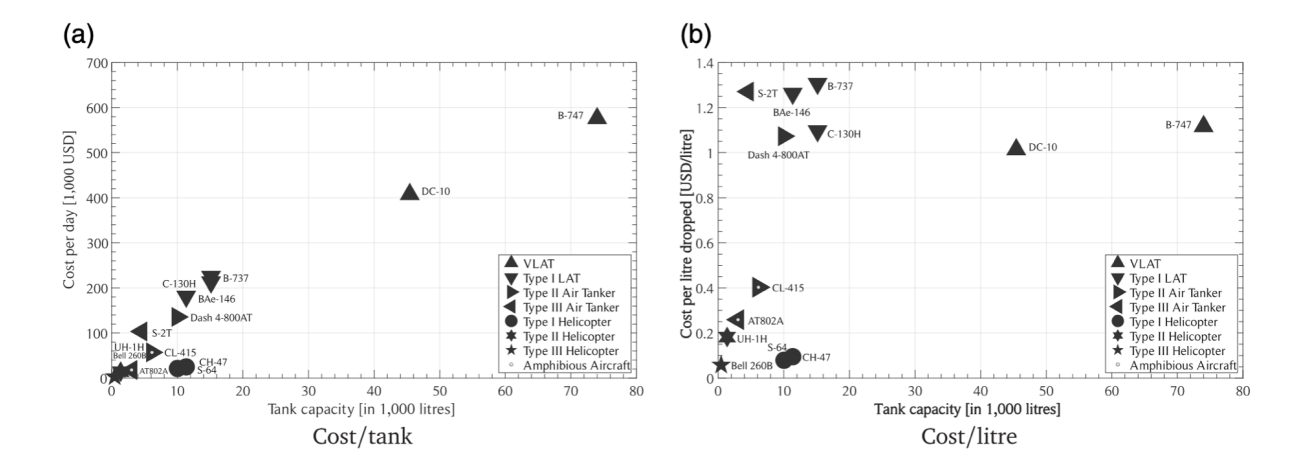


Figure 1.10

In figure 1.10 its possible to see that, in terms of cost per day, the bigger the tank is the bigger is the cost. Scoopers and Helicopters have a relatively low cost per day of operations but a reduced tank capacity. In general we can say that, more or less, helicopters and amphibious aircraft are in the same area of the graph. This is probably due to the possibility of a in-air refill. The second graph in image 1.10 is pretty similar to the first one and, it represent, the cost per liter of dropped retardant VS the tank capacity. In this case, an important parameter is the bombing rate, that affects the cost per liter, in fact, as expected, helicopters in this case are the cheaper and in general the in-air refill tankers take big advantages on the large tanker in which the bombing rate is affected by the necessity to reach a equipped runway to operate.

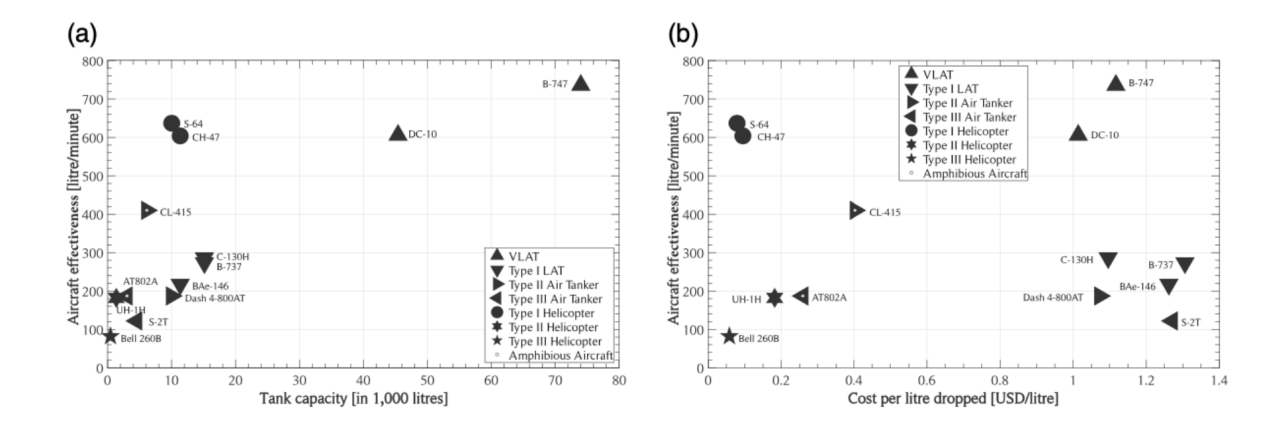


Figure 1.11

In image 1.11 we can evaluate the performance in terms of effectiveness  $\frac{Quantity}{Time}$  rather than cost as we did before. In this case we can see an interesting situation: All the small Helicopters are more or less in the same area characterized by low Aircraft-Effectiveness and that is due to the small tank capacity. Big helicopters do the best because they guarantee the best effectiveness with the smaller tanks. That is because of the bombing rate combined with pretty large tanks.

Very large tankers do the best in terms of effectiveness with the bigger. They are pretty the same than big Helicopters because the trade off between the huge tanks and the reduced bombing rate. Also in this case we see the CL-415 in a intermediate area between the different worlds of very big tanks and very small tanks.

An interesting analysis can be surely done observing the second graph in figure 1.11 in which is represented the effectiveness vs the operational cost in terms of cost per liter. What is immediately clear is that four main groups are forming. On the left we said almost only helicopters, has seen before they have the lower cost of operation because they can be refilled almost on place and they don't spend to much time flying around searching for a water source. The left part of the graph is, divided in upper and lower zone. In the upper zone we see big Helicopters which, with the good size tank can drop, large amount of retardant at a high rate. In the lower zone we see small helicopters, surely cheap, but less effective because of the reduced tanks. In terms of operations small helicopters still remains a choice especially in site in which refilling is difficult for example in private pools or very small lakes. The right part contains mainly airplanes divided by the tank capacity in upper and lower zone, we see that, non amphibious aircraft, regardless the tank capacity are affected by very high costs because of the necessity to fly over and over againg to reach the retardant and do the refilling. In the exact center of the graph we see the CL-415 with good capacity and so effectiveness and relatively good costs of operations.

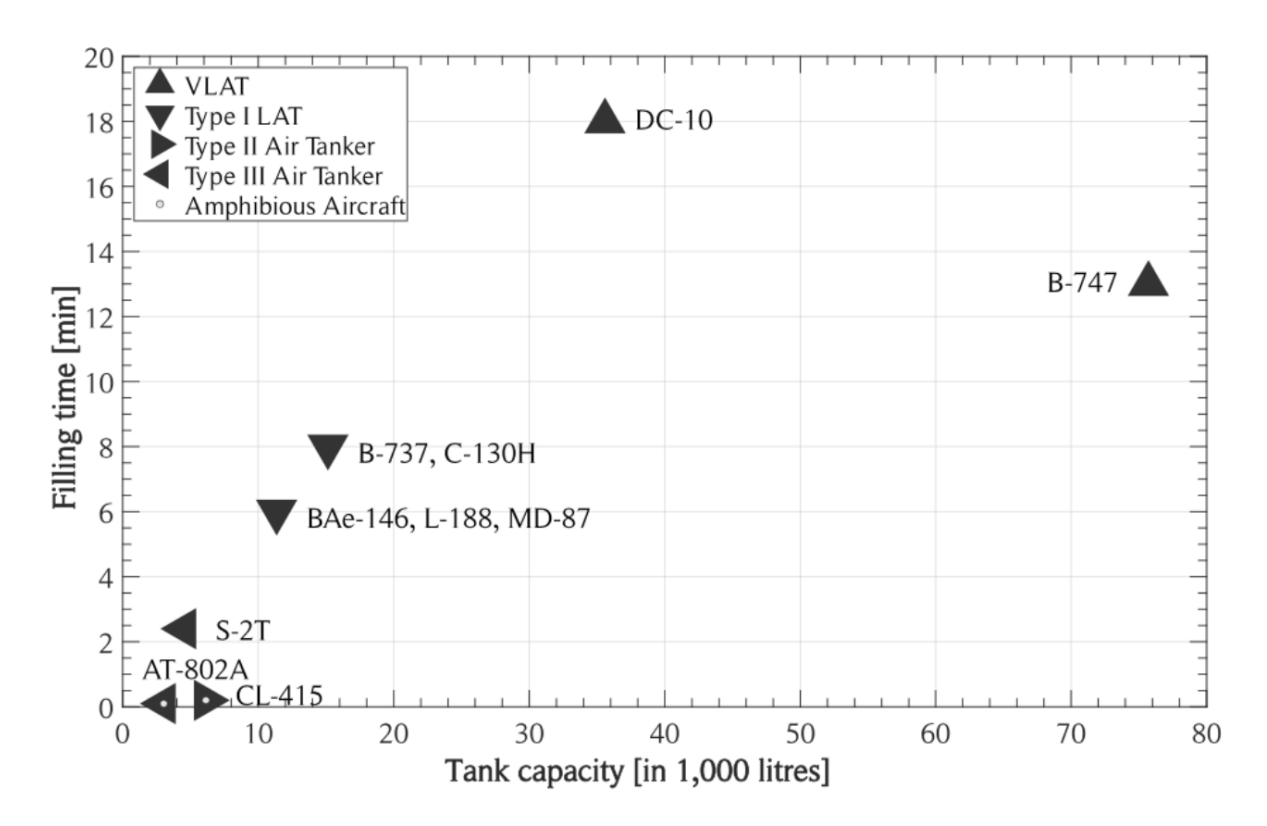


Figure 1.12

The graph in figure 1.12 is pretty clear, amphibious aircraft and Helicopters have really the best filling time rather than bigger non amphibious plane that, due to the tank capacity takes lots of minute to refill. In particular we can see that the DC-10 is doing the worst in this specific performance.

#### 1.3.5 Operating principles of water bomber aircraft

The idea of water bombing aircraft is basically store water in internal or external tanks for throwing it in the exact point at the exact time for extinguish or preventing fire. The element who stores water is the hopper

The hopper can be driven by the hydraulic system and should be near the center of mass of the plane in order to not destabilize the flight during the dropping. Water can fall for gravity or can be expelled by pumps. The pressure inside the hopper should be the higher possible for obtaining a coherent drop. If the column is not coherent it may be possible to loose a lot of coverage and so the effectiveness of the operations. If the water just falls for gravity for having good pressure values we will need to design the hopper as high as possible to make the static pressure  $p = \rho gh$  as high as possible.

Since we are trying to use the PrandtlPlane architecture we may have problems with the height of the fuselage and for that we may need a pressurized system for the water dropping as said before.

The coverage, depends on different parameters, the pressure is just one of them. Other important things to keep in mind are the speed of the plane and the height at which the drop begins. Depending on the type of vegetation the requested coverage for effective drop goes from 1 to 2.5  $\left[\frac{l}{m^2}\right]$ . There are specific models to describe the water column useful for defining trajectory and the speed for the drop in a optimal way.

## 1.4 Aircraft type selection

Specifically, in this work is chosen to focus on the conceptual design of a scooper because of, in a typical operation scenario wee clearly see that scooper such as the CL-415 represents a good compromise between all the different performances. The main objective of this work, in conclusion, is to place some other marks on these five performance graph trying to introduce the PrantdlPlane concept into the firefighting world.

What is expected to find is new configurations with bigger tanks and pretty the same costs of operations in terms of cost per day and cost per liter. It would be fantastic to find new possible planes with increased effectiveness with reduced costs.

For determine where to place the "new marks" on this graphs it is necessary to determine the main aspects of the plane and to simulate his flight on the mission on which the graph are build

## Chapter 2

# **Matching Chart**

To initialize the design process it is first necessary to make some evaluations on the amount of thrust or power needed. In this phase we still don't know if the plane will be equipped with turbofan or turboprop engines, these are important information to know in order to draw the matching chart so we decided to represent both case, the one with turbofan engine and the other with propeller.

### 2.1 Purpose and Meaning of the Matching Chart

The Matching Chart is a graph where we represent, on the x-axis the wing load factor  $\frac{W}{S} \left[ \frac{kg}{m^2} \right]$  and on the y-axis the specific power  $\frac{P}{W} \left[ \frac{kW}{kg} \right]$  or specific thrust  $\frac{T}{W} \left[ \frac{kg}{kg} \right]$ . Basically what we do is to impose the equilibrium of the forces on the plane and to find which are the the couples of  $\frac{T}{W}$  and  $\frac{W}{S}$  that make the equilibrium possible. Since the forces acting on the aircraft depend on the flying condition we need to analyze the equilibrium for different flight conditions.

The power and thrust on the matching chart has to be intended as necessary value for the correct execution of the specific maneuver.

For all of this condition we make some Hypothesis:

- The aircraft is assumed to be a concentrated mass
- The thrust axis coincide with the x-body axis
- The diagram is computed at sea level

Lets take in to account all the different flying conditions required for this plane. The thrust in-flight equilibrium equation is written below

$$\begin{cases} \frac{T}{W} = \frac{\frac{1}{2}\rho V^2 C_{D,0}}{\frac{W}{S}} + 2\frac{k}{\rho V^2} \left(\frac{W}{S}\cos\gamma\right)^2 + \sin\gamma \\ \left(\frac{T}{W}\right) = \left(\frac{T}{W}\right)_{sl} \frac{\rho}{\rho_{sl}} \end{cases}$$
(2.1)

Were:

- $\rho$  is the air density
- $\bullet$  V is the airspeed
- $C_{D0}$  is the parasite drag coefficient.
- k is the coefficient of the non-linear term of the drag polar curve expressed as:  $C_D = C_{D,0} + k \cdot C_L^2$
- $\gamma$  is the climb angle

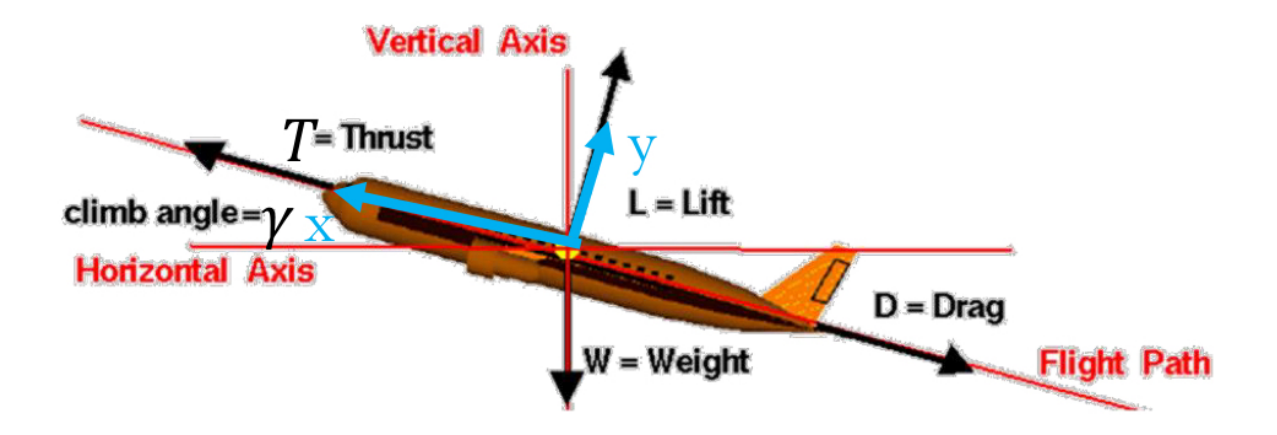


Figure 2.1: Forces layout for a generic Aircraft

•  $\rho_{sl}$  is the air density at sea level and it is set to  $1.225 \frac{kg}{m^3}$ 

Below the same equilibrium equation in terms of power:

$$\begin{cases} \frac{P}{W} = \frac{\frac{1}{2}\rho V^3 C_{D,0}}{\frac{W}{S}} + 2\frac{1}{\rho}k \left(\frac{W}{S}\cos\gamma\right)^2 + \sin\gamma \cdot V \\ \left(\frac{P}{W}\right) = \left(\frac{P}{W}\right)_{sl} \left(\frac{\rho}{\rho_{sl}}\right)^{0.7} \end{cases}$$
(2.2)

#### 2.2 Cruise

For the cruise we can see we need to set some parameters for drawing the graph, for example, its necessary to decide at which flight level we want to cruise and at what speed. It's possible to fix  $\gamma = 0$ . The cruise level is fixed at 6500ft and the cruise speed at  $100\frac{m}{s}$ . In this way we have all the information in order to draw the curve for the curve

### 2.3 Climb

The climb section is divided in two main part because, if we were considering just one section for all this flight segment, we would commit a big model error because of the variation of density, speed and climb angle that have to occur since this is a transition moment between the ground and the cruise condition.

The equation we use in this case is the same that in the cruise segment but assuming different parameters.

$$\begin{cases}
\frac{T}{W} = \frac{\frac{1}{2}\rho V^2 C_{D,0}}{\frac{W}{S}} + \frac{1}{2}\rho V^2 k \left(\frac{2\frac{W}{S}}{\rho V^2}\cos\gamma\right)^2 + \sin\gamma \\
\left(\frac{T}{W}\right) = \left(\frac{T}{W}\right)_{sl} \frac{\rho}{\rho_{sl}}
\end{cases} (2.3)$$

The parameters are represented in the table below.

Parameter	FIRST SEGMENT	SECOND SEGMENT
$\begin{array}{c} \textbf{Min} \ \gamma \ \textbf{OEI} \\ \textbf{condition} \end{array}$	Twin: 0.0% Quad: 0.5%	Twin: 2.4% Quad: 3.0%
Start when	$V_{ m LOF}$ reached	Gear fully retracted
Slats / Flaps Configuration	Takeoff	Takeoff
Engine rating	TOGA / FLEX	TOGA / FLEX
Speed reference	$1.1 \cdot V_s$	$1.3 \cdot V_s$
Landing gear	Retraction	Retracted
Ground effect	Without	Without

Table 2.1: Climb Segment Performance Requirements (Engine-Out)

With all this information we can use the equilibrium equations and compute the curve for these two data set.

#### 2.4 Take Off

For the take off phase we need to define a method for evaluating the equilibrium in different moments. During the ground roll, rotation and lift-off, the force system apply on the body is really different and can result difficult to do the same as we did discussing the cruise and climb phases. In this case we decide that the cheaper way to evaluate the specific thrust or power needed for the take off its an empirical model that allows, with a very small effort, to find all its necessary to know.

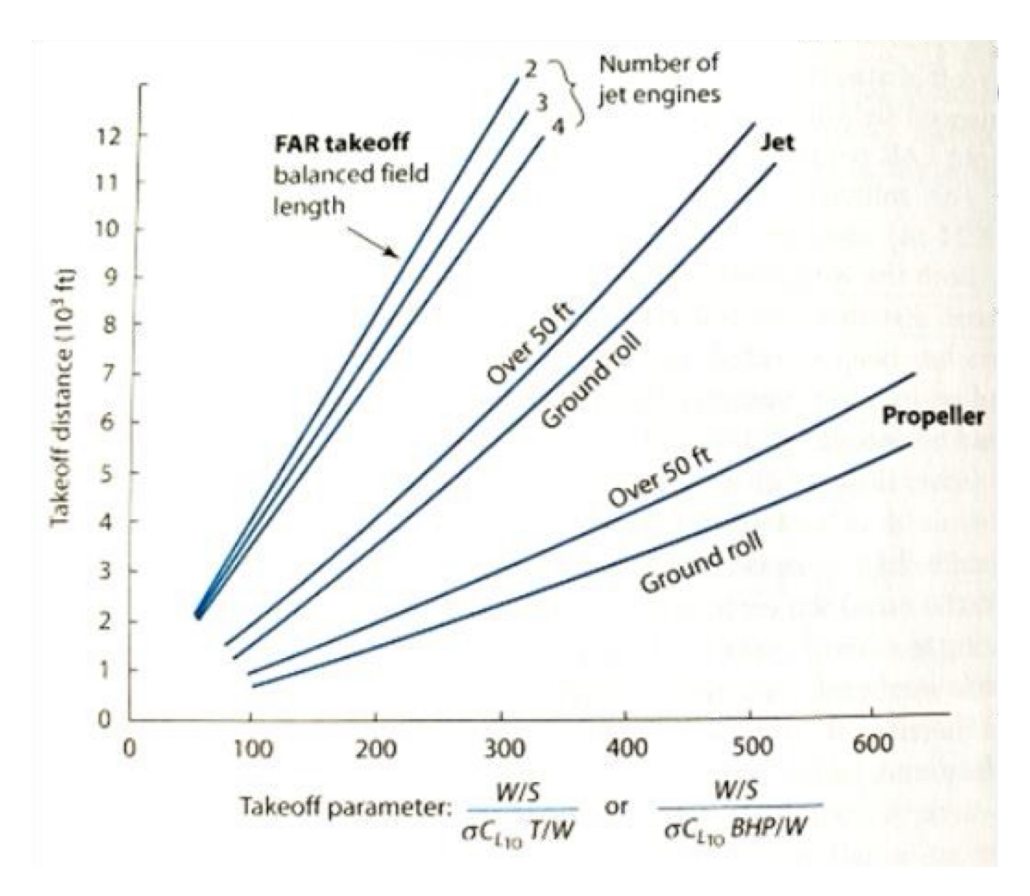


Figure 2.2: TOD vs TOP

From the 2.2 graph we can compute the Take Off Parameter from imposing the Take off Distance. So, deciding a proper take off distance for the aircraft, we find the take off parameter and, for the following equation we can draw the curve we are searching for. Referring to 2.2 graph we can see that the value of take off parameter depend on the type and the number of engine onboard. Since we are taking into considerations both the turboprop and turbofan architecture we'll need to vary the value of TOP in a proper way.

$$\frac{W}{S} = (TOP) \, \sigma C_{L,TO} \left(\frac{T}{W}\right) \tag{2.4}$$

and so

$$\frac{T}{W} = \frac{\left(\frac{W}{S}\right)}{\left(TOP\right)\sigma C_{L,TO}}\tag{2.5}$$

For the case of a turboprop engine, where we need to talk about power instead of thrust the equation becomes as it follows:

$$\frac{P}{W} = \frac{\left(\frac{W}{S}\right)}{(TOP)\,\sigma C_{LTO}} V_1 \tag{2.6}$$

Where  $\sigma = \frac{\rho}{\rho_{sl}}$  and  $C_{L,TO}$  is the lift coefficient in the take off configuration so with flaps and slats extended.

#### 2.4.1 Evaluation of the $C_{L,TO}$

For evaluating the  $C_{L,TO}$  there are lots of possible methods. For example we can use potential method or CFD method, or, in this situation, where we have a conventional wing section its possible to choose a simpler method, starting from  $C_{L,max}^{2D}$  of the chosen section.

We can estimate the value of the  $C_{L,max}^{3D}$  as indicated on the Raymer texbook with the following equation:

$$C_{L,max}^{3D} = 0.9 \cdot C_{L,max}^{2D} \cdot \cos(\Lambda_{25})$$
 (2.7)

Where the  $C_{L,max}^{2D}$  can be easily found in tables. In this case we assume a value of 2.70 And with flaps and slats extended this value increases of:

$$\Delta C_{L,max}^{flap,3D} = 0.92 \cdot \Delta C_{L,max}^{flap} \cdot \frac{S_{flapped}}{S} \cos(\Lambda_{25})$$
 (2.8)

 $\Delta C_{L,max}^{flap,2D}$  is the  $C_L$  augmentation due to flap or slat configuration. In this case we assume a value of 1.45 as we find on the Raymer textbook. The  $S_{flap}$  is the portion of the wing affected by the presence of the flaps or slats.

#### 2.4.2 Regulations

For the take off we need to consider that, if a failure occur during the ground roll it is necessary to decide wether to continue with the take off or or to stop and brake. The idea is that the Accelerate and stop distance (ASD) and the Take off Distance (TOD), depend on the speed at which the engine failure occur. So there will be a point at which these two distances will be equal. The speed at which the ASD is equal to the TOD is called decision speed or V1. The distance at which the ASD and the TOD are equal is the BFL or Balanced Field Length.

For the regulations it is necessary to take into account a "Recognition Time" that is the time estimated for the pilot to take a decision after the engine failure occur.

V2 is the speed to reach at a height of 35ft above the runway surface,  $V_2$  has to be more than 1.2  $V_s$  where  $V_s$  is the Stall Speed that can be computed with the following equation:

$$V_S = \sqrt{\frac{2\frac{W}{S}}{\rho C_{L,maxTO}}} \tag{2.9}$$

#### 2.5 Stall

For a fire fighting aircraft is particularly important to make consideration upon the stall condition. Stall occur when the angle of attack is to high for the speed and so the flow separates from the back of the wing the lift drops the equilibrium is broken so the plane basically falls.

Lets use the stall speed equation as follows to find the maximum load factor for not breaking the stall limit:

$$\left(\frac{W}{S}\right)_{stall} = \frac{1}{2}\rho V_s^2 C_{L,max} \tag{2.10}$$

## 2.6 Other Flight Condition

Other possible flight conditions are the ones that occur when a landing is aborted. The diversion can occur in different moments. If the diversion is decided when the plane is in the approach condition its necessary to climb at a moderate rate, flaps and landing gear are not extended and that means a certain amount of power.

If the diversion occur when the plane is already on the ground or in the immediate proximity this maneuver requires lot more thrust: first of all the climb angle must vary a lot because, since we are near the runway we need to climb at a very high ratio but its not enough, the plane in this condition is ready for the landing so, flaps and slats are fully extended, landing gear is extended and, for that the drag is considerable.

The approach climb, Landing Climb and the touch and go must be feasible also in OEI (One Engine Inoperative) condition.

#### 2.7 Tank Refill

For the tank refill maneuver several contributions must be taken into consideration.

Airflow applies a force on the lifting system, this force can be seen as Drag and Lift and can be evaluated with the usual method:

$$\begin{cases} D = \frac{1}{2}\rho V^2 S C_D = \frac{1}{2}\rho V^2 S \left( C_{D,0} + \frac{C_L^2}{\pi \cdot AR \cdot e} \right) \\ L = \frac{1}{2}\rho V^2 S C_L \end{cases}$$
 (2.11)

Obviously there is the weight and the thrust contribution and, differently from before, there are forces acting on the hull for which we need to define a model. For now, the first step, is to put all together and find the equation we are looking for.

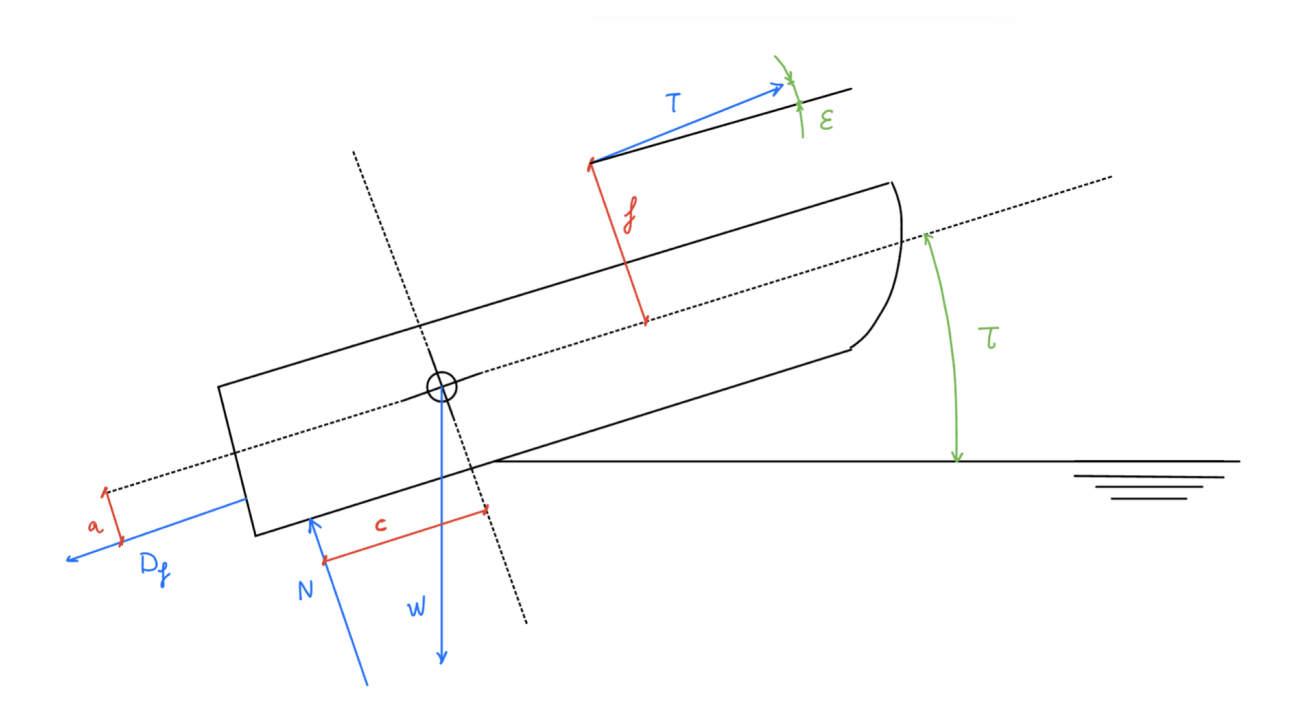


Figure 2.3: Force diagram on during refilling

The equilibrium on the plane is represented in figure 2.3 is written as follows:

$$\begin{cases}
T \cdot \cos \tau - D - D_h = 0 \\
L + T \cdot \sin \tau - W + L_h = 0
\end{cases}$$
(2.12)

Because of  $\tau$  is never above 10° we can reduce the equilibrium to:

$$\begin{cases}
T - D - D_h = 0 \\
L - W + L_h = 0
\end{cases}$$
(2.13)

Rewriting the equations in a more comfortable way we find the specific thrust or specific power

required in this particular situation:

$$\frac{P}{W} = \frac{1}{2} \frac{1}{\eta_p} \rho V^3 \left(\frac{W}{S}\right)^{-1} \left(C_{D,0} + \frac{4\left[\frac{L_h}{S} - \frac{W}{S}\right]^2}{\rho^2 V^4}\right) + \frac{D_h V}{\eta_p}$$
(2.14)

Were:

- $\frac{P}{W}$  Is the specific power
- $\eta_p$  is the propeller efficiency
- rho is the air density @ sea level
- $C_{D,0}$  is the parasite drag coefficient
- $L_h$  is the hull lift
- $D_h$  is the hull drag

Now the issue becomes to find a model to evaluate the value of  $D_h$  and  $L_h$ .

#### 2.7.1 Geometry of the planning hull

This design case is about a planning hull. Referring to [13] we can write some empirical equations for determine the amount of lift and drag the hull exchange with the fluid. To understand the working principle of a planning hull we need to think about the limit case: a infinite plane surface (flat bottom surface) forced on a water surface at a certain speed.

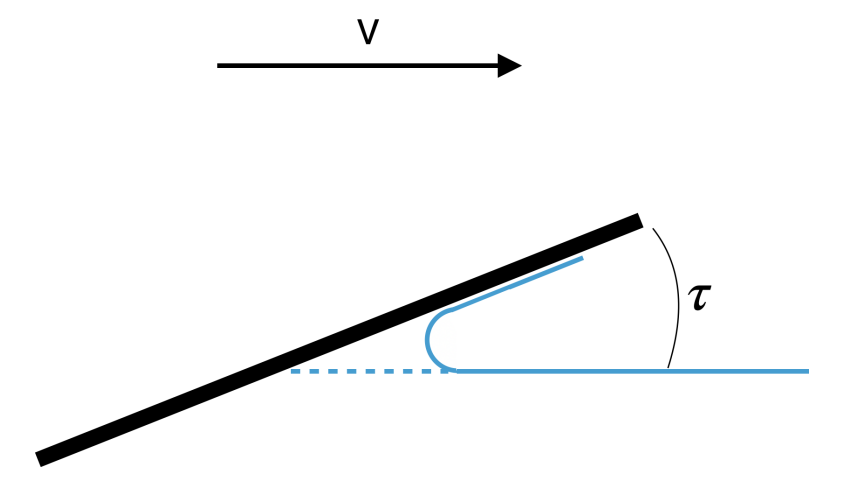


Figure 2.4: Plane surface planning

As we can see in picture 2.4 there is a layer of water who is sprayed forward by the surface. As we can imagine this layer of fluid means that a drag force is applied to the plane opposing to motion. This is, simplifying, the reason why a deadrise angle is introduced. With a deadrise angle its possible to reduce the negative effect caused by the spray increasing, at the same time, the lateral-directional stability which, in the case of a flat bottom surface is not guaranteed. Introducing a deadrise angle we obtain a Hull design and so, we can study the forces applied on the hull by the water and the disposition of spray root and spray layer.

In fact in figure 2.6 we see, from a lateral point of view, the way water surround a planning hull. Its possible to observe some characteristic dimensions. The effective pressure area is the

wetted length  $\lambda$ . The contact length between the hull and the undisturbed water is  $L_k$  and the length at which we find the spray root is  $L_c$ . Now there are relations between these different length.

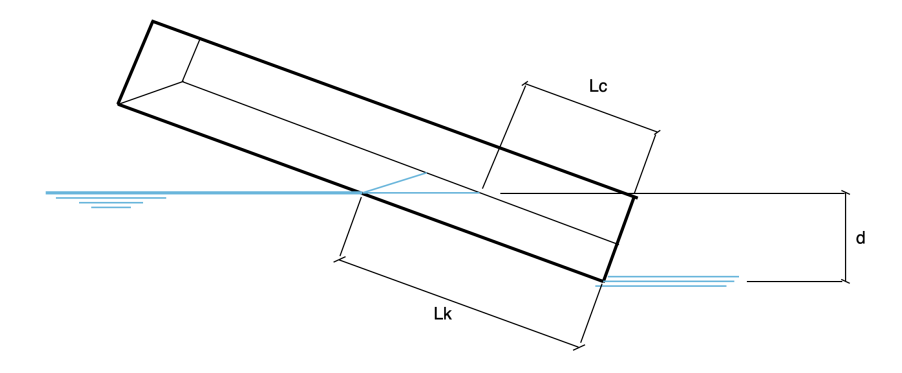


Figure 2.5: Model of prismatic Hull Lateral View

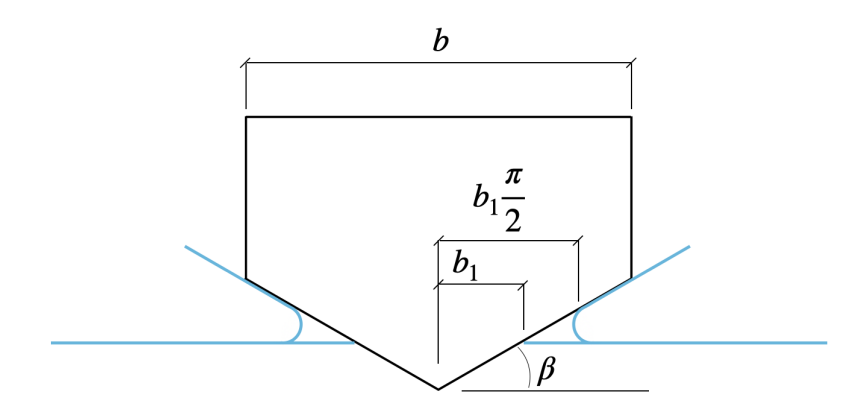


Figure 2.6: Model of prismatic Hull Front View

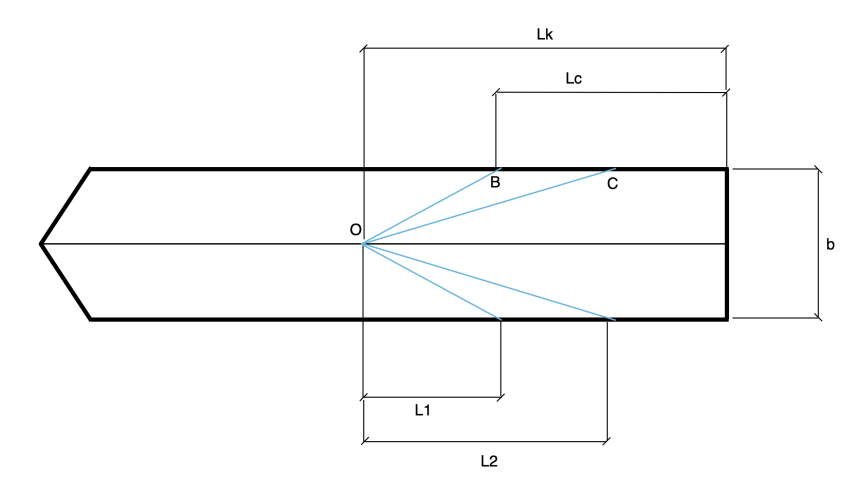


Figure 2.7: Model of prismatic Hull Bottom view

The difference between  $L_c$  and  $L_k$  is found to be in [13]:

$$L_k - L_c = \frac{b}{\pi} \frac{\tan \beta}{\tan \tau} \tag{2.15}$$

and, defining  $L_k$  as:

$$L_k = \frac{d}{\sin \tau} \tag{2.16}$$

Substituting and rearranging in the definition of the mean wetted length-beam ratio  $\lambda$ , defined as:

$$\lambda = \frac{L_k + L_c}{2 \cdot b} = \frac{\left[\frac{d}{\sin \tau} - \frac{b}{2\pi} \frac{\tan \beta}{\tan \tau}\right]}{b} \tag{2.17}$$

#### 2.7.2 Lift on the planning hull

The lift of a planning surface is due on 2 main contribution:

- Buoyant contribution due to static pressure acting on the hull
- Dynamic reaction of the fluid against the moving surface

The Buoyant effect can be seen mostly at low speed and it is basically due to gravity. As the speed increases dynamic reaction begin to be more influent; at the beginning we have that the dynamic effect tend to decrease the load the prismatic surface can support. Then, at big value of speed coefficient the dynamic lift become predominant. The equation for hull lift must take in to account both this contribution.

To empirically find an equation for the lift coefficient of a prismatic body planning on water we use the aerodynamic theory which says that: for high **AR** ( Aspect Ratio ) bodies ( Bodies with a small span and high length ) the lift coefficient is proportional to  $\tau^2$  and for low  $\lambda$  bodies lift coefficient is proportional to  $\tau$ . In [13] is shown that for bodies with an aspect ratio of a likely planning solid, we find that:

$$\frac{C_L}{\tau^{1.1}} = f(\lambda, C_v) \tag{2.18}$$

Where:

$$L_h = \frac{1}{2}\rho_{water}V^2b^2C_{l,\beta} \tag{2.19}$$

The empirical formula we can find combining the aerodynamic theory and a huge amount of experimental data is the following:

$$C_{L,0} = \tau^{1.1} \left[ 0.0120 \cdot \lambda^{\frac{1}{2}} + \frac{0.055 \cdot \lambda^{\frac{5}{2}}}{C_v^2} \right]$$
 (2.20)

With  $0.60 \le C_v \le 13.00$  and  $2^{\circ} \le \tau \le 15^{\circ}$  and  $\lambda \le 4$  else the model is not valid.

This is the lift coefficient on a planning surface with deadrise  $\beta = 0^{\circ}$ . When  $C_v$  is very small, between 0.6 and one, the lift coefficient due to dynamic contribution falls and the surface experiences like a sinking effect. Its now possible to correct the lifting coefficient for a flat surface in the following way adding a deadrise angle  $\beta$ .

$$C_{L,\beta} = C_{L,0} - 0.0065 \cdot \beta \cdot C_{L,0}^{0.60}$$
(2.21)

Where  $C_{L,\beta}$  is the lift coefficient for a deadrise surface and  $\beta$  is the deadrise angle for the surface. The effect of the deadrise angle is to diminish the value of the dynamic lift.

#### 2.7.3 Drag for a planning surface

The total hydrodynamic drag of a planning surface is, as for the lift, the sum of two different contribution:

- Hydrostatic drag due to a component of the static pressure force acting normally to the motion
- Viscous drag acting tangentially on the spray and wetted area.

The drag becomes:

$$D = \Delta \cdot \tan \tau + \frac{D_f}{\cos \tau} \tag{2.22}$$

Where in [13]  $\Delta$  represent the total load (the weight of the boat or plane **W**),  $D_f$  is the friction drag, acting tangentially to the motion which can be evaluate as follows:

$$D_f = \frac{C_f \rho V_1^2 \left(\lambda b^2\right)}{2 \left(\cos \beta\right)^4} \tag{2.23}$$

Where  $C_f$  is the Shroenherr turbulent friction coefficient and  $V_1$  is the average bottom velocity which we can evaluate with the following method.

When  $C_v$  reaches high values its possible to write the  $C_{L,0}$  as:

$$C_{L,0} = 0.0120 \cdot \tau^{1.1} \lambda^{\frac{1}{2}} \tag{2.24}$$

Then, correcting for a deadrise angle, becomes:

$$C_{L,\beta} = C_{L,0} - 0.0065 \cdot C_{L,0}^{0.60}$$
 (2.25)

So

$$C_{L,\beta,d} = 0.0120\tau^{1.1}\lambda^{\frac{1}{2}} - 0.0005753 \cdot \beta \tau^{0.66}\lambda^{0.3}$$
(2.26)

So the dynamic load on the bottom is:

$$\Delta_d = \frac{1}{2} \rho V^2 b^2 (C_{L,\beta,d})$$
 (2.27)

And the average dynamic pressure on the bottom is:

$$p_d = \frac{\Delta_d}{\lambda b^2 \cos \tau} = \frac{\rho V^2 C_{L,\beta,d}}{2\lambda \cos \tau} \tag{2.28}$$

Applying the Bernoulli equation knowing the average dynamic pressure we find the average bottom velocity as a fraction of the velocity:

$$V_1 = V\sqrt{1 - \frac{2 \cdot p_d}{\rho V^2}} = V\sqrt{1 - \frac{C_{L,B,d}}{\lambda \cos \tau}}$$
 (2.29)

So summarizing we find the drag applied on the planning surface with deadrise to be:

$$D = \Delta \tan \tau + \frac{\rho V_1^2 C_f \lambda b^2}{2 \cos \beta \cos \tau}$$
 (2.30)

Where the  $C_f$  is defined as:

$$C_f = \frac{0.0576}{Re^{\frac{1}{5}}} \tag{2.31}$$

And,  $Re = \frac{V_1 \lambda b}{\nu}$  where  $\nu$  is the kinematic viscosity,  $\lambda$  is the average wetted surface, b is the hull span.

#### 2.7.4 Drag on the water intake

A simplified model for the water intake drag is found applying the conservation of momentum. The water intake door is represented as we can see in figure 2.8. For the calculation we need to set few hypothesis:

- The water flux is 1-Dimensional
- There is no viscosity

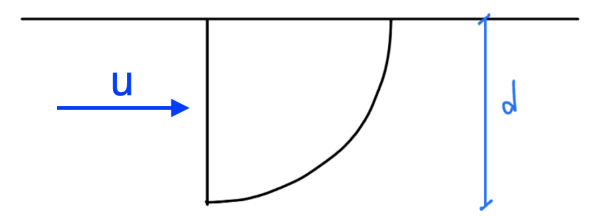


Figure 2.8: Water intake model

For the model we define a permeable volume in which we impose the conservation of momentum:

$$\vec{R} = \int \vec{n} \cdot (\rho \vec{u}) \, d\Sigma \tag{2.32}$$

Where  $\vec{R}$  is the total force applied to the water intake, which is composed by the force on the water intake and the surfaces force such as the pressure forces.

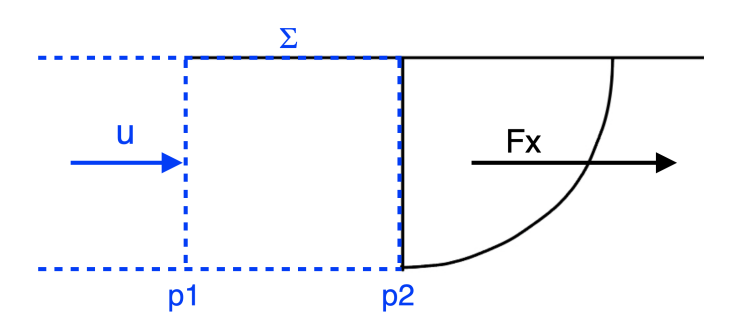


Figure 2.9: Control Volume

As we can see the calculation unfolds as follows:

$$F_x - p_1 A_1 + p_2 A_2 = -\rho u_1 A_1 + \rho u_2 A_2 \tag{2.33}$$

The section is supposed to remain constant in along the flow path since the water is supposed to be incompressible. The static pressure is  $p = p^{\circ} - \frac{1}{2}\rho u^2$  we can substitute in the previous equation obtaining:

$$F_x = p_1 - p_2 - \rho u_1 = -\rho u_1 + p_1^{\circ} - \frac{1}{2}\rho u_1^2 - p_2^{\circ} + \frac{1}{2}\rho u_2^2 = -\rho u_1 - \frac{1}{2}\rho u_1^2$$
 (2.34)

The speed of the water in 1 is equal to the speed of the plane. The water stops in the space of the intake and so the speed in 2 is zero in the reference system of the plane. The total pressure between 1 and 2 is conserved and so the result obtained is:

$$F_x = -\rho u_1 - \frac{1}{2}\rho u_1^2 \tag{2.35}$$

This is the drag of the water intake and so we sum it to the drag of the hull.

#### 2.8 Representation of the Matching Chart

For the very first drawing of the matching chart parameters are set as similar as possible to CL-415 in order to verify if the model gives plausible result. The matching chart, in terms of necessary specific power is shown in figure 2.10.

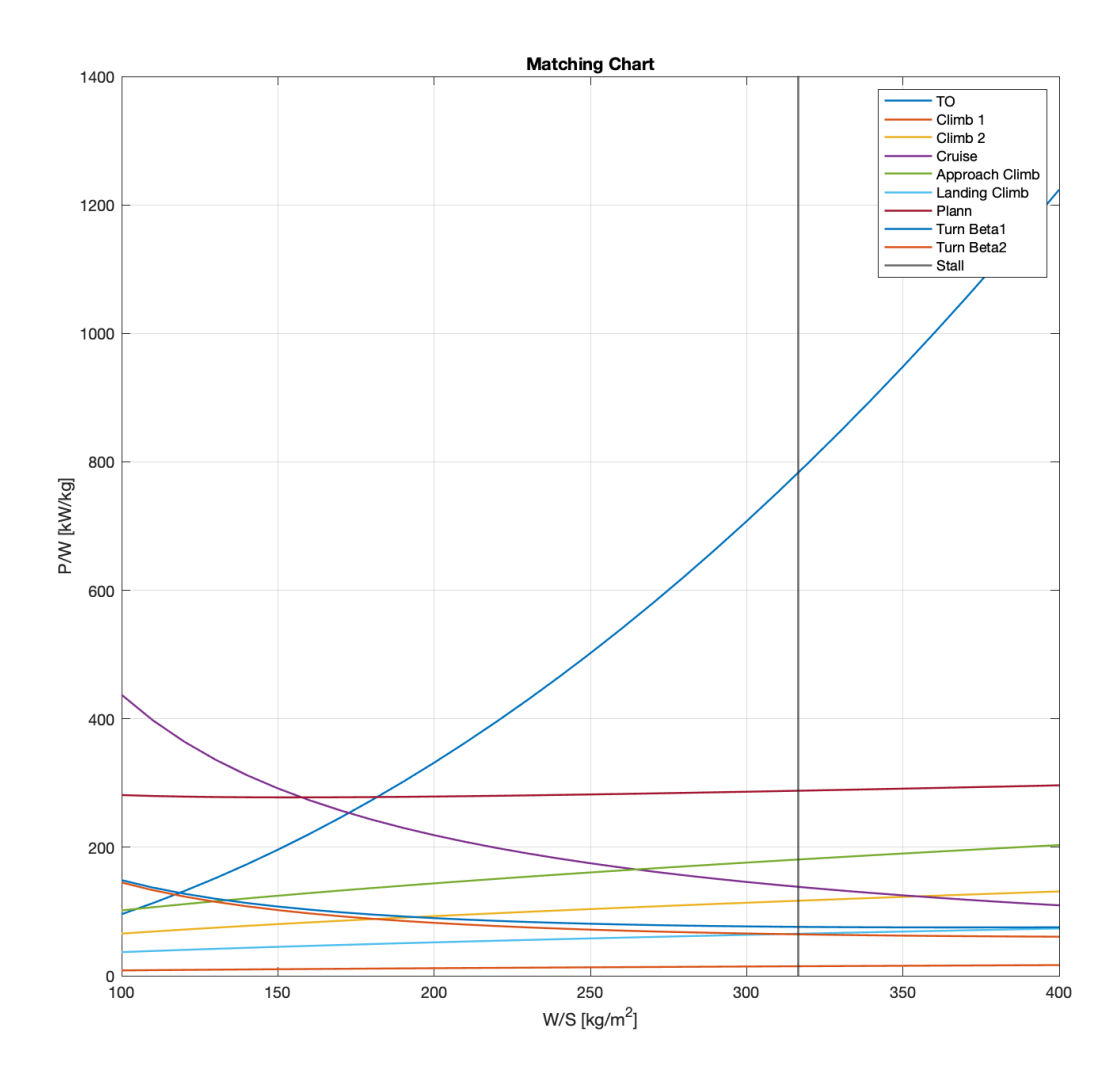


Figure 2.10: Specific Power Matching Chart

The matching chart in terms of specific thrust necessary is shown in figure 2.11.

As we can see in terms of specific thrust the refill maneuver is more incisive than in the case of specific power.

For now, the option which seem to be more feasible is the propeller. We can say that, in a certain way, the propeller is more indicated for low speed operations such as firefighting aircraft.

For now, we consider both the turboprop and the turbofan and wait to see later which one is the best.

#### 2.8.1 Results analysis

It is necessary to understand which are the parameters, regarding the refill maneuver, which have the worst effect on the necessary power or thrust. In fact big engines weight more and

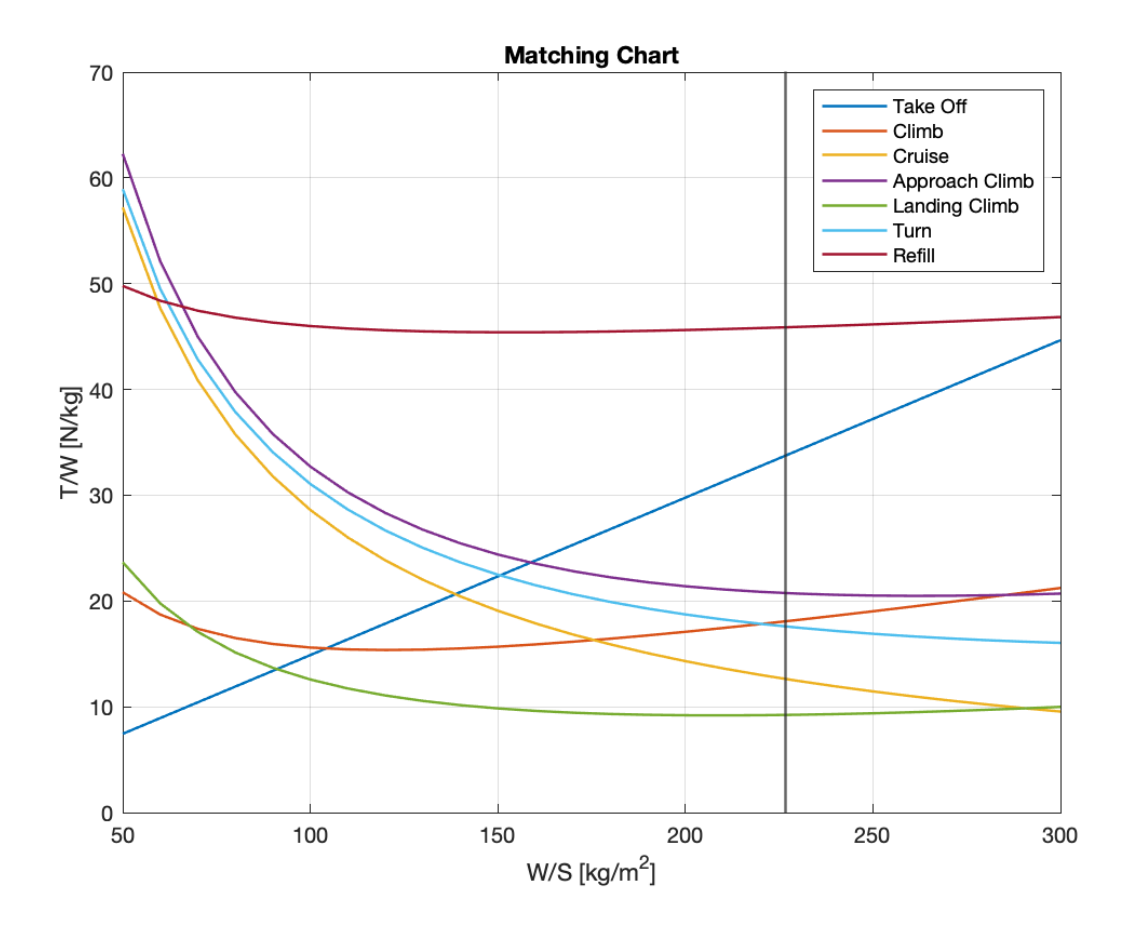


Figure 2.11: Specific Thrust Matching Chart

involve more quantity of fuel and so, again, weight. So its very important to keep the necessary specific power/thrust as small as possible for having a well functioning plane.

#### Effect of Deadrise angle

First of all lets see how the deadrise angle value affects the necessary specific power during the refill maneuver. The graph is shown in figure 2.12.

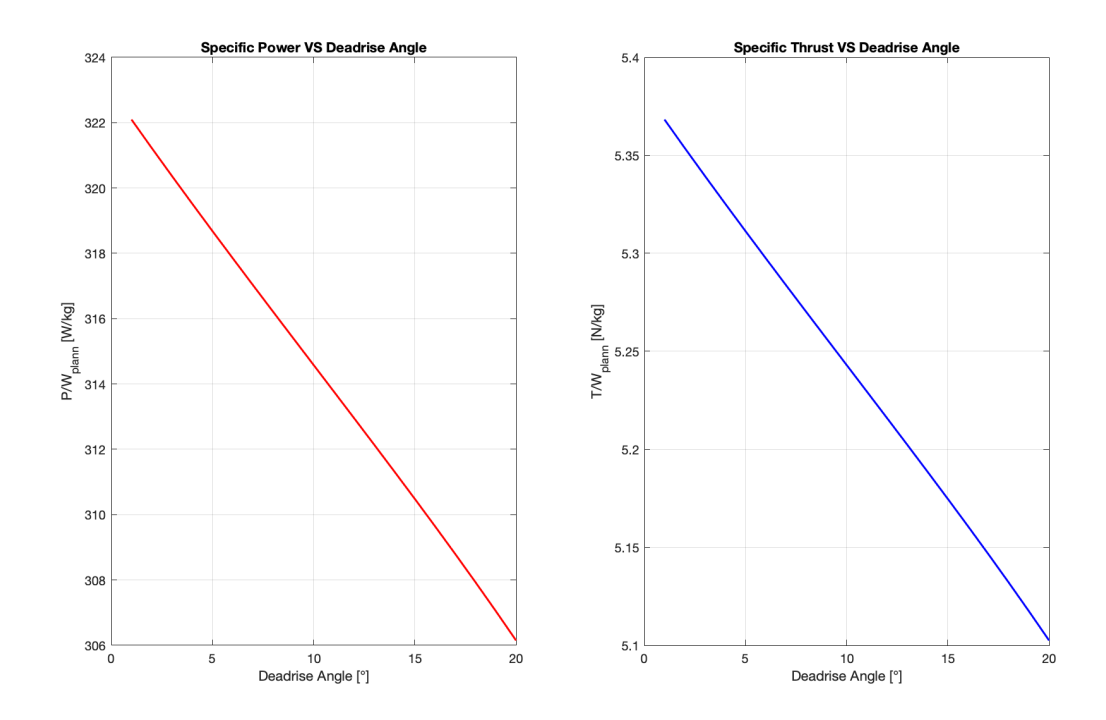


Figure 2.12

As we can see the amount of necessary power/thrust diminish with the deadrise angle, this is due to the model equation. The hull lift diminish with the deadrise angle because the effect of the deadrise guide the spray laterally. The hull drag decreases with the deadrise angle as we can see in figure 2.13 due to the formulation of the Hull Drag.

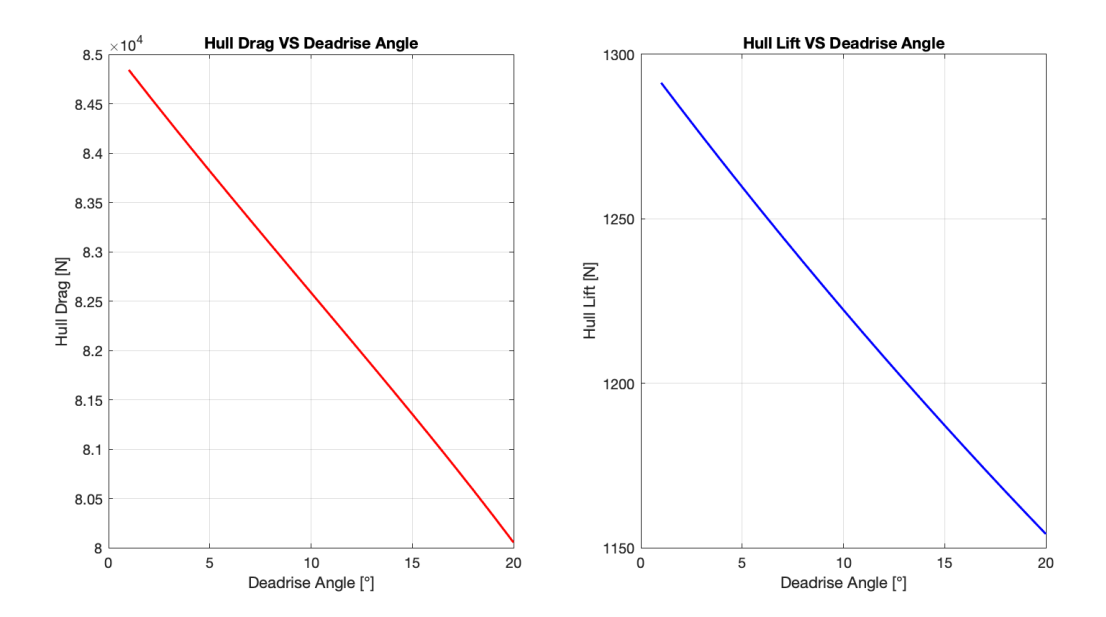


Figure 2.13

The reason why the necessary power/thrust decreases is because the drag diminish more than lift. For the deadrise angle we see that it can be a good design variable since we should keep as low as possible but considering the issue that this has with stability and refilling.

#### Effect of Trim Angle

The trim angle  $\tau$  is another interesting parameter to vary for a better understanding of the functioning of the model and the prediction of the future interaction with the whole aircraft.

The matching chart is represented at a trim of 4° and, while doing this kind of considerations, its necessary to take in to account three main aspects:

- Wing and Propeller clearance
- Refilling Port functioning
- · Cockpit visibility

Its important to specify that, since wings are attached to the hull, varying the trim angle has an influence on the  $C_L$  but, in this case we do not consider that because the purpose of this analysis is mainly to asses how the trim angle value affects the drag and the lift of the hull. In general, the refill phase will not take place in a extreme trim angle configuration, because of the water intake and visibility issue cited before.

The variation of necessary specific power/thrust with the trim angle is represented in figure 2.14

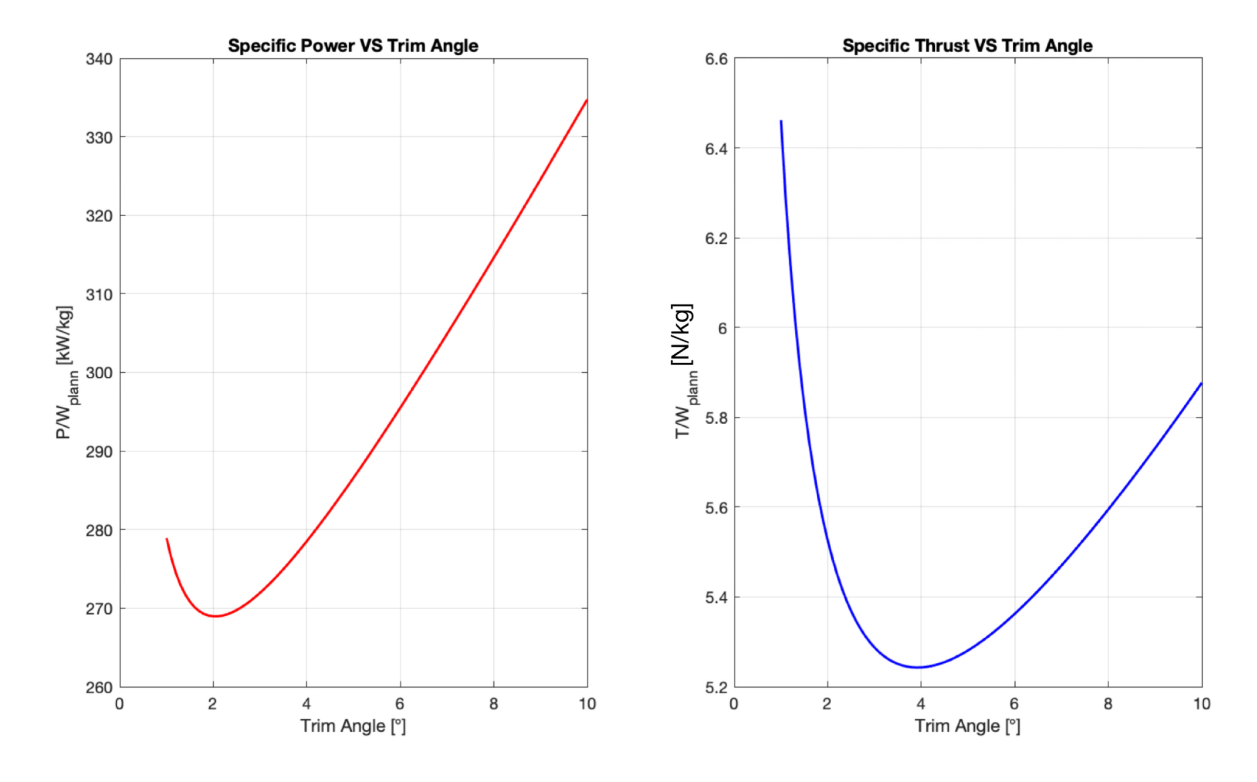


Figure 2.14

From the 2.14 we see clearly two minimum value of necessary specific Thrust and Power which occurs at a different trim angle. So What we see is that with a trim angle of  $4^{\circ}$  we minimize the  $\frac{T}{W}$  and with the value of  $2^{\circ}$  we minimize the  $\frac{P}{W}$ .

#### Effect of Vertical Depth of the trailing edge of the boat

The effect of the vertical depth of the trailing edge of the boat is represented in graph 2.15.

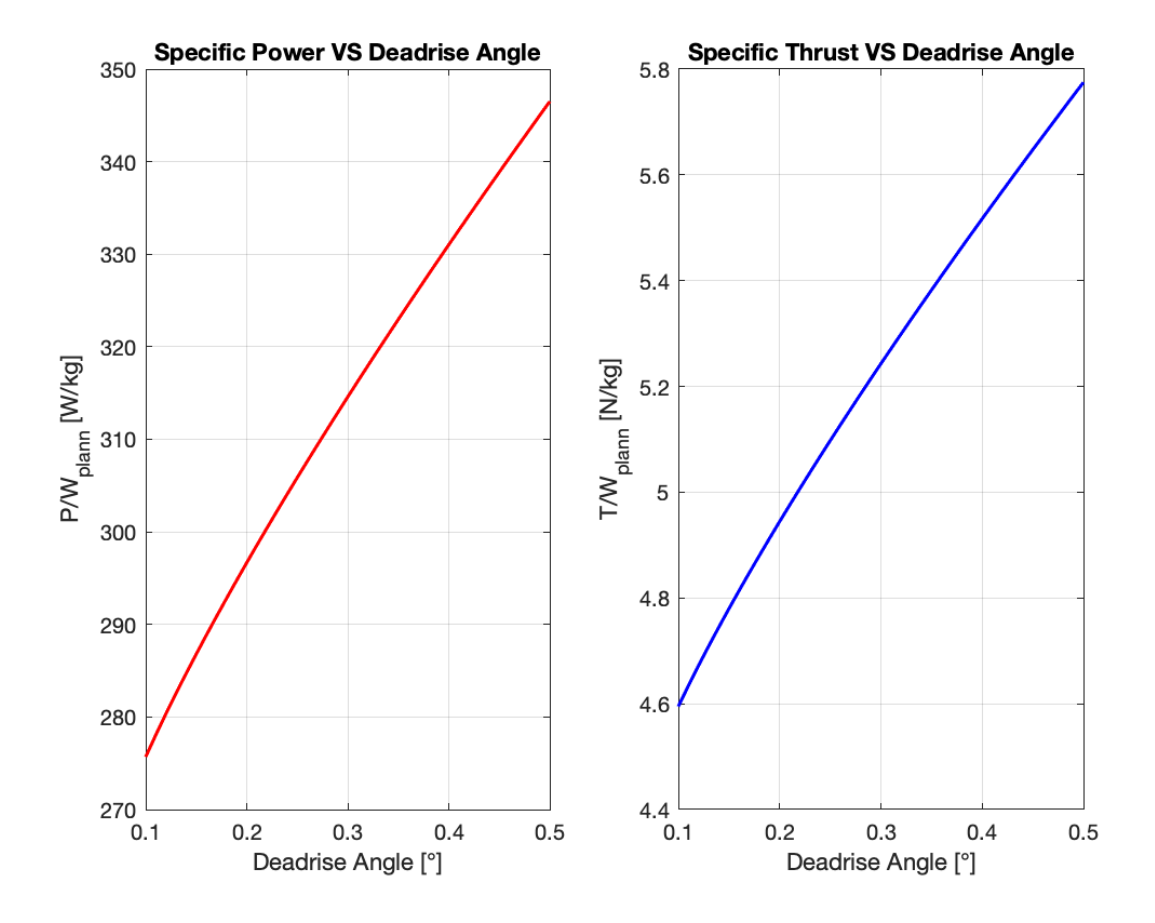


Figure 2.15

As we can see the more the trailing edge is deep inside the water the more the necessary power/thrust increases. That happens because of the big increasing of the drag. Also the lift is augmented by the vertical depth but less than the drag and this make the necessary power lots higher.

Also in this case the lower is the depth the lower the power but, for the functioning of the water intake a trade off is fundamental.

#### Effect of the beam of the planning surface

The beam of the planning surface is a very important parameter to consider because certainly it has an effect on the necessary power/thrust for the refill maneuver.

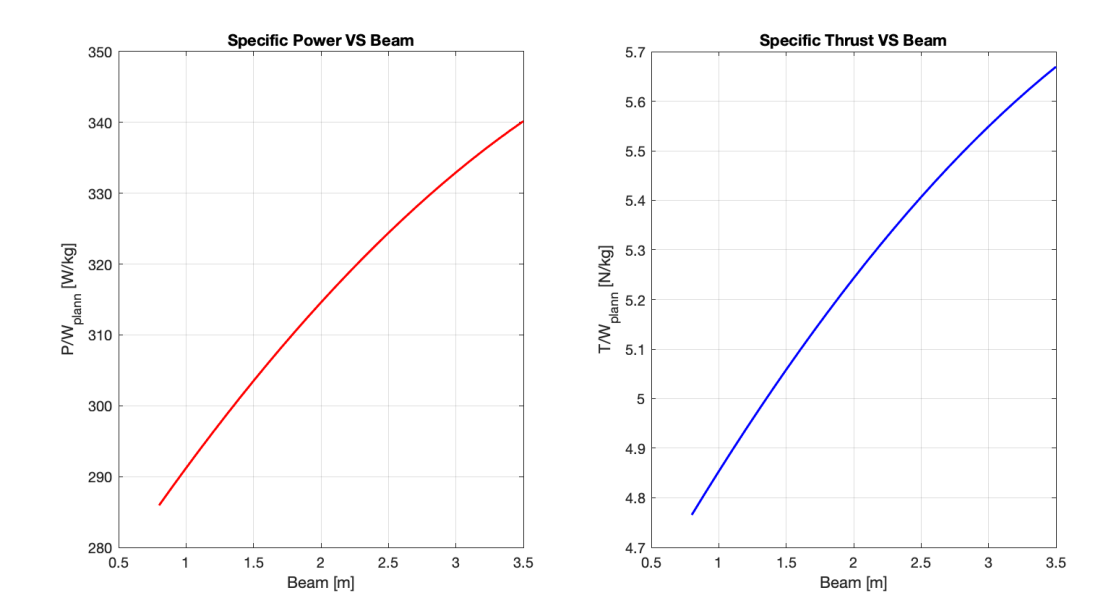


Figure 2.16

As we can see in figure 2.16 the necessary power/thrust, as expected, increases. We can find a reason in this observing that, despite an increased lift, big drag values bad affect the results.

# Chapter 3

# Weights

In this chapter the aim is to define strategies to evaluate the contribution of each component to the mass of the plane.

The aircraft mass is composed by three main parts:

$$MTOW = OEM + m_{fuel} + m_{payload} (3.1)$$

Regarding the  $m_{fuel}$  contribution it will be necessary to define a strategy for his evaluation. In this case  $m_{pay}$  is mostly represented by the mass of water/retardant stored in the tanks. For the OEM contribution there are several parts to evaluate:

- Principal structure components
- Secondary structures
- Propulsion
- Systems

# 3.1 Wing/Lifting System

The lifting system, which is part of the principal structure, is one of the most important part of the plane, the wing is what allows the plane to stay in the air, generate all the lift and allows to control the plane. In this particular case, introducing a box-wing type lifting system, to define the structural weight of the wing is a more complex task. What we can find is that there are different kind of methods.

The simplest method is empirically. Different textbook show different formulas. Raymer present a method based on the following formula:

$$\begin{cases}
W_{wing} = 0.93 \cdot I_w + 6.44 \cdot S + 390 & S \ge 900 f t^2 \\
W_{wing} = 4.24 \cdot I_w + 0.57 \cdot S & S \le 900 f t^2
\end{cases}$$
(3.2)

Where  $I_w$  is a geometrical parameter define as:

$$I_w = \frac{n_{ult} \cdot AR^{1.5} \left(\frac{W_{zf}}{W_{to}}\right)^{0.5} (1 + 2\lambda) \left(\frac{W}{S}\right)^{1.5} \cdot 10^{-6}}{\left(\frac{t}{c}\right) (\cos \Lambda_{25})^2 (1 + \lambda)}$$
(3.3)

Where:

- $n_{ult}$  is the ultimate load factor
- $AR = \frac{b^2}{S}$  is the wing aspect ratio

- $\frac{W_{sf}}{W_{to}}$  is  $\frac{OEW + PAYLOAD}{MTOW}$
- $\lambda$  is the taper ratio
- $\Lambda_{25}$  is the wing sweep at 25% of the chord
- $\frac{t}{c}$  is the thickness ratio of the wing

This geometrical parameters have a big impact on the wing weight and on the wing aerodynamics performance in terms of L/D.

The Torembeek approach is similar to the Raymer procedure but with a slightly different formulation that can be written in this approximate way:

$$\frac{W_{wing}}{W_g} = k_w b_s^{0.75} \{ 1 + \sqrt{\frac{b_{res}}{b_s}} \} n_{ult}^{0.55} \left( \frac{b_s/t_r}{W_g/S} \right)$$
(3.4)

Where:

- $k_w$  constant for the wing
- $b_s = b/\cos\Lambda_{25}$
- $t_r$  is the taper ratio
- $W_q = MTOW$

Both the method give an estimation on the wing structural weight based on data available. This is a problem for unconventional design as the one we are considering.

Another way to estimate the structural weight is to perform a FEM analysis. However, such an analysis requires knowledge of the internal arrangement of spars, ribs, and webs, and since we are in a very early design phase, this approach does not appear feasible.

In this work, we therefore choose to build a brand-new stick model in *MATLAB*, approximating the wing as a bi-dimensional beam embedded in three-dimensional space, subjecting it to the ultimate loads that the components are expected to carry, and computing the resulting internal actions. As stated above, a stick model is adopted to evaluate the wing's structural weight. Other approaches-such as simplified DoE-type models as described in [?] and [10]-do exist for the early design stage of box-wing configurations; nevertheless, these also require knowledge or credible estimates of the internal wing-box structure, and their integration within the Aerostate code would be nontrivial.

In the proposed formulation, the beam-stick model is described by nodes; although such methods can themselves be used within optimization loops, in our case the weight estimation must be as rapid as possible, providing a coarse (yet conservative) estimate of stress in each section and, more generally, of the quantity of metal required per section, without committing to a detailed placement of internal components. Certainly, methods like those mentioned above can be useful later in this project to refine the mass estimate of the wing structure and to support the detailed interior layout of ribs, spars, and panels.

#### 3.1.1 Stick model for wing weight calculation

Nodes are 1-D entities in the space described only with their coordinates, since we are looking for a stick model, the elements will be 2-Dimensional beam whose position and orientation in the space is described by two nodes. Each node in the space has 6 Degree of Freedom (from now DOF): three DOF describes the possibility for the node to translate in the space in the three direction and the others the possibility for the node to rotate in the space. Since two nodes describe a beam element each of them has twelve DOF.

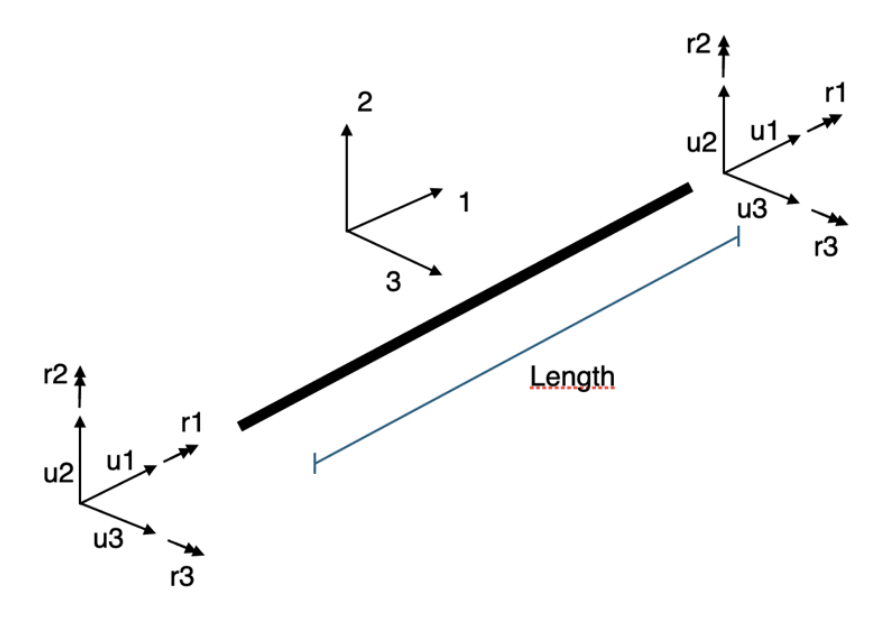


Figure 3.1: Beam Element

Its decided to divide the structure in equal-length elements in order to find a solution less affected as possible by discretizations errors.

Now the question is, once applying loads and constraints to this object how does it moves in the space?

For answering this question we need to solve the equation:

$${F} = [K] {x}$$
 (3.5)

Where  $\{F\}$  is the load vector, [K] is the stiffness matrix and  $\{x\}$  is the displacement vector. The load vector for a beam element is defined as:

$$\begin{cases}
F_{1_1} \\
F_{2_1} \\
F_{3_1} \\
M_{1_1} \\
M_{2_1} \\
M_{3_1} \\
F_{1_2} \\
F_{2_2} \\
F_{3_2} \\
M_{1_2} \\
M_{2_2} \\
M_{3_2}
\end{cases}$$
(3.6)

The displacement vector for a beam element is defined as:

$$\begin{cases}
 u_{1_1} \\
 u_{2_1} \\
 u_{3_1} \\
 r_{1_1} \\
 r_{2_1} \\
 r_{3_1} \\
 u_{1_2} \\
 u_{2_2} \\
 u_{3_2} \\
 r_{1_2} \\
 r_{2_2} \\
 r_{3_2}
\end{cases}$$
(3.7)

Where  $u_{i,j}$  represent the force applied on the j-node in the i-direction and  $r_{i,j}$  represent the torque applied on the j-node in the i-direction.

The stiffness matrix of a generic beam element is determined as follows:

$\int \frac{E \cdot A}{L}$	0	0	0	0	0	$-rac{E\cdot A}{L}$	0	0	0	0	0 ]
0	$rac{12EJ_3}{L^3}$	0	0	0	$rac{6EJ_3}{L^2}$	0	$rac{-12EJ_3}{L^3}$	0	0	0	$rac{6EJ_3}{L^2}$
0	0	$rac{12EJ_2}{L^3}$	0	$-rac{6EJ_2}{L^2}$	0	0	0	$-rac{12EJ_2}{L^3}$	0	$-rac{6EJ_2}{L^2}$	0
0	0	0	$\frac{GJ_1}{L}$	0	0	0	0	0	$-rac{GJ_1}{L}$	0	0
0	0	$-rac{6EJ_2}{L^2}$	0	$rac{4EJ_2}{L}$	0	0	0	$rac{6EJ_2}{L^2}$	0	$\frac{2EJ_2}{L}$	0
0	$rac{6EJ_3}{L^2}$	0	0	0	$\frac{4EJ_3}{L}$	0	$-rac{6EJ_3}{L^2}$	0	0	0	$\frac{2EJ_3}{L}$
$-\frac{EA}{L}$	0	0	0	0	0	$rac{EA}{L}$	0	0	0	0	0
0	$-rac{12EJ_3}{L^3}$	0	0	0	$-rac{6EJ_3}{L^2}$	0	$rac{12EJ_3}{L^3}$	0	0	0	$-rac{6EJ_3}{L^2}$
0	0	$-rac{12EJ_2}{L^3}$	0	$\frac{6EJ_2}{L^2}$	0	0	0	$rac{12EJ_2}{L^3}$	0	$rac{6EJ_2}{L^2}$	0
0	0	0	$-rac{GJ_1}{L}$	0	0	0	0	0	$rac{GJ_1}{L}$	0	0
0	0	$-rac{6E*J_2}{L^2}$	0	$\frac{2EJ_2}{L}$	0	0	0	$rac{6EJ_2}{L^2}$	0	$rac{4EJ_2}{L}$	0
0	$rac{6EJ_3}{L^2}$	0	0	0	$\frac{2EJ_3}{L}$	0	$-rac{6EJ_3}{L^2}$	0	0	0	$\frac{4EJ_3}{L}$

#### Where:

- $\bullet$  E is the Young Module and depends on the material
- A represent the surface of the section of the beam element
- L represent the length of the beam element
- $J_2, J_3$  are the beam moment of inertia in the bending directions and  $J_1$  is the polar moment of inertia of the section:  $J_1 = J_2 + J_3$

The core of this FEM-type calculation is to properly determine a stiffness matrix for the whole structure. Once defined the structure stiffness matrix we will use it to calculate the displacement of each node composing the structure and so the internal force characteristics (Shear and bending moment).

As we can see in figure 3.1 the reference system in which the stiffness matrix is defined is 123. This local reference system could be different between two adjacent elements as the force and displacements vectors could. So if we want to put together the matrix of each element in order to determine the matrix of the whole structure it is necessary to find a method for rotating each local reference system in to the general "XYZ" in which the coordinates of the nodes are expressed.

Rotation between 123 and XYZ For the rotation between the two reference system in the tri-dimensional space we will need to define the characteristics of "123" axis with respect to the "XYZ" system.

- Axis "1", the first basis vector of the "123" space, is the  $\tau$  vector which we can see in figure 3.2
- The "2" axis is, perpendicular with "1" and contained in to the "XY" plane
- The "3" vector can easily be found with the external product between "1" and "2"

So the first vector "1" components are:

$$\vec{\tau} = \{\tau_X, \tau_Y, \tau_Z\} \tag{3.8}$$

And are found as follows:

$$\vec{\tau} = \left\{ \begin{array}{c} \tau_X \\ \tau_Y \\ \tau_Z \end{array} \right\} = \left\{ \begin{array}{c} X_1 - X_2 \\ Y_1 - Y_2 \\ Z_1 - Z_2 \end{array} \right\} \tag{3.9}$$

And the unit vector  $\tau$ :

$$\hat{\tau} = \frac{\vec{\tau}}{|\tau|} \tag{3.10}$$

To find the second basis vector "2" its necessary to write the following system of equation which imposes:

- Perpendicularity with vector 1
- Parallelism with "XY" plane

Consider a vector with generic components:

$$\vec{2} = \{a, b, c\} \tag{3.11}$$

We impose the following conditions:

$$\begin{cases} \vec{1} \cdot \vec{2} = 0\\ \vec{2} \cdot n\vec{X}Y = 0 \end{cases}$$
 (3.12)

Where  $n_{XY} = \{0,0,1\}$  is the normal to the plane XY.

We obtain:

$$\begin{cases} \tau_X \cdot a + \tau_Y \cdot b = 0 \\ c = 0 \end{cases} \tag{3.13}$$

The solution to this system could be:

$$\vec{2} = \{ -\tau_Y, \tau_X, 0 \} \tag{3.14}$$

The third vector of the base is found with the external product between  $\vec{1}$  and  $\vec{2}$ .

$$\vec{3} = \vec{1} \times \vec{2} \tag{3.15}$$

Now, having the three orthonormal base for the "123" reference system we define the rotation matrix which bring us from global to local and its inverse, that in this case is equal to the transpose since the base is orthonormal as follows:

$$R = \begin{bmatrix} | & | & | \\ \vec{1} & \vec{2} & \vec{3} \\ | & | & | \end{bmatrix}$$

$$39$$

For our problem a  $3 \times 3$  matrix as R is not enough to explete the rotation. We define matrix T as the Kroneker product between R and  $I^{4\times 4}$  as follows:

$$T = R \otimes I^{4 \times 4} \tag{3.17}$$

$$T = \begin{bmatrix} R & 0 & 0 & 0 \\ 0 & R & 0 & 0 \\ 0 & 0 & R & 0 \\ 0 & 0 & 0 & R \end{bmatrix}$$

At this point the matrix K rotated in the global system is found as follows:

$$K_{glob} = T^{-1} \cdot K_{loc} \cdot T \tag{3.19}$$

For each element we can define a  $\vec{\tau}$  which is centered in the mean point of the element and goes from the first node towards the second on a element-parallel direction.

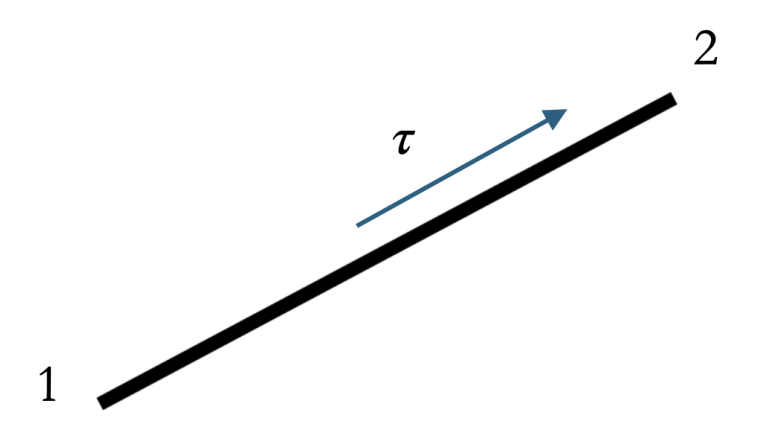


Figure 3.2:  $\tau$  vector

And for example:

$$F_{global} = T^{-1} \cdot F_{local} \tag{3.20}$$

$$F_{local} = T \cdot F_{qlobal} \tag{3.21}$$

Composing the stiffness matrix Having the stiffness matrix of each element expressed in the global reference system we can sum rows and columns acting on the same DOF with the method in figure 3.3. Since contiguous element share DOF we need to compose the stiffness matrix in the following way.

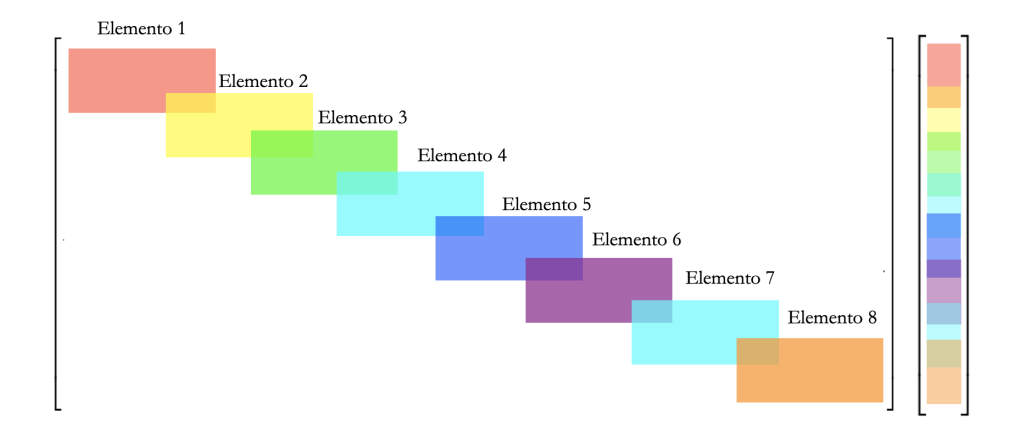


Figure 3.3: Construction of the stiffness matrix

As we can see the stiffness matrix is quite sparse because, with structures composed by large number of internal elements, there are just few elements around the diagonal. We can treat it as a sparse matrix on Matlab for making the computing more efficient.

**Loads and Constraints** For the computing its necessary to proper define the load vector. The load vector F is a column with a number of rows equal to the total number of Degree of Freedom of the structure. The force vector can be given in the global or in the local reference system. For the test case in which we consider the CSR-01 what we do is to compute the load to apply on each node of the structure in the "Z" dyrection.

We know the MTOW value for the CSR-01 which is about 77000 kg. In this procedure we apply to the wing the maximum load which is:

$$F_{maximum} = n_{ult} \cdot \frac{MTOW}{2} \tag{3.22}$$

Where  $n_{ult}$  is the ultimate load factor for the plane. For the CSR-01 the ultimate load factor is set to 2.5 but, for the new firefighter plane it may be reasonable to set a value of at least 3.5 since the maneuver which this kind of aircraft is supposed to face are more demanding. The MTOW value is divided by 2 because we consider just one wing at a time. Once computed the  $F_{maximum}$  value its needed to choose how to apply it on the structure. For the CSR-01 the choice is to divide equally the load fo each node composing the wing structure. The load for each node is found as follows:

$$F_{node} = \frac{F_{maximum}}{N_{nodes}} \tag{3.23}$$

Where  $N_{nodes}$  is the number of nodes contained in the wing structure.

For the firefighter plane the approach is pretty the same. From the AVL we will obtain a lift distribution but, in general, at this moment it does not seem to be bad to use a constant lift distribution.

For what concerns constraints, its possible to set the Degree of Freedom which are constrained and so removed from the stiffness equation which is computed just for the "free" Degree of Freedom. For the CSR-01 the constraint model set clamp on root section. For the firefighter box-wing aircraft we have two root section, one for the upper and one for the lower wing and so the choice is to set two clamps.

Compute of displacements Once computed the stiffness matrix and assigned loads and constraints in the proper way we can finally compute the displacements vector in the global reference system "XYZ". What we obtain solving the system is a vector which describes the displacement and rotation of all the nodes in the "XYZ" coordinates. This vector is useful in

order to represent the deformed wing, since it enough to sum the original position of each node with the corresponding displacement found in the " $U_{qlob}$ ".

The vector  $U_{glob}$  is not so useful in terms of the computation of the internal force characteristics for whose is necessary to transpose the displacement vector in all the "123" systems of each element. This operation is pretty simple since we already know the  $T_{glob2loc}$  matrix which can we use as follows:

$$U_{loc} = T_{glob2loc} \cdot U_{glob} \tag{3.24}$$

The local reference system allows us to make consideration about the deformation.

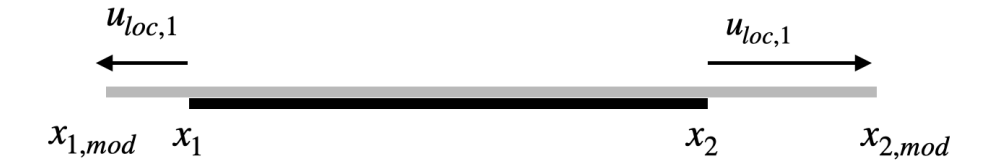


Figure 3.4: Deformation along the axis line

Along the axis of the beam we can evaluate the normal stress. In fact we can compute the elongation of each element:

$$\epsilon = x_{2,mod} - x_{1,mod} - (x_2 - x_1) = x_2 + u_{loc,2} - x_1 + u_{loc,1} - x_2 + x_1 = u_{loc_2} - u_{loc,1}$$
 (3.25)

So the normal characteristic is:

$$N = E \cdot \epsilon \tag{3.26}$$

and

$$\sigma_{xx} = \frac{N}{A} = \frac{k \cdot \epsilon}{A} \tag{3.27}$$

The vertical displacement:

$$\nu = U_{loc,2} \tag{3.28}$$

We talk about the displacement in the only Z direction because of the unique components, in our model, able to carry normal stress are the upper and lower panel and so, a bending moment around the "3" axis will have the effect of producing a normal stress in the spars which can not be taken in to account. Nevertheless the bending moment is negligible in that direction and is mostly around the "2" axes.

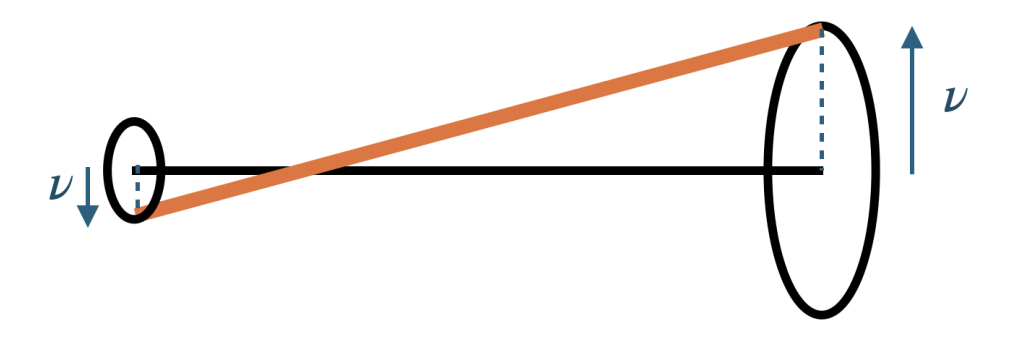


Figure 3.5: Displacement out of the axis line

Once computed the vertical displacement we can apply the equation of the elastic curve for compute the characteristic of bending moment and shear.

Deriving one time the vertical displacement allows to find the section rotation around axis "2" for the beam.

$$\phi = \frac{\partial \nu}{\partial x} \tag{3.29}$$

Deriving one more time we can find the bending momentum of every section of the wing.

$$M_y = J_2 E \cdot \frac{\partial^2 \nu}{\partial x^2} \tag{3.30}$$

Deriving one more time the bending momentum we find the shear module on every section.

$$T_y = \frac{\partial^3 \nu}{\partial x^3} \tag{3.31}$$

And, one more time, we can find the load on our structure

$$q = \frac{\partial^4 \nu}{\partial x^4} \tag{3.32}$$

Wing-Box modeling For the wing section it is decided to use a simplified scheme which we can see in 3.6.

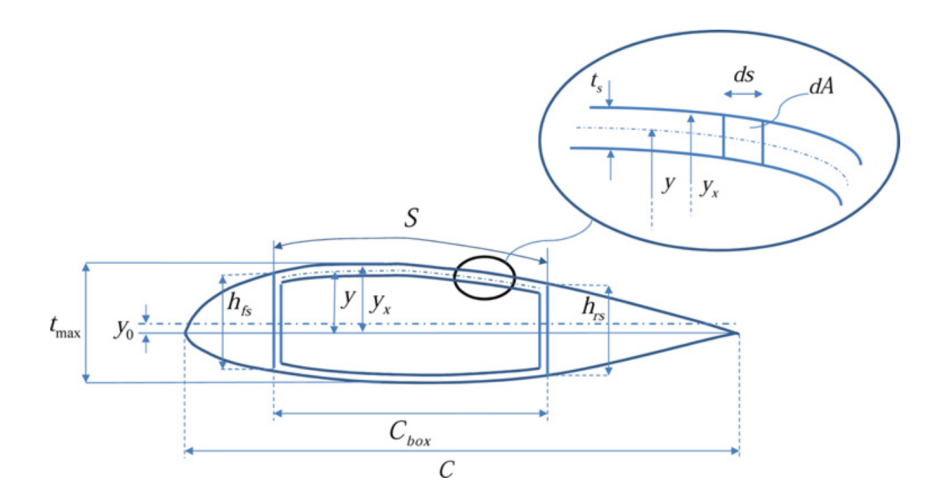


Figure 3.6: Wing Box

As we can see in figure 3.6 this model takes in to account only the center part of the wing box. The hypotesis are:

- Upper and lower panel carry normal stresses
- Front and Rear spar carry shear stresses

In the wing there are other structural components that in this case we don't consider since we use a model for which we see upper and lower panel as equivalent rectangular panels considering the Stringer and rivets part of the mass composing this component.

For the determination of the thickness of equivalent upper and lower panel we use the following formula:

$$\begin{cases} t_{s,u} = \frac{\frac{M}{\sigma_{max,u}}}{\eta_t t_{max} S_u} \\ t_{s,l} = \frac{\frac{M}{\sigma_{max,l}}}{\eta_t t_{max} S_l} \end{cases}$$

$$(3.33)$$

Where:

•  $\sigma_{max,u/l}$  is the maximum allowable stress for the specific material which can be found in [4], in the panel and depends on the task of the specific panel. For the lower panel, which is pulled, the maximum allowable is the strain stress for the material and, for the upper panel, which is compressed we may take in to account the buckling. The formula we use for the computing of the allowable is the following:

$$\sigma_{max,upper} = \min\left(\sigma_y, F\sqrt{\frac{M \cdot F}{\eta_t t_{max} C_{box} L}}\right)$$
(3.34)

Where F = 1.30 is the stiffened panel efficiency, M is the bending momentum, E is the young model of the material,  $t_{max}$  is the maximum thickness of the wing profile,  $C_{box}$  is the distance between the two spars and L is the ribs pitch.

•  $\eta_t$  is the effective distance between the two equivalent panel which is estimated by Torembeek and depends on the section maximum thickness and height of the front and rear spar

$$\eta_t = \frac{1}{3} \left( 1 + \left( \frac{h_{fs}}{t_{max}} \right)^2 + \left( \frac{h_{rs}}{t_{max}} \right)^2 \right) - 0.025$$
(3.35)

Pay attention to this formula because its expressed in imperial system.

•  $S_{u/l}$  are the length of the curve upper or lower panel

The model produces the following scheme:

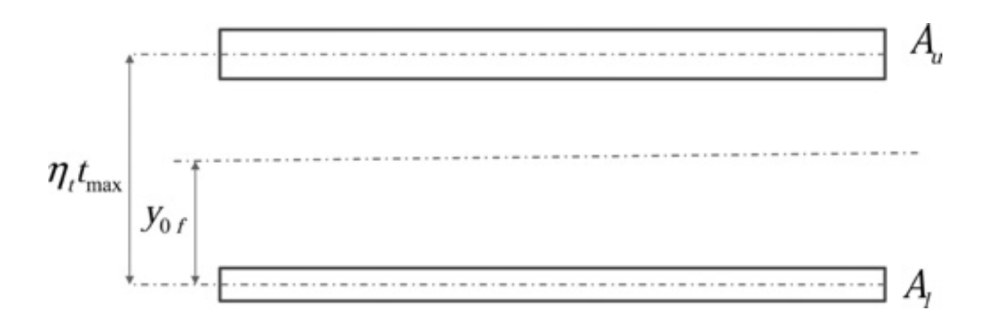


Figure 3.7: Equivalent Panel Model

We can, in a simple way, estimate the thickness of the front and rear spar. First of all we need to know the shear flux in the panels composing the wing box and, in particular, in the spars because of they are the unique element capable to carry shear stress.

The shear flux is due to the shear module and to the torsional moment acting on the beam section so:

$$q = q_{M_t} + q_T \tag{3.36}$$

The component of the shear flux due to torsional moment is found as follows:

$$q_{M_t} = \frac{M_t}{2 \cdot A_{hor}} \tag{3.37}$$

Where  $A_{box}$  is the surface enclosed within the panels. For the shear flux the formula used is the following:

$$\begin{cases} q_{T,f_s} = \frac{h_{f_s}}{\left(h_{f_s}^2 + h_{r_s}^2\right)} \cdot T \\ q_{T,r_s} = \frac{h_{r_s}}{\left(h_{f_s}^2 + h_{r_s}^2\right)} \cdot T \end{cases}$$
(3.38)

In this way we found the total shear flux in each spar and, with this we have:

$$t_{fs,rs} = \frac{q_{fs,rs}}{\tau_{max}} \tag{3.39}$$

**Determination of the weight** With this method what we are doing is:

- Computing the stiffness matrix
- Computing the load characteristics
- Computing the panel thickness

As we can clearly see in this procedure we need to know before the start the thickness of the panels composing the section for computing the stiffness matrix and, with this, the thickness so it chosen to use an iterative procedure represented in figure 3.8

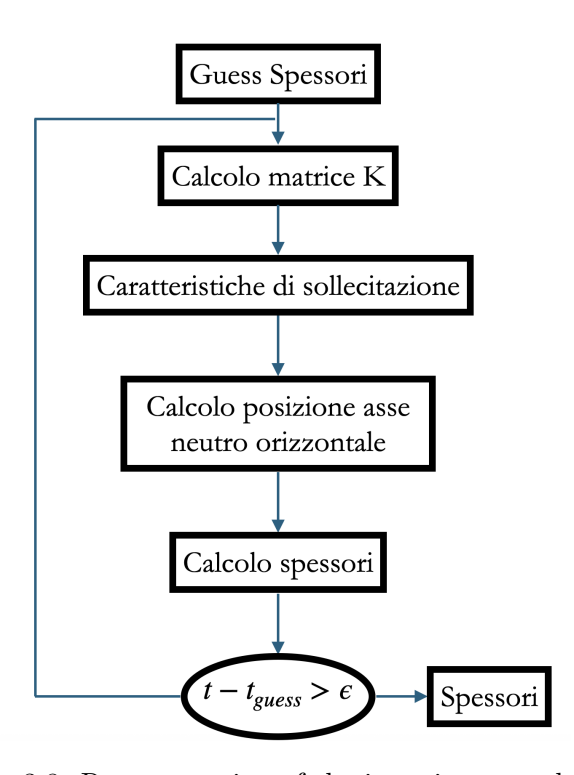


Figure 3.8: Representation of the iterative procedure

In this way, when the algorithm converge to a unique value, we find the thickness of the wing and, after this, computing the mass is a very easy task since we know the length and the area of the beam section.

#### 3.1.2 Wing structural mass results

For the very first comparison we consider the airbus a320 wing characteristic.

This wing characteristic are available online on the website [1], the plane considered is the CSR-01 alias Airbus a320.

The wing planform can be found on the website and is represented in figure 3.9. All the geometric characteristic of the wing are put in a .txt file which will be the input for the stick model Matlab code.

The input is given by tables where we indicate:

• Main section coordinates

- Connectivity between the various section
- Aerodynamic Profile
- Twist of the main sections which, is imposed to follow a linear trend
- The length of the element in which the structure is divided for computing
- Wing chord in the main section, which is imposed to follow a linear trend
- Thickness to Chord ratio of the main section which is imposed to follow a linear trend
- First Guess of the Thickness for the panels composing the load-bearing of the wing box
- MTOW value for the plane
- Material Characteristic such as: Young Module, Shear Module, Yeld stress and shear value for all the panels

The values have to be expressed with the international system.

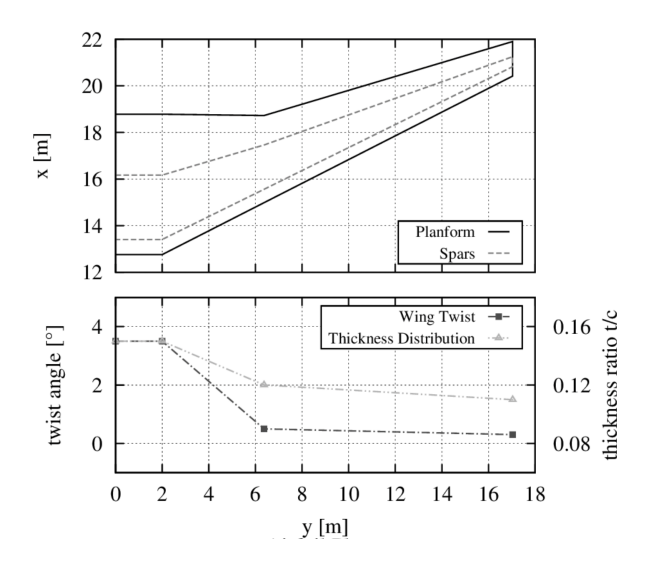


Figure 3.9: Airbus a320 wing planform and twist distribution

We can read the weight value of 8097 kg for the wing from the website. We need to be careful because this number is the sum of different contributes which are not taken in to account by the stick model Matlab code. Is possible to read all the contribution in figure 3.10.



Figure 3.10: Mass breakdown standard for CSR-01

Another way to compare the CSR-01 wing with the result of the stick model Matlab code is using the Raymer [12] formula to compute the wing weight. This procedure is very useful since there is the possibility to change the main aerodynamic/geometric parameters which are considered in the Raymer formula and compare the trends. Moreover the Raymer formula consider just the structural weight and ignores the other parts which affect the wing-mass breakdown of the CSR-01.

Convergence analysis As said before the wing sections are divided in a finite number of element with the same length defined in "input.txt". This number should not affect the result and so its important to do a convergence analysis.

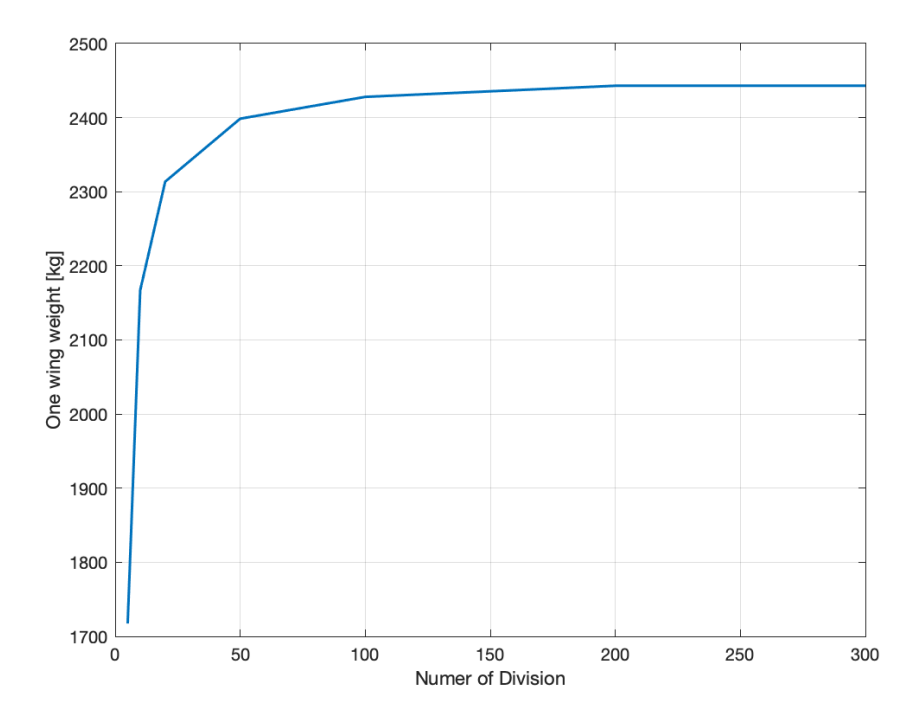


Figure 3.11: One Wing weight

As we can see in figure 3.11 the wing weight increases with the number of division since a structure composed of less elements is more rigid. Increasing the division number the weight increases and, over 200 division the weight converges at a value of little more than 2400 kg.

CSR-01 With the settings described in the previous paragraph the stick model produces the weight of: 2460 kg for one wing and so 4920 kg for the entire lifting system instead of the real value that we assume to be the one indicated on CSR-01 of 8097 kg with a difference of 35.5%. This difference is due to the different mass breakdown standard: The masses taken in to account by CSR-01 are represented in figure 3.10. The Matlab stick model compute only the mass necessary to carry the aircraft weight with the front and rear panel which are not supposed to carry any weight, considering the given material allowed stress.

To harmonize the two outcomes, we could consider trying to add two loads on the wing: the main gear, in the Airbus a320 is placed in to the wing structure, so, the gear support structure is located in the wing structure. Another load which is considered in the CSR-01 case is the pylon attachment who carries the engine and which is ignored by the stick model. For what concerns secondary structures which carries other component of the lifting system such as flaps and slats that we neglect in the stick model.

For a proper evaluation of this supplementary weight a method can be to add concentrated load where this systems such are placed for simulating the presence of an extra rib to carry on the shear flux. Nevertheless the value found on the CeRAS website is useful because gives, at a minimum, a validation of the order of magnitude of results.

**Raymer** On the Raymer textbook is presented an empirical method for the computing of the wing structural weight. The method is based on the following formula:

$$\begin{cases}
W_{wing} = 0.93 \cdot I_w + 6.44 \cdot S + 390 & S \ge 900 f t^2 \\
W_{wing} = 4.24 \cdot I_w + 0.57 \cdot S & S \le 900 f t^2
\end{cases}$$
(3.40)

Where S is the wing reference surface and  $I_w$  is a geometrical parameter which depends on the wing geometrical main characteristic as follows:

$$I_{w} = \frac{n_{ult} \cdot AR^{1.5} \left(\frac{W_{zf}}{W_{to}}\right)^{0.5} (1 + 2\lambda) \left(\frac{W}{S}\right)^{1.5} \cdot 10^{-6}}{\left(\frac{t}{c}\right) (\cos \Lambda_{25})^{2} (1 + \lambda)}$$
(3.41)

Where  $n_{ult}$  is the ultimate load factor set to 3.5, AR is the wing aspect ratio set to 9.48,  $\frac{W_{zf}}{MTOW}$  is the ratio between the Weight of the aircraft without fuel and MTOW,  $\lambda$  is the wing taper ratio and, for the a320 is set to 0.24,  $\frac{W}{S}$  is the wing load factor,  $\frac{t}{c}$  is the thickness to chord ratio of the wing section and its set to 12.64%,  $\Lambda_{25}$  is the sweep value at 25% of the wing chord and is set to 22°.

The result given by this method is 2314 kg which carries an error, with respect to the stick model, of 5.57%.

Since the model we've done is physic based, we expect it to follow quite the same trend of the Raymer formula.

Results analysis The sweep value surely affect the structural weight of the wing since it causes the coupling between shear and torsion. So increasing the Sweep value we expect the wing weight to increase. The trend obtained in shown in figure 3.12.

As we see in the figure the wing weight, as expected, increases with the sweep angle maintaining the same wingspan.

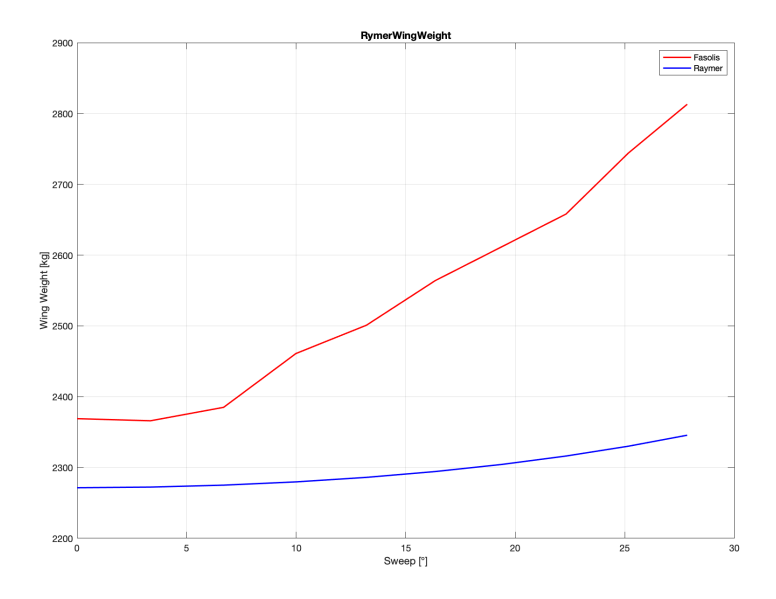


Figure 3.12: Wing weight variation with the Sweep Angle

## 3.2 Weight of the wing box computed with the stick model

For the very first trial with the box-wing we choose to set the same MTOW and wing-span of the CL-415 and try to compute how much is the wing weight. For now the lift is suppose to be 70% on the front wing and 30% on the rear one For what concerns the weight of the Box Wing we need to define the coordinate which describes the main section of the wing. In the very first phase what is done is to impose:

- Wing-Span "b"
- Height and Length of the vertical section of the wing.
- $\Lambda_{25}$  of the front wing
- $\Lambda_{25}$  of the rear wing
- $\Gamma$  of the front wing
- $\Gamma$  of the rear wing

With this parameter set all the section coordinates are completely defined. In the table below its possible to find all the set parameters:

Table 3.1: Geometric and structural parameters of the box-wing

Parameter	Value			
GEOMETRY				
Wingspan	14 m			
Vertical strut height	2 m			
Vertical strut length	2 m			
Front wing sweep angle (Lambda_front_wing)	20°			
Rear wing sweep angle (Lambda_rear_wing)	25°			
Front dihedral angle (Dihedral_front)	10°			
Rear dihedral angle (Dihedral_rear)	5°			
Division step size	0.03 m			
AERODYNAMIC SECTION				
Airfoil profile	NACA4611			
Profile assignment ID	1			
Twist angles at nodes	$3.6, 3.6, 0.25, 0.2^{\circ}$			
Guess thicknesses (Upper, Lower, Front Spar, Rear Spar)	0.04, 0.04, 0.04, 0.04 m			
Thickness-to-chord ratio	12, 12, 12, 12			
Chord lengths at nodes	4, 4, 4, 4 m			
MATERIAL				
Material	Aluminium			
Young's modulus	$6.9 \times 10^{10} \text{ Pa}$			
Shear modulus	$2.6 \times 10^{10} \text{ Pa}$			
Density	$2700 \text{ kg/m}^3$			
$\sigma_{ m max,\ Upper}$	$5.1 \times 10^{8} \text{ Pa}$			
$\sigma_{ m max,\ Lower}$	$5.1 \times 10^{8} \text{ Pa}$			
$ au_{ m max,\ Front\ Spar}$	$5.1 \times 10^{8} \text{ Pa}$			
$ au_{ m max,\ Rear\ Spar}$	$5.1 \times 10^{8} \text{ Pa}$			
LOAD				
Total aircraft weight	24000 kg			

The mass of the wing system with this input data gives 5823 kg as result.

Also in this case may be useful, for design purposes, to understand what influences the geometrical parameters of the wing have.

#### 3.2.1 Sweep and Dihedral

For geometrical consideration we can say that, changing the Sweep angle of the two wing affect the weight. For first we are changing the sweep of the front wing between 0 degree and 30 degree. In figure 3.13a we can appreciate how the weight of the entire wing system vary because of the variation of the sweep of the front wing. We can see that the weight of the wing have a maximum at  $5^{\circ}$ . In figure 3.13b we see the deformation of the wing. The sweep of the front wing affect the geometry of the wing system itself because of the wing main section coordinates are built in the following way: Starting in the [0,0,0] point we find the second one adding the front wing, then the vertical piece is added knowing his height and length and then, from the second point the third is found by adding the rear wing. In this way, without knowing the position of the two wing roots the wing is fully defined but, varying parameters like sweep or dihedral vary the position of the wing root.

Coordinates are shown in table below:

$$\mathbf{Wing} = \begin{bmatrix} 0 & 0 & 0 \\ b & b\tan(\Lambda_{\mathrm{front}}) & b\tan(\Gamma_{\mathrm{front}}) \\ b & b\tan(\Lambda_{\mathrm{front}}) + r & b\tan(\Gamma_{\mathrm{front}}) + h \\ 0 & b\tan(\Lambda_{\mathrm{front}}) + r + b\tan(\Lambda_{\mathrm{rear}}) & b\tan(\Gamma_{\mathrm{front}}) + h + b\tan(\Gamma_{\mathrm{rear}}) \end{bmatrix}$$

Where "r" is the length of the vertical part and "h" is the height.

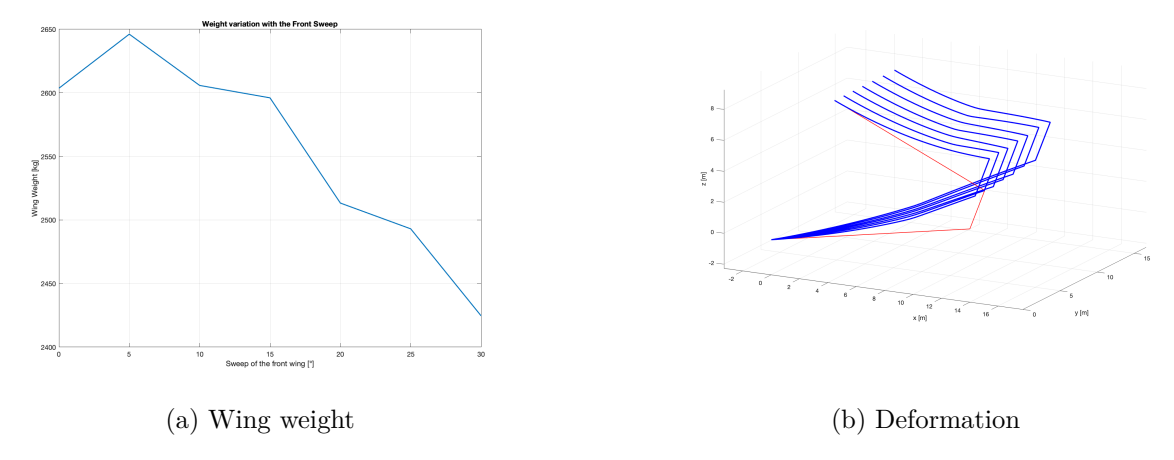


Figure 3.13: Variation of the front sweep

In the same way we can evaluate the impact of the sweep of the rear wing whose weight its represented in figure 3.14a and its deformation in figure 3.14b. As we can see the weight of the wing with the rear sweep increases. This is an interesting point since the two sweeps seems to have opposite behavior and so we may take advantage, in terms of weight of the wing structure keeping the rear sweep as little as possible and the front sweep as big as possible. This preliminary considerations doesn't consider aerodynamics aspects.

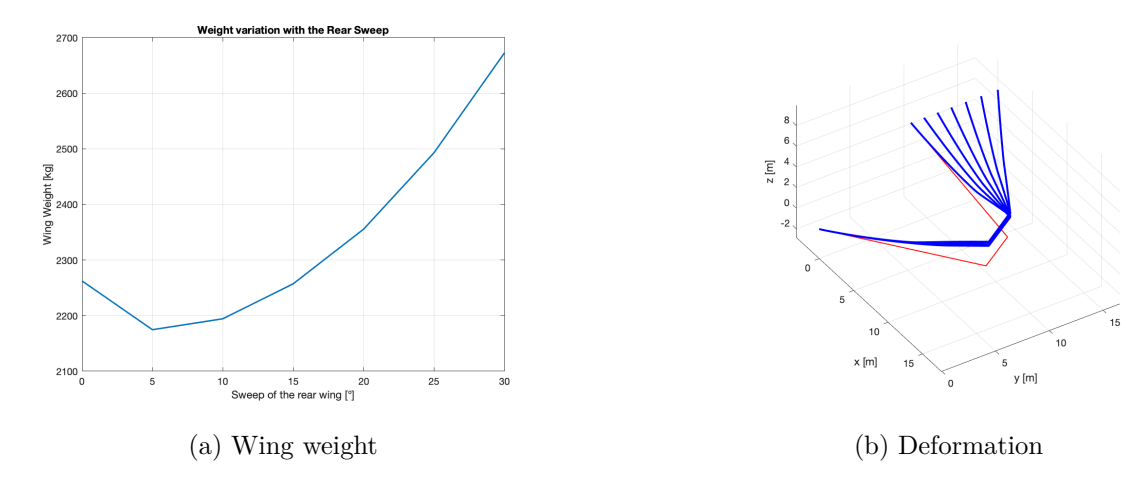


Figure 3.14: Variation of the rear sweep

The same proof can be done varying the dihedral of the front and rear wing plotting the results.

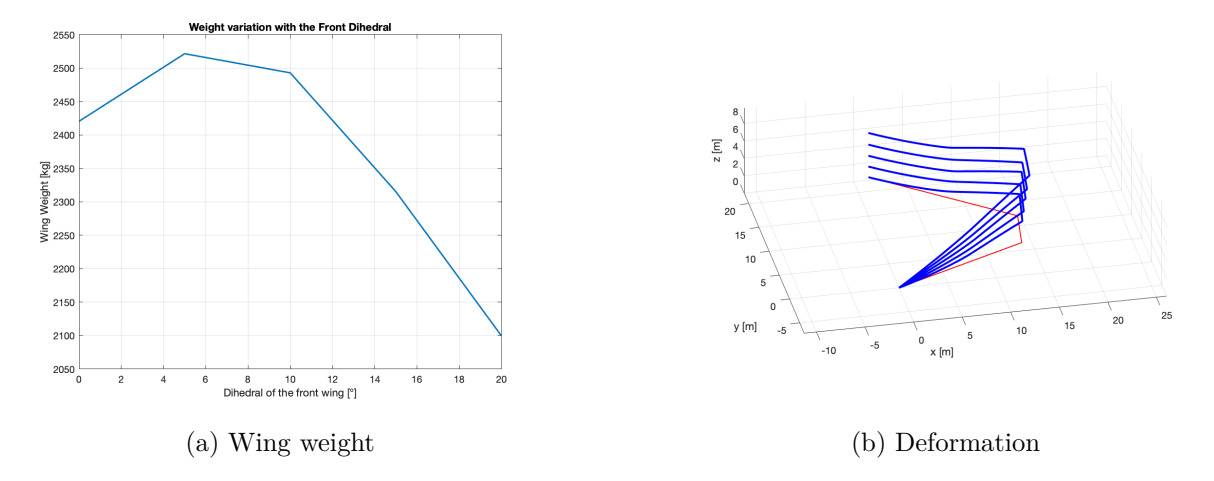


Figure 3.15: Variation of the front dihedral

For what concerns the rear dihedral of the wing the method is the same and the results are plot in figure 3.16a

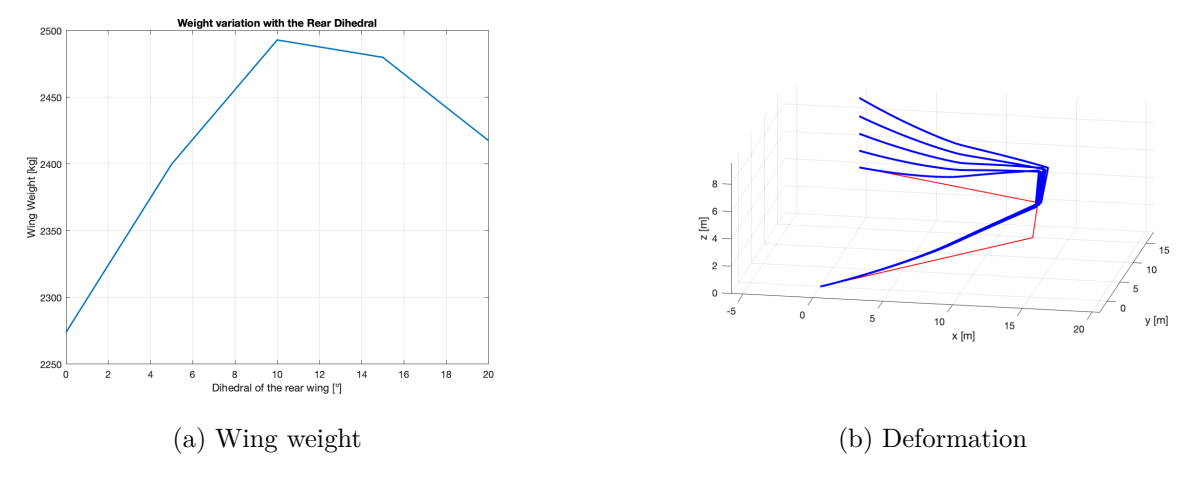


Figure 3.16: Variation of the rear dihedral

As we can see for the dihedral for both the wing we find a maximum value for the weight at two different value which is, lower for the front wing (more or less 5 deg) and higher for the rear wing (more or less 10 deg). We may expect that the value of minimum weight will be found at low values of dihedral for the rear wing and high for the front.

For investigating this phenomena its chosen to do a combined analysis between the two angles:

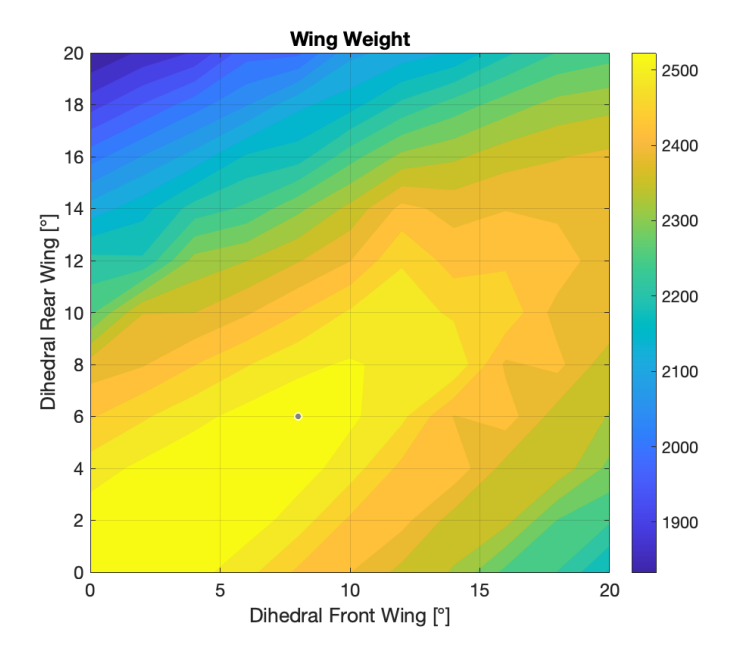


Figure 3.17: Dihedral for the front and the rear wing

## 3.3 Other weights

For what concerns the weight other components its chosen to use an empirical method found on the Raymer [12] textbook. Formulas for all the components are indicated in table 3.2.

Component	Variable	Formula
Fuselage	W_fuselage	$0.3280 K_{\text{door}} K_{Lg} (W_{dg} N_z)^{0.5} L^{0.25} S_f^{0.302} (1 +$
		$\left(K_{ws}\right)^{0.04} \left(\frac{L}{D}\right)^{0.10}$
Main Landing Gear	W_main_landing	$0.0106 K_{mp} W_i^{0.888} N_l^{0.25} L_m^{0.4} N_{mw}^{0.321} N_{mss}^{-0.5} V_{\text{stall}}^{0.1}$
Nose Landing Gear	W_nose_landing	$0.032 K_{np} W_i^{0.646} N_l^{0.2} L_n^{0.5} N_{nw}^{0.45}$
Nacelle Group	W_nacelle	$0.6724 K_{ng} N_{Lt}^{0.10} N_w^{0.294} N_z^{0.119} W_{ec}^{0.611} N_{en}^{0.984} S_n^{0.224}$
Engine Controls	W_engine_controls	$5.0 N_{en} + 0.80 L_{ec}$
Starter	W_starter	$49.19 \left(\frac{N_{en}W_{en}}{1000}\right)^{0.541}$
Fuel System	W_fuel	$2.405 V_t^{0.606} \left(1 + \frac{V_i}{V_t}\right)^{-1.0} \left(1 + \frac{V_p}{V_t}\right) N_t^{0.5}$
Flight Controls	W_flight_controls	$2.405 V_t^{0.606} \left(1 + \frac{V_i}{V_t}\right)^{-1.0} \left(1 + \frac{V_p}{V_t}\right) N_t^{0.5}$ $145.9 N_f^{0.554} \left(1 + \frac{N_m}{N_f}\right)^{-1.0} S_{cs}^{0.20} (I_y \cdot 10^{-6})^{0.07}$
APU Installed	W_APU_installed	$2.2W_{ m APU~uninstalled}$
Instruments	W_instruments	$4.509 K_t K_{tp} N_c^{0.541} N_{en} (L_f + B_w)^{0.5}$
Hydraulics	W_hydraulics	$0.2673 N_f (L_f + B_w)^{0.937}$
Electrical	W_electrical	$7.291 R_{kva}^{0.782} L_a^{0.346} N_{gen}^{0.10}$
Avionics	W_avionics	$1.73  W_{uav}^{0.983}$
Furnishings	W_furnishings	$0.0577 N_c^{0.1} W_c^{0.393} S_f^{0.75}$
Air Conditioning	W_air	$62.36 N_p^{0.25} \left(\frac{V_{pr}}{1000}\right)^{0.604} W_{uav}^{0.10}$
Anti-Ice System	W_anti_ice	$0.002W_{dg}$
Handling Gear	W_handling	$3.0 \times 10^{-4} W_{dg}$
Military Cargo Handling System	W_military_cargo	$2.4 \times (\text{cargo floor area, ft}^2)$

Table 3.2: Weight estimation formulas for aircraft components imperial system

The empirical constants are represented in the table below with the relative values used for the computation of the mass of the water bomber box-wing aircraft.

Symbol	Description
$B_w = 14m$	Wing span, ft
D = 2.59m	Fuselage structural depth, ft
$D_e = ?$	Engine diameter, ft
$F_w = ?$	Fuselage width at horizontal tail intersection, ft
$H_t = ?$	Horizontal tail height above fuselage, ft
$H_t/H_v=1$	0.0 for conventional tail; 1.0 for "T" tail
$H_v = ?$	Vertical tail height above fuselage, ft
$I_y = ?$	Yawing moment of inertia, lb · ft <sup>2</sup>
$K_{cb} = 2.25$	2.25 for cross-beam (F-111) gear; 1.0 otherwise
$K_d = ?$	Duct constant
$K_{door} = 1.06$	See values based on door config.
$K_{dw} = 1.0$	0.768 for delta wing; 1.0 otherwise
$K_{dwf} = 1$	0.774 for delta wing aircraft; 1.0 otherwise
$K_{Lg} = 1.12$	1.12 if fuselage-mounted main landing gear; 1.0 otherwise
$K_{mc}$	1.45 if mission completion required; 1.0 otherwise
$K_{mp}$	1.126 for kneeling gear; 1.0 otherwise
$K_{ng}$	1.017 for pylon-mounted nacelle; 1.0 otherwise

Symbol	Description
$K_{np}$	1.15 for kneeling gear; 1.0 otherwise
$K_p$	1.4 for engine with propeller or 1.0 otherwise

$K_r = 1$	1.133 if reciprocating engine; 1.0 otherwise
$K_{rht} = 1$	1.047 for rolling tail; 1.0 otherwise
$K_t = 0.739$	0.793 if turboprop; 1.0 otherwise
$K_{tp} = 0.826$	0.826 for tripod gear; 1.0 otherwise
$K_{tr}=1$	1.18 for jet with thrust reverser or 1.0 otherwise
$K_{uht} = 1$	1.143 for full-moving horizontal tail; 1.0 otherwise
$K_{vg}=1$	1.62 for variable geometry; 1.0 otherwise
$K_{ws} = 1$	1.19 for variable sweep wing; 1.0 otherwise
$K_{vsh} = 1$	1.425 if variable sweep wing; 1.0 otherwise s
$K_{ws,formula}$	$0.75(1+2\Lambda)/(1+\Lambda)(B_w \tan \Lambda/L)$
$K_y = 0.33 \cdot 1$	Pitching radius of gyration, ft ( $\approx 0.3L$ )
$K_z = L_t = ?$	Yawing radius of gyration, ft ( $\approx L_t$ )
L = 19.89m	Fuselage structural length, ft
$L_a = ?$	Electrical routing length
$L_d = ?$	Duct length, ft
$L_e = ?$	Length from engine front to cockpit
$L_f = ?$	Tail length, ft

Symbol	Description
$L_m = ?$	Length of main landing gear, in
$L_n = ?$	Nose gear length, in
$L_s = ?$	Single duct length
$L_{sh} = ?$	Engine shroud length, ft
$L_t = ?$	Tail length (quarter-MAC to quarter-MAC), ft
$L_{tp} = ?$	Tailpipe length, ft
M = 0.4	Mach number
$N_c = 3$	Number of crew
$N_{ci}=2$	1.0 if single pilot; 1.2 w/ backseater; 2.0 with copilot
$N_{en}=2$	Number of engines
$N_f = ?$	Number of functions performed by controls
$N_{gen} = ?$	Number of generators (typically = $N_{en} = 2$ )
$N_l = 7$	Ultimate landing load factor = $N_{gear} \times 1.5$
$N_{Lt} = ?$	Nacelle length, ft
$N_m = ?$	Number of mechanical functions (0-2)
$N_{mss} = ?$	Number of main gear shock struts
$N_{mw}$	Number of main wheels
$N_{nw}$	Number of nose wheels
$N_p$	Number of personnel onboard (crew and pax)
$N_s$	Number of flight control systems

Symbol	Description
$N_t$	Number of fuel tanks
$N_u$	Number of hydraulic utility functions
$N_w$	Nacelle width, ft
$N_z$	Ultimate load factor (= $1.5 \times$ limit load)
q	Dynamic pressure at cruise, lb/ft <sup>2</sup>
$R_{kva}$	System electrical rating (kV · A)
$S_{cs}$	Control surface area, ft <sup>2</sup>
$S_{csw}$	Wing-mounted control area, ft <sup>2</sup>
$S_e$	Elevator area, ft

$S_f$	Fuselage wetted area, ft <sup>2</sup>	
$S_{fw}$	Firewall surface area, ft <sup>2</sup>	
$S_{ht}$	Horizontal tail area	
$S_n$	Nacelle wetted area, ft <sup>2</sup>	
$S_r$	Rudder area, ft <sup>2</sup>	
$S_v$	Vertical tail area, ft <sup>2</sup>	
$S_w$	Trapezoidal wing area, ft <sup>2</sup>	
$\mathbf{SFC}$	Engine specific fuel consumption	
T	Total engine thrust, lb	
$T_e$	Thrust per engine, lb	
$V_i, V_p, V_t$	Fuel volumes (integral, protected, total), gal	
$V_{pr}$	Volume of pressurized section, ft <sup>3</sup>	
W	Fuselage structural width, ft	
$W_c$	Maximum cargo weight, lb	
$W_{dg}$	Design gross weight, lb	
$W_{ec}$	Engine + contents weight, lb	
$W_{en}$	Engine weight (each), lb	
$W_{fw}$	Fuel weight in wing, lb	
$W_l$	Landing design gross weight, lb	
$W_{press}$	Pressurization weight penalty	
$W_{uav}$	Uninstalled avionics weight, lb	
Λ	Wing sweep at 25% MAC	

With this method we obtain a value for the mass of all the component except for the wing which we evaluating with the stick model.

## 3.4 Fuel weight

For the fuel weight estimation, a simulation-based approach was adopted. To simulate the mission is not the unique approach possible. For example we could have estimated the consumption of fuel empirically in some flight segment and with the Breguet formula in others. In this case, having a firefighter aircraft, is really not convenient to use empirical solution since the mission is no like other cargo airplanes.

#### 3.4.1 Airspeed

The IAS value is the Indicate Air Speed value indicated by the instruments. For finding the TAS value (i.e. Thrue Air Speed) which is the speed measured by an external observer steady on the ground in calm air condition we need to do some correction due both to the variation of the static pressure and temperature with the altitude and to the compressibility effects affecting this value at high speed.

From the IAS value is possible to find the EAS value(i.e. Equivalent Air Speed) with the following formula:

$$EAS = \sqrt{2\frac{a^2}{\gamma_{air} - 1} \left(\frac{\rho}{\rho_0}\right) \left(\left(\frac{p_t}{p}\right)^{\frac{\gamma_{air} - 1}{\gamma_{air}}} - 1\right)}$$
(3.43)

Where  $a = \sqrt{\gamma RT}$  is the speed of the sound at the current flight level,  $\rho$  and  $\rho_0$  are the air density at flight level and sea level.  $\gamma_{air}$  is the ratio between specific heat value. The total pressure  $p_t$  is computed with the IAS value:

$$p_t = p + \frac{1}{2}\rho \cdot IAS^2 \tag{3.44}$$

To find the TAS value, which is used for the power evaluation, we use the following formula:

$$TAS = EAS\sqrt{\frac{\rho_0}{\rho}} \tag{3.45}$$

#### 3.4.2 Design-mission

For the simulative approach its firstly necessary to define which is the design-mission on which the simulation has to take place. We expect the typical mission of this aircraft to be as follows:

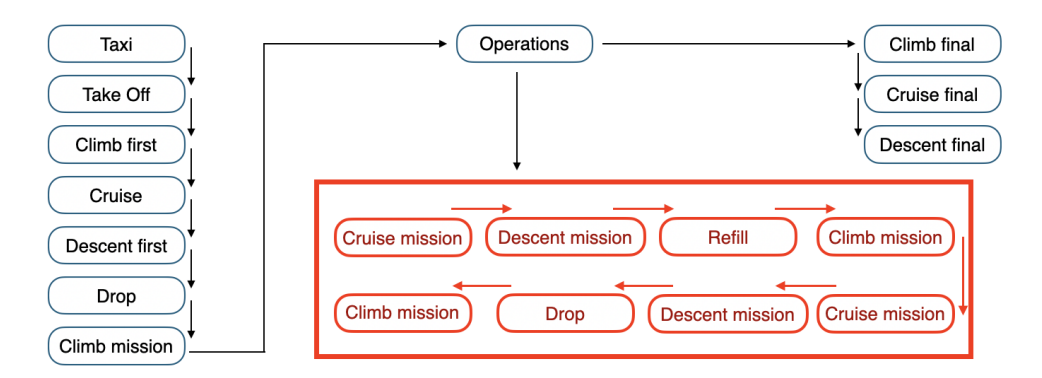


Figure 3.18: Mission

As we can see in figure 3.18 the mission is composed by the "black" part and the "red" one. The reason why the mission has been divided in this two section is because of the "red" one is repeated "n" times and the "black" one is just one time per flight. The first issue is to define the each mission part.

#### 3.4.3 Simulation of the mission

To simulate the mission consist of imposing the forces equilibrium on the airplane in every phase of the flight for computing the power which the engine is delivering and, knowing the Specific Thrust/Power Fuel consumption of the aircraft, mass of fuel burned for each time interval.

For what concerns the refilling and the emptying of the water tanks what is done for simulation purposes is to instantly sum or subtract the full weight of the water from the mass of the plane so, when computing the fuel consumption its necessary to consider that the initial weight of the aircraft is gross.

The general equation is basically the second Newton law:

$$\Sigma \vec{F}(t) = m(t) \cdot \ddot{x}(t) \tag{3.46}$$

And the power delivered by the engine can be written as follows since we impose the accelerations on the system to be equal to 0 and so:

$$\Sigma \vec{F}(t) = \vec{0} \tag{3.47}$$

Imposing the trajectory to be fully contained in plane x-z in general we obtain:

$$\begin{cases} \Sigma F_x(t) = \vec{0} \\ \Sigma F_z(t) = \vec{0} \end{cases}$$
 (3.48)

In flight conditions the equations become as follows:

$$\begin{cases}
L = W \cdot \cos \gamma \\
T = W \cdot \sin \gamma + D
\end{cases}$$
(3.49)

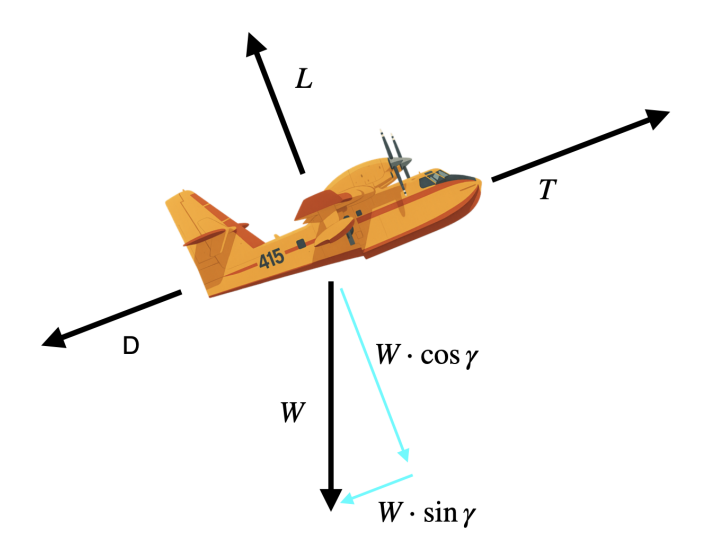


Figure 3.19: Forces equilibrium

Rewriting the forces:

$$\begin{cases}
C_L = \frac{2\frac{W\cos\gamma}{S}}{\frac{S}{\rho V^2}} \\
T \cdot V = P_{fly} = V \cdot W\sin\gamma + \frac{1}{2}\rho V^3 S\left(C_{D0} + \frac{C_L^2}{\pi\lambda e}\right)
\end{cases}$$
(3.50)

In this way, knowing all this data we can compute the power delivered by the engine and so the fuel consumption per time unit as follows:

$$\dot{W} = k_p \cdot P_{fly} \tag{3.51}$$

And so, knowing the value of the initial weight we can integrate the last equation obtaining:

$$W\left(t\right) = W_0 - \dot{W}dt\tag{3.52}$$

Notice that even if the  $P_{fly}$  value becomes negative, meaning for example that the ramp value is to negative and that the propeller has become passive, the fuel level onboard can't in any case rise but, at least, remain constant. With the same value we can compute the motion:

$$V(t) = \frac{\partial s}{\partial t} \tag{3.53}$$

$$\begin{cases} x(t) = s \cdot \cos \gamma = (s_0 + \dot{s} \cdot dt) \cdot \cos \gamma \\ z(t) = s \cdot \cos \gamma = (s_0 + \dot{s} \cdot dt) \cdot \sin \gamma \end{cases}$$
(3.54)

This method is useful but not in all the flight phases. When the plane is on ground its necessary to compute the component of the weight acting on the landing gears and on the wings which depends on the speed. Moreover in phases such as take off or taxi we can not consider the speed to be constant and so, the Euler method, is no longer usable. In the next paragraphs we will discuss all the flight phases in detail.

For describing the mission we set the "Operational altitude" to 1500ft which, for our model, is the altitude at which the plane have to fly when operating on site. We also define a "Cruise altitude" of 5000ft as the altitude at which we expect to cruise from the airport to the area of operations and vice versa.

Taxi The taxi phase occurs before the take off and it is basically the plane rolling on the ground from the starting point to the beginning of the runway. Supposing the airport to be at 0 ft we have to write the forces acting on the plane when taxing. Since the forces scheme is very far from the Hypothesis made before and, seen that in any case the fuel consumption in this phase will be minimal, at this stage, its decided to set the throttle to 7% of the maximum power supposing that this quantity power is enough to move the plane on ground. The duration of this phase, in our case, its set to 10 minutes.

Take off The take off phase is very tricky since, in this moment, for sure, big acceleration and couples are acting on the aircraft in the x and y direction this makes the differential equation of motion written before more difficult to integrate since become a second order differential equation. To avoid the problem as like the taxi phase, the choice is to set the throttle to 100% (TOGA power) for ensuring the plane will surely take off. Even in the case of a significant overestimation of the required power, this would not pose a serious issue, as the phase lasts only 2 minutes.

Climb first The phase called "climb first" brings the plane from the ground to the cruise altitude. In this moment the airplane, which took off from the airport, is climbing toward the operation site at a constant IAS value of 150kt with a 5° ramp value. In this way its possible to find the power delivered by the engine in this phase. Its important to discuss the state of the tank. The mission is designed to:

- To respond on site as fast as possible
- To operate on site as long as possible

For this two reasons the choice made is to maintain the tank fully loaded when on ground to be able to take off and deliver water as fast as possible. The tank fully loaded means more weight in the very first phase of the flight and so more fuel consumption.

Cruise first The "cruise first" phase occurs after take off and is the path necessary for the plane to arrive on the operational site. The cruise speed is set to an IAS value of 150kt and an altitude of 5000ft. This phase last 30 minute in which the plane make almost 130km.

**Descent first** The "Descent first" happens right after the "Cruise First. This phase brings the plane down to 0ft with a ramp value of  $-5^{\circ}$  and a constant IAS value of 150kt.

**Drop** The drop phase is one of the most important in terms of the operations for this kind of aircraft. This phase is surely characterized by big variations in weight caused by the water tanks rapidly emptying which imply big changes in the lift values and so in the dynamics of the flight which, under this hypothesis, we should not consider.

What is important for a good water drop is, mostly, that the pressure, airspeed and altitude are in a correct range for obtaining a good, coherent water column which guarantee at least the expected coverage value.

For this, at this early stage of the design process, we chose to consider the water drop to happen at a constant altitude of 0ft with a specified airspeed of 70kt and to last 2 minutes. We know that, in real operations, the throttle will be set by the pilots at the correct value but, in this case, for takin in to account the worst case, also for safety reasons, the throttle is set to 100% as for the takeoff. Exactly as we did before this simplifications can be used because of the very short duration of this maneuver which will not have a big impact on the entire fuel consumption.

**Cycle of operations** This plane, as every well designed amphibious aircraft should do, will last longer than one single drop on the operation site. The Cycle of Operation is made of different phases which repeats equal for a finite amount of times. These phases can be resumed in:

- "Cruise mission" which separate the operating site from the water source at 1500 ft for 10 minutes
- "Descent mission" from the operational altitude to 0 ft where the water source is supposed to be, with a ramp of  $-5^{\circ}$
- "Tank refill" which is the phase in which we touch the water and refill the tank. Since this phase is pretty demanding in terms of power/thrust its reasonable to set the throttle to 100% and the duration at 1 minute. We set the altitude at 0ft
- "Climb mission" The phase climb mission happens right after the tank refill and brings the plane from 0ft to the cruise altitude with a ramp of  $5^{\circ}$
- "Cruise mission" This phase is already been explained
- "Descent mission" This phase is already been explained
- "Drop" This phase is already been explained
- "Climb mission" This phase is already been explained

The number of repetition for the operation cycle can be set and, it may be used as a parameter for the design process since it has certainly a big impact on the overall aircraft performance.

**Climb final** The climb final phase bring the aircraft from the operational altitude to the cruise altitude with the ramp angle of  $5^{\circ}$ .

Cruise final The "Cruise final" is the same as the cruise first

**Descent final** The descent final phase altitude brings the plane from the cruise final altitude to the airport which we consider to be, as said before, at sea level. This is the last phase of the mission model since we consider the landing negligible in terms of fuel consumption.

#### 3.5 Results

Imposing a initial mass of 19890 kg, which is the MTOW value for the CL-415 used as reference in this first test case we simulate the mission as described before obtaining a final mass of 10142 kg. The weight loss is not due just on fuel consumption but depends on the water discharge which takes place during the mission. The Aircraft will take off with the tank fuel for the reasons told before and will obviously land with the tanks emptied. If the water quantity is set to 8000 kg, for example, its easy to compute that the mass of fuel burnt during the whole mission is 1747 kg.

In the following figures is shown the mission profile in terms of z and x, the number of cycles of operation is, in this case, set to 15 and this is a parameter which affects the fuel consumption the most.

We can see the mission profile in figure 3.20.

The weight loss is shown in figure ??

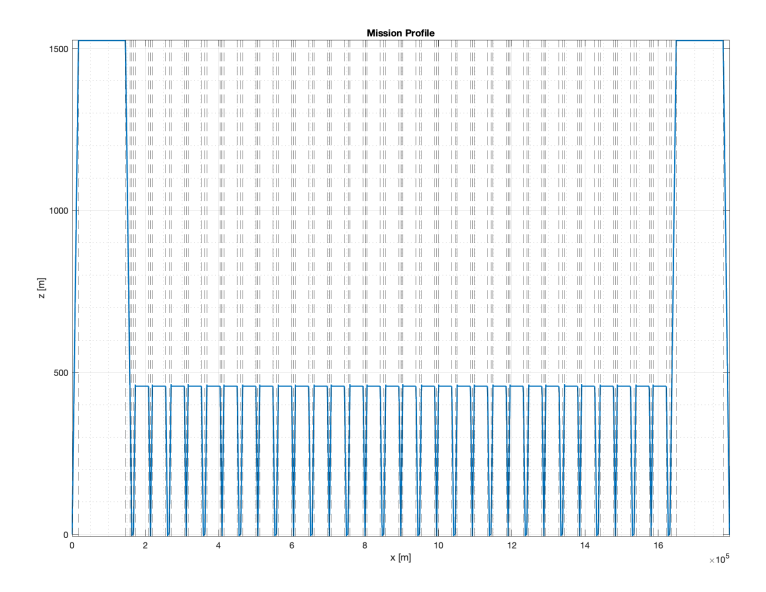


Figure 3.20: Mission profile

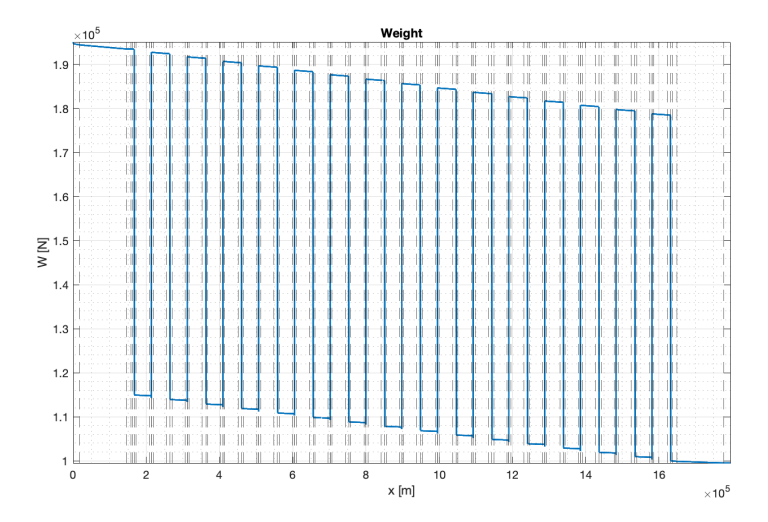


Figure 3.21: Weight of the aircraft

By means of the same code, it is possible to observe the value of the lift coefficient required for the longitudinal trimming of the aircraft. As previously stated, if the aircraft is trimmed, the following equation holds:

$$W = L = \frac{1}{2}\rho V^2 S C_L \tag{3.55}$$

Hence:

$$C_L = 2\frac{\frac{W}{S}}{\rho V^2} \tag{3.56}$$

Consequently, for each instant of flight it is possible to compute the corresponding lift coefficient. As shown in Figure 3.22, the most critical portion of the mission is, as expected, the drop phase. In this phase, the goal is to decelerate the aircraft as much as possible in order to perform an effective water release. The target airspeed should be below 50 m/s. Assuming a given reference surface and considering that the drop occurs at an altitude essentially equal to zero, corresponding to standard atmospheric density, the resulting lift coefficient values are in any case greater than unity. In order to achieve the values of the lift coefficient reported in Figure

3.22, it will be necessary to adopt a high-lift configuration, thereby increasing the maximum achievable  $C_L$  of the wing when required. This would allow the aircraft to maintain a trimmed condition even during the most demanding phases of flight.

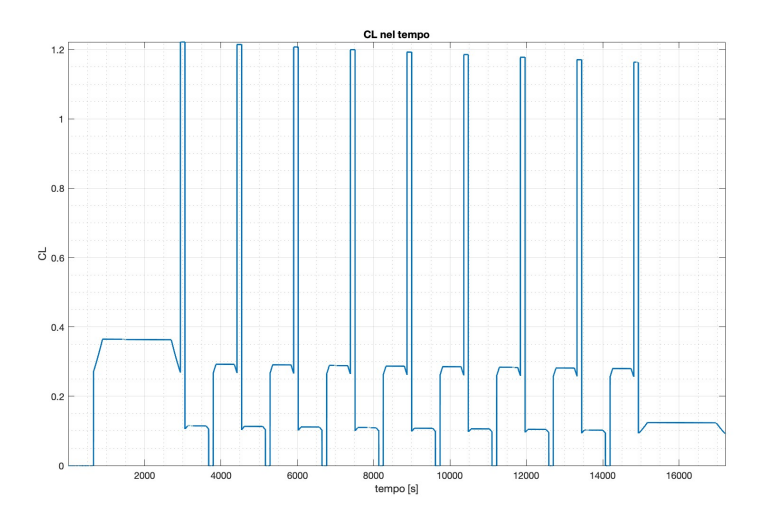


Figure 3.22: Lift coefficient as a function of mission time

The high-lift configuration is not considered at this stage, but it will be studied in detail in future analyses. Selecting the drop phase as the discriminating design condition will result in a wing highly suited for very low-speed flight, while being poorly adapted to high-speed regimes. This is both due to compressibility effects, which would be extremely challenging to manage with a wing optimized for incompressible flow, and because such optimization would naturally lead to wings with nearly zero sweep and large surface areas in order to keep the wing-loading low.

# Chapter 4

# Aerodynamics

Aerodynamics performance is a crucial aspect while designing an aircraft, and, in this case, introducing a brand new lifting technology its particularly interesting to investigate how the wing geometrical parameters influence the fire-fighting performances.

For the aerodynamics design its chosen to use an optimization method based on the AEROSTATE software. AEROSTATE is a Matlab-based optimization tool which allows to evaluate the aerodynamics performance of a biplane configuration using AVL.

AVL (Athena Vortex Lattice) is an aerodynamics computer based on potential flux method. To better understand the working of AVL its necessary to explain what potential flux stands for.

## 4.1 AEROSTATE underlying theory

As said before AEROSTATE is an aerodynamics optimization tool and so we have to understand the numerical optimization methods and numerical aerodynamics solver which are the two main component of this software.

## 4.2 AVL functioning

AVL (Athena Vortex Lattice) is a software developed by the Massachusets Institute of Technology [2] for the computing of the aerodynamics performance with VLM (Vortice Lattex Method) plus the resolution of slender body as fuselage and nacelles.

**Vortex Lattex Method** VLM is a method used for the computing of the aerodynamic performance of wings. This method is based on potential flux and consists in the following steps:

- Modeling of the wing planform
- Discretizations of the wing planform in a finite numbers of rectangular panels
- Modeling of each rectangular surface with a horseshoe vortex system
- Computing of the induced velocity on the control point of each rectangular surface
- Imposing the NON-penetration condition in the control point of each rectangular section
- Solution of the algebraic system which allows to find the intensity of each horseshoe vortex
- With the potential flow theory, knowing the intensity of the vortex placed on each rectangular panel is possible to compute the lift and drag coefficient on the panel.

There are several hypothesis done on the original problem in order to executed the VLM.

- Flux:
  - Inviscid
  - Irrotational
  - Incompressible
  - Small  $\alpha$ ,  $\beta$ ,  $\delta$
- Geometry:
  - Plane surface we model the camber line
  - Discretization in rectangular panels
  - Modeling panel as horseshoe vortex systems

Induced velocity by a vorticous line The problem is represented in the following figure:

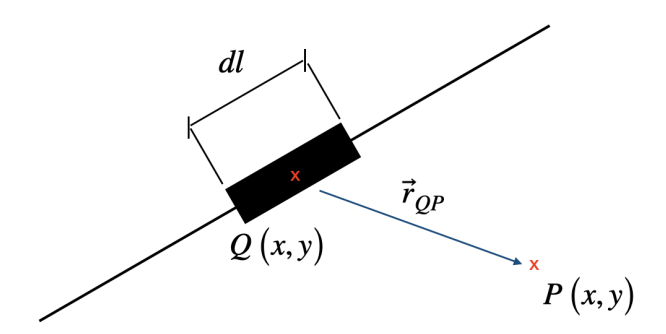


Figure 4.1: Biot-Savart problem

For the computing of the velocity induced in P by the infinitesimal vortex with length dl placed in Q with intensity  $\Gamma$  we use the Biot-Savart formula as follows:

$$d\vec{v} = \frac{\Gamma}{4\pi} \cdot \frac{\vec{dl} \times \vec{r}_{QP}}{|r_{QP}|^3} \tag{4.1}$$

So in case of an horseshoe vortex where we have, one finite length vortex and two infinite vortex with we use superposition of effects computing all the different contributions separately and then summing them as shown in figure below.

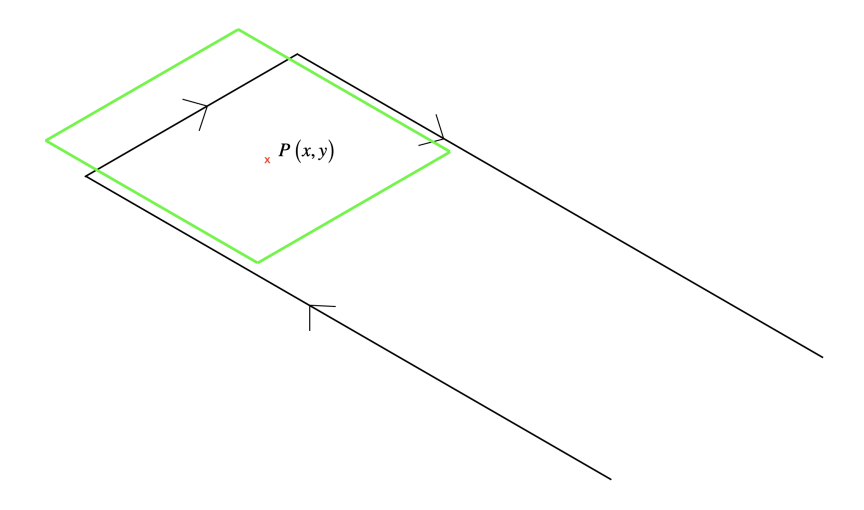


Figure 4.2: Horseshoe vortex and panel modeling

**Non penetration condition** For the determination of the lift acting on one panel composing the surface we need to know the intensity of each horshoe vortex acting on each panel of the surface.

For the beginning lets take in to account just one panel which is hit by a freestream flow  $U_{\infty}$  with an inclination of  $\alpha$  and  $\beta$  with respect to the rectangular panel. The panel generate an horseshoe vortex which is composed by a bound vortex placed on the quarter chord line and two semi infinite vortex line. Since the panel represents the wing we have to impose the non penetration condition. We impose the condition in the P point as shown in figure 4.2. The P point is placed on the third quarter of the chord.

The Non penetration condition is represented in the equation below:

$$(V_{\infty} + V_{ind}) \cdot \vec{n} = 0 \tag{4.2}$$

Where  $V_{\infty}$  is the freestream flow velocity,  $V_{ind}$  is the velocity induced in point P by the horseshoe vortex and  $\vec{n}$  is the normal vector to the surface in point P.

The induced velocity will be the product of a constant value and the intensity of the vortex  $\Gamma$ :

$$\vec{V}_{ind} = \vec{K} \cdot \Gamma \tag{4.3}$$

While the  $\vec{n}$  for a thin surface which can be seen as z(x,y) = f(x,y) can be computed as follows:

$$\vec{n} = \left(-\frac{\partial f}{\partial x}, -\frac{\partial f}{\partial y}, 1\right) \tag{4.4}$$

The freestream flow is represented as  $V_{\infty} = (V_{\infty} \cos \alpha \cos \beta, V_{\infty} \sin \alpha, V_{\infty} \sin \beta)$ 

Projecting vector  $V_{\infty}$  in the  $\vec{n}$  direction the following expression is found considering  $\alpha$  and  $\beta$  to be small:

$$\vec{V}_{\infty} \cdot \vec{n} = V_{\infty} \left( \frac{\partial f}{\partial x} + \beta \frac{\partial f}{\partial y} + \alpha \right) \tag{4.5}$$

Substituting in the non penetration condition we find:

$$V_{ind} \cdot \vec{n} \approx V_{\infty} \left( \frac{\partial f}{\partial x} + \beta \frac{\partial f}{\partial y} + \alpha \right)$$
 (4.6)

and then

$$\Gamma \cdot k \cdot \vec{n} \approx V_{\infty} \left( \frac{\partial f}{\partial x} + \beta \frac{\partial f}{\partial y} + \alpha \right)$$
 (4.7)

To find the value of  $\Gamma$  as become an easy task because we have found a simple linear equation.

**Full wing** For the full wing the task is a little more complex because each panel is seen as a horseshoe vortex and, each horseshoe induces a velocity on each panel. So the non perturbation condition for the i panel take on a different expression:

$$\sum_{j=1}^{N} k_{j\to i} \cdot \Gamma_j \approx V_{\infty} \cdot \vec{n}_i \tag{4.8}$$

For each i-panel, we consider the induced speed by each j-panel and this as to be equal to the projection of the freestream flow on the normal of the i-panel. In this way we obtain a linear algebraic system which has dimensions of  $N \times N$  where N is the number of panels with N unknowns who are the intensity of the horseshoe vortex for each panel.

#### 4.2.1 Lift and drag on panels

Lets take in to consideration the Navier-Stokes equation:

$$\begin{cases} \frac{\partial \rho}{\partial t} + \nabla \cdot (\rho \vec{q}) = 0\\ \frac{\partial (\rho \vec{q})}{\partial t} + \nabla \cdot (\rho \vec{q} \cdot \vec{q}) = -\nabla \rho + \nabla \cdot \vec{\tau} + \rho \vec{f}\\ \frac{\partial (\rho E)}{\partial t} + \nabla \cdot (\rho E \vec{q}) = -\nabla \cdot (\rho \vec{q}) + \nabla \cdot (\bar{\tau} \cdot \vec{q}) + \rho \vec{f} \cdot \vec{q} + \nabla \cdot (k \nabla T) \end{cases}$$

$$(4.9)$$

Solving this system of equation is a very complex matter because of the high non-linearity and instability of the solutions. CFD (Computational Fluid Dynamics) gives a numerical solutions of this system over time and allows certainly to evaluate, with a high precision level the performances of the lifting system. What is sure is that, in the preliminary phase of the design, when we need to try lots of different geometrical configurations in order to find the optimum CFD methods are way too expensive. What is possible to do is to impose some hypothesis for in order to simplify the equations and low the computational cost.

The hypothesis are:

- The fluid is ideal
- No volume forces
- Isentropic fluid

We obtain the following equations written in x-direction:

$$\begin{cases} \frac{\partial \rho}{\partial t} + \frac{\partial}{\partial x} (\rho u) = 0\\ \frac{\partial (\rho u)}{\partial t} + \frac{\partial}{\partial x} (p + \rho u^2) = 0\\ \frac{\partial (\rho E)}{\partial t} + \frac{\partial}{\partial x} (\rho E u) + \frac{\partial}{\partial x} (\rho u) = 0 \end{cases}$$
(4.10)

The Euler equation represents a good starting point but present non-linearity that makes CFD necessary.

If, to the previous hypothesis we add:

- Stationary flux
- Irrotational flux  $\nabla \times \vec{q} = 0$

Since the rotor of the gradient of a generic vector field is always equal to zero, we can say that, since the rotor of the  $\vec{q}$  field is equal to zero, there is a scalar field  $\phi$  defined as follows:

$$\vec{q} = \nabla \phi \tag{4.11}$$

Where  $\phi$  is the potential function.

In the same way, knowing that the conservation of the mass have to be respected, we can write:

$$\vec{q} \cdot \nabla \rho + \rho \nabla \cdot \vec{q} = 0 \tag{4.12}$$

and so

$$\nabla \cdot (\rho \vec{q}) = 0 \tag{4.13}$$

$$\frac{\partial}{\partial x}(\rho u) + \frac{\partial}{\partial y}(\rho v) = 0 \tag{4.14}$$

Defining the  $\vec{b}$  field perpendicular to the  $\vec{q}$  field as follows:

$$\vec{b} = (-\rho v)\vec{i} + (\rho u)\vec{j} \tag{4.15}$$

The  $\vec{b}$  field is irrotational:

$$\nabla \times \vec{b} = \begin{bmatrix} \vec{i} & \vec{j} & \vec{k} \\ \frac{\partial}{\partial x} & \frac{\partial}{\partial y} & \frac{\partial}{\partial z} \\ -\rho v & \rho u & 0 \end{bmatrix} = \left[ \frac{\partial}{\partial x} \left( \rho u \right) + \frac{\partial}{\partial y} \left( \rho v \right) \right] \vec{k} = 0$$
 (4.16)

As we can see the  $\vec{b}$  field is irrotational and so its possible to define his own potential  $\psi$  which is called the steam function:

$$\vec{b} = \nabla \psi \tag{4.17}$$

Since we defined  $\vec{b}$  to be perpendicular to  $\vec{q}$  and so:

$$\vec{q} \cdot \vec{b} = \nabla \phi \cdot \nabla \psi = 0 \tag{4.18}$$

Another think which is possible to show is that both the stream and the potential functions solve the Laplace equation and so are harmonic.

And we can subsequently find that the lift on the thin plane surface with a circulation  $\Gamma$  is:

$$L = \rho \vec{V} \times \vec{\Gamma} \tag{4.19}$$

#### 4.2.2 Numerical optimization

Numerical optimization deals with finding, for a system defined by a finite number of parameters, the combination of these parameters that minimizes a particular objective function defined within the system. Optimization problems are divided into different categories:

- Single-objective and multi-objective problems
- Constrained and unconstrained problems

Below is the general formulation of a constrained single-objective optimization problem.

$$\min_{\mathbf{x} \in R^n} f(\mathbf{x})$$
subject to  $g_i(\mathbf{x}) \le 0, \quad i = 1, \dots, m$ 

$$h_j(\mathbf{x}) = 0, \quad j = 1, \dots, p$$
(4.20)

As stated in [9]. Exploring the admissible solution space, aiming to the minimization of the objective function its possible to follow a variety of criteria. In the case of AEROSTATE tool the search for the minimum is done with a local point of view and also in a global way so the algorithm don't present a local minimum as the optimum point but search for the global minimum of the function in the admissible space.

For usage of the AEROSTATE tool its necessary to accurately set the starting point for the optimization. To set the point its necessary to act, in the Geometry folder, on the proper Matlab structure which contains all the geometric parameters which define the plane.

Once the starting point's selected, its possible to set the objective function in the "obj.mat" script and the and the constraints from the script "confun.m".

### 4.3 Aerodynamics design method

The very first concern about the design of a firefighter aircraft should be related to the wing loading. For a box-wing configuration, having two surfaces contributing to the lift of the plane, its necessary to define two different wing loading, one for the front wing and one for the rear wing. The wing loading of a single wing is defined, as shown in [?], as the lift generated from the wing divided by his reference surface. The total wing loading for the plane can be computed with the following formula:

$$\left(\frac{W}{S_{tot}}\right) = \left(\frac{L}{S}\right)_{FW} \cdot \left(\frac{S_{FW}}{S_{tot}}\right) + \left(\frac{L}{S}\right)_{RW} \cdot \left(\frac{S_{RW}}{S_{tot}}\right) \tag{4.21}$$

For evaluating the total wing loading its necessary to set the vertical trim:

$$W = L = \frac{1}{2}\rho V^2 S C_L \tag{4.22}$$

Obtaining:

$$\frac{W}{S} = \frac{1}{2}\rho V^2 C_L \tag{4.23}$$

One of the main focuses in aerodynamic design is the selection of the design condition. In this context, the design condition is intended as a combination of altitude, speed, and weight. For the aircraft considered in this study, several possible conditions could be used for the aerodynamic design of the lifting system.

The most critical condition in aerodynamic terms is the drop condition. In this case, the speed must fall below 55 m/s, while the aircraft operates at a very low altitude with a very high load, since this phase follows the scooping phase. This condition is therefore certainly critical; however, it is expected that the aircraft will face it with the wing in a flapped configuration. Consequently, when designing the clean wing, it would not make sense to select this point as the design condition, since it would lead to configurations with an excessively high lift coefficient.

Another possible approach, ultimately adopted, is to select the lift coefficient a priori. We assume that, in the design condition at sea level and at full load immediately after scooping, the lift coefficient is  $C_L = 0.35$ . The aircraft is expected to operate near this value because each airfoil has an angle of attack of best efficiency, which the designer should take into account. Even in this study, where overall aerodynamic efficiency is not the primary driver, sizing the wing for a relatively low lift coefficient preserves margin to fly at higher angles of attack without approaching stall. The remaining task is to determine the flight speed required for level flight. For this calculation we use the well-known CL-415 as a reference.

The calculation is structured as follows. Let us assume that the CL-415 has a design lift coefficient of 0.35, a wing area of 100 m<sup>2</sup>, and an after-scooping weight of 21319 kg, as reported in [12]. This yields the following result through the equation:

$$V = \sqrt{\frac{2 \cdot \frac{M \cdot g}{S}}{\rho C_L}} = 98 \,\text{m/s} \tag{4.24}$$

Once this design speed for the wing is obtained, the design process can begin. This value of  $C_L$  is translated into a constraint in terms of wing loading due to the structure of the Aerostate code. The corresponding wing loading for this condition is:

$$\frac{W}{S} = \frac{1}{2}\rho V^2 C_L = 209 \,\text{kg/m}^2 \cdot g \tag{4.25}$$

The value of  $209 \text{ kg/m}^2$  represents the maximum wing loading that a well-designed configuration should have. In the Aerostate code, it is possible to impose such a constraint, as explained later.

The value of  $209 \text{ kg/m}^2$  is also consistent with what is reported in [12] regarding the wing loading of the CL-415, which, depending on the flight condition, falls approximately within the same range.

For a proper aerodynamic design of the aircraft, a careful selection of the wing airfoil, or possibly a set of airfoils along the span, is required. Airfoil choice is a key step in the process and should be driven by the characteristics and mission of the aircraft.

Airfoils suitable for subsonic flight can differ markedly from those intended for transonic flight. At high Mach number, the local flow around the wing may reach  $M \geq 1$  even if the flight Mach number is lower. Transonic airfoils aim to delay this condition and to place the shock as far aft as possible, so that an overly forward shock on the chord does not induce separation over the entire suction side.

Although the detailed selection of the airfoil is deferred to later phases of the design, in the present case a relatively thick airfoil is preferable to a thin one. In particular, a trailing edge stall, rather than a leading edge stall, is desirable in order to obtain a gentle stall behavior. This is important because the aircraft will often operate in demanding conditions. This characteristic is especially required for the rear wing, which can help recover from stall if properly designed.

## 4.4 Discussion on the assessment of the Design Weight

In the previous part of this study, a method for evaluating the Maximum Take-Off Weight (MTOW) was presented. The MTOW represents the maximum weight at which the aircraft can safely take off from the runway. In this particular case, the discussion on design weight must also consider the amphibious nature of the aircraft. A specific MTOW value for water operations has to be determined, as it depends both on buoyancy conditions and on the power required for water take-off. This aspect will be analyzed later; for now, the focus is on determining the appropriate design weight of the aircraft. Since the water tank, in flight conditions, can be either full or empty, the design weight spans a wide range of variation, as the amount of water potentially stored in the tank is approximately 13,000 kg. The decision on which weight should be adopted as the design weight arises from considerations related to stall conditions. Suppose the design weight were defined with the tank empty: in this case, the lifting surfaces would be sized for a lighter aircraft. When the tank is full, however, the wing loading significantly increases, which worsens stall characteristics. Considering that stall is most likely to occur during the waterdrop phase of the mission-when the tank is full-the design weight must therefore be based on the full-tank condition. Nevertheless, the design weight will not be exactly equal to the MTOW: it will be computed by considering the fuel level at the end of the first cruise segment, i.e., when the operational phase of the mission effectively begins. Consequently, the design weight will be slightly lower than the MTOW value.

Having determined the wing loading and knowing the design weight its possible to evaluate the total reference surface of the whole plane.

$$S_{tot} = \frac{W_{design}}{\left(\frac{W}{S}\right)} \tag{4.26}$$

In the real configuration, the front and rear wing surfaces will not be equal. However, in the initial stage of the aerodynamic design, it can be useful to assume them to be equal in order to obtain a correct estimation of the wing chords, given that the wingspan will be 28 meters. For this preliminary assessment, the main dimensions of the CL-415 are taken as a reference.

The surface area of one wing, assuming a trapezoidal shape, can be expressed as follows:

$$S_{fw,rw} = \frac{(C_{root} + C_{tip})}{2} \cdot b \tag{4.27}$$

Where S and b are known, while  $C_{\text{root}}$  and  $C_{\text{tip}}$  are the unknowns.

Since we know from the beginning that the two wings will have the same wingspan, we can impose a system of equations to determine the chords of the two wings in this first stage, under this preliminary hypothesis and considering a taper ratio for the front wing to be  $\lambda = 0.35$ :

$$\begin{cases}
S_{fw} = \frac{C_{R,fw} + C_{tip}}{2} \cdot b \\
S_{rw} = \frac{C_{R,rw} + C_{tip}}{2} \cdot b \\
\lambda = \frac{C_T}{C_{R,FW}}
\end{cases}$$
(4.28)

Solving this equation provides values that are useful for determining the starting point of the optimization problem. These values are 'physics-based,' in the sense that they are computed while taking into account wing loading and stall considerations.

For what concerns the other leading variables to set in to the geo structure in order to give the code a good starting point we need to set:

- Incidence
- Coordinates of the sections
- Chords
- Theta
- Span
- Sweep
- Dihedral

#### 4.5 Constraints determination

For a proper definition of the problem constraints, within the AEROSTATE tool we can define high-velocity constraints, geometrical constraints, and low-velocity constraints.

Geometrical constraints refer to the geometric characteristics derived from the aircraft layout. It is important to note that values such as the wingspan or the design weight  $(W_{des})$  are predefined in the code and do not vary, since they drive the overall design process.

As an example of geometric constraints, in this case it is chosen to impose that the leading edge of the rear wing, summed with its root chord, does not exceed the total fuselage length. A second example specific to this case is that the x position of the leading edge of the front wing, added to the root chord of the front wing, must be less than the front of the water tank position, ensuring that there is no interference between the tank structure and the wing box structure.

Regarding the geometric constraints, a constraint on the wing loading is also included, representing a true cornerstone of aerodynamic design. Having established in a previous section of this chapter the appropriate design wing loading value that the aircraft must have in order to sustain the design flight conditions, it is necessary to impose on the optimizer the maximum allowable wing loading value.

To understand this choice, it must be clarified that the wing loading constraint essentially corresponds to a constraint on the assignable wing area of the aircraft. By its nature, the optimizer tends to increase the wing loading value, since a higher wing loading implies a smaller chord and therefore a more elongated wing, which results in lower form drag, a more efficient lift distribution, and consequently, higher aerodynamic efficiency. For this reason, the wing loading value must be strictly upper-limited.

There are several ways to impose an upper limit on the wing loading value. One possible approach could be to constrain the wing loadings of the two wings separately. It is possible to include this type of constraint within the code, considering that, for stability and stall resistance reasons, the wing loading of the front wing should generally be higher than that of the rear wing. However, this approach is avoided in the present case.

Instead, a slightly different operation is chosen by imposing the constraint in the following form:

$$\frac{1}{2}\rho V^2 C_{L,\text{Tot}} < \left(\frac{W}{S}\right)_{\text{max}} \tag{4.29}$$

In this way, since the upper limit for the overall aircraft wing loading is known, while the individual wing loading limits are not precisely defined, and considering that the total wing loading can be expressed as:

$$\left(\frac{W}{S_{tot}}\right) = \left(\frac{L}{S}\right)_{FW} \cdot \left(\frac{S_{FW}}{S_{tot}}\right) + \left(\frac{L}{S}\right)_{RW} \cdot \left(\frac{S_{RW}}{S_{tot}}\right) \tag{4.30}$$

it is considered more effective in this case to impose the constraint on the total wing loading.

For the taper ratio constraint, it is necessary for structural reasons to keep it less than one.

After the geometrical constraints are set, aerodynamic constraints are introduced. AEROSTATE allows the definition of two specific flight conditions, one called 'High Speed' and another called 'Low Speed'. In this way, it is possible to impose constraints related to high-speed flight conditions as well as those related to low-speed conditions, which are equally important because they concern phases such as landing or, in this particular case, the drop/refill operations.

For the first analysis, high-speed constraints are considered:

$$\begin{cases}
MS_{min} \leq MS \leq MS_{max} \\
-0.025 \leq \frac{x_{cp} - x_{CG,max}}{c} \leq 0.025 \\
1 - \epsilon \leq \frac{\frac{1}{2}\rho V^2 SC_L}{W} \leq 1 + \epsilon \\
\max (C_l(y))_{\text{ant, post}} \leq 0.7
\end{cases}$$
(4.31)

As can be observed, the stability margin must remain between  $MS_{min} = 0$  to ensure longitudinal stability and  $MS_{max} = 0.4$  to avoid excessive pitch stiffness.

The center of pressure and the aircraft center of gravity must coincide as closely as possible in order to ensure pitching moment balance.

A very important constraint concerns the vertical equilibrium in pitch: the lift generated by the wings must equal the aircraft weight.

The maximum value for local  $C_l$  is imposed at 0.7, since exceeding this limit is unacceptable for both structural and aerodynamic reasons related to stall of the aerodynamic profile.

### 4.6 Optimization starting point

An important part of the optimization process is the correct selection of the starting point, that is, the initial configuration from which the optimizer begins the iterative calculation described earlier. The initial configuration of the wing system can be observed in Figure 4.3. As shown, the starting point is defined according to the chord values described previously.

In the initial configuration, assuming the absence of compressibility effects, the taper ratio is initially set to zero. Since the code tends to produce tapered wings, which are generally more efficient, a tapered wing is generated. The dihedral angle of the front wing is set to a non-zero value in order to respect the imposed boundaries.

Regarding the position of the two wings, a realistic arrangement is applied. As mentioned earlier, sufficient space must be left for the water tank; therefore, an adequate distance between the two wings is imposed. From this point of view, the optimization process can begin.

The choice of the initial point is also important because it allows for a preliminary estimation of the aircraft weight, as discussed in the following chapters.

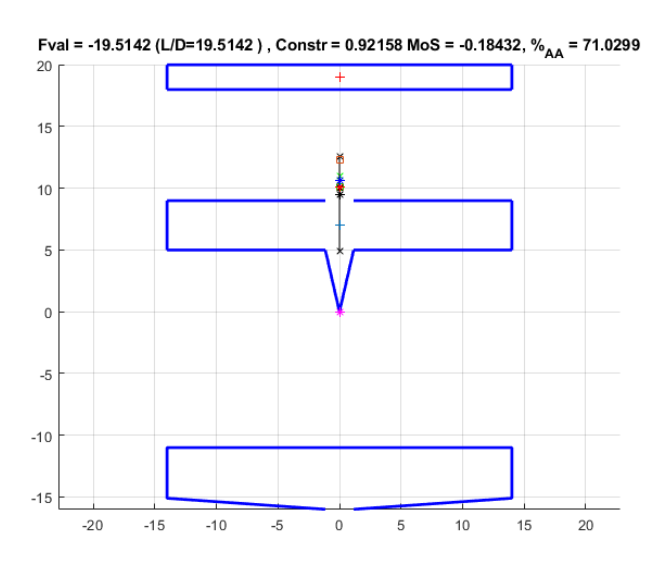


Figure 4.3: Starting point of the optimization process

### 4.7 Boundaries definition

For the optimization tool AEROSTATE, it is necessary to set proper boundaries for the design variables defining the problem, since we must define, as accurately as possible, the admissible design space in which the solution can be found. Within the definition of  $x_0$  inside the geometric structure, for each lifting surface the structures  $geo.ala\_ant.var$  and  $geo.ala\_post.var$  are defined, as shown in the figure below.

In Figure 4.4 it is possible to see that, for each geometrical parameter used to fully define the aerodynamic characteristics of the lifting system, a value of either zero or one is assigned. When a variable is set to 1, it means that the specific parameter will be used as a variable in the optimization cycle; if set to 0, the parameter will remain constant throughout the process.

For each variable that is switched on in the .var structure, proper boundaries must be defined.

The criteria to be considered when defining the proper boundaries are the following:

- Admissibility of the value. If a value is not admissible for any reason, either geometrical or aerodynamic, it should be excluded from the boundaries.
- Number of active variables. The greater the number of variables activated in the geo structure, the higher the dimensionality of the design space. This increases the probability of finding the optimal solution, but also leads to longer computational times for convergence.

1
[1,0,0]
[1,1,1]
[1,1,1]
[0,0,0]
[1,0]
[1,1]
[1,1]
[0,0]

Figure 4.4: "geo.ala ant.var" structure

• Width of the boundaries. Wider boundaries increase the likelihood that the optimum lies within the design space. However, this also extends the execution time of the optimization process, since a larger space must be explored.

In the following figure the boundary chosen are represented:

Min	Variable	Max
4.396 m	XLEala_ant	8.85 m
3 m	C1 ala_ant	5 m
-6°	Thetal ala_ant	8°
3 m	C2 ala_ant	5 m
-5°	Theta2 ala_ant	7°
3 m	C3 ala_ant	5 m
-6°	Theta3 ala_ant	5°
1 m	b1 ala_ant	8 m
3°	Dihed1 ala_ant	15°
0°	SW1 ala_ant	10°
3°	Dihed2 ala_ant	15°
0°	SW2 ala_ant	10°
-7°	Angleala_ant	7°
11.3 m	$XLEala\_post$	21.3 m
1.5 m	C1 ala_post	3 m
-6°	Theta1 ala_post	7°
1.5 m	C2 ala_post	3 m
-6°	Theta2 ala_post	6°
8 m	b1 ala_post	16 m
-10°	Dihed1 ala_post	0
-15°	$SW1 ala\_post$	0
-6°	Angleala_post	6°

Table 4.1: Boundaries set for each design variable

The x position of the leading edge of the front wing is subject to several geometric constraints. The wing cannot be placed too far forward to avoid interference with the cabin door and the hull structure, while it must be sufficiently elevated to prevent interaction with the hull and

sufficiently advanced to avoid interference with the water tank, which occupies entire sections of the fuselage. This constraint on the forward position relative to the tank is imposed as a constraint rather than as a boundary, since the design variable refers to the leading edge position, and variations in the chord length could otherwise result in interference.

The chord values are imposed according to the following criterion. Knowing the aerodynamic design condition of the aircraft, it is possible to determine the reference wing area using the previously estimated design weight used for the optimization, obtaining a value of approximately  $150 \text{ m}^2$ . Once the total surface area of  $150 \text{ m}^2$  is obtained, a 2/3-1/3 distribution between the two wings is assumed, leading to a root chord of about 3.6 m for the front wing and 1.8 m for the rear wing. The boundary values were therefore defined based on these results, ensuring that the optimized values remain within these ranges.

As for the dihedral angle values, the rear wing is given almost complete freedom, whereas the front wing requires stricter constraints. Due to the refilling condition of the water tank, it may be advantageous for the front wing to have a slightly higher tip compared to the root. Being a low wing, during the scooping phase it is desirable to avoid contact between the wing and the water surface, as well as to allow for the possible installation of floating devices that would otherwise lack space.

The wing sweep values are also strongly constrained. The flight conditions of this aircraft will never be particularly restrictive in terms of compressibility effects. The design condition corresponds to Mach 0.28, which does not pose any issue regarding wave drag. Wing sweep could become useful at higher flight regimes, but in this case the aircraft is unlikely to operate within the transonic range.

### 4.8 Computation of the Mass Center

For stability reasons its necessary for the optimization tool to define the position of the center of gravity of the Aircraft. The method for the definition of the position of the center of gravity uses the position of the center of gravity of all the components of the Aircraft and their own mass. Thanks to [12] its possible to compute all the aircraft components mass and center of mass as we can see in the next section for some of them.

Wing In the Aerostate tool, as described in [?], it is necessary to evaluate the wing mass in order to compute the aircraft center of mass. For this reason, a simplified model is used:

$$W_{wing,ant,post,bulk} = 2 \cdot \rho_{wing} \cdot S_{tot} \tag{4.32}$$

As is clear, with this method the software does not account for variations in the wing geometry that occur during the execution. The wing weight depends only on the reference surface and on the wing surface density, which can be set by the user.

In future implementations of the code, a physics-based method will be considered for wing mass evaluation, such as the one presented in this work, which is able to compute the wing mass directly from the overall geometry and therefore with greater accuracy.

Payload mass and CG For the payload, this aircraft represents a particular case, since it is limited to the water used as fire retardant, which is essentially concentrated in the tank. The location of the tank therefore determines the payload center of mass. In this configuration, it is not convenient to place the payload center of mass too far forward in the fuselage, because the front wing must be positioned relatively aft in order to avoid interaction between the water spray and the front wing. The payload mass, is fixed at 47% of the fuselage.

In the following table its summarized the position of the center of mass of the components of the aircraft.

Table 4.2: Components of weight and longitudinal center of gravity position (as a percentage of fuselage length)

Component	Mass [kg]	x-cg
Fuselage	4710.80	40%
Vertical Tail	67.50	$X_{CG,VT}$
Front Wing	$2\rho_1 S_{FW}$	$X_{CG,FW}$
Rear Wing	$2\rho_2 S_{RW}$	$X_{CG,RW}$
Payload (max)	12828.98	47%
Fuel	2273.00	$0.7 X_{CG,FW} + 0.3 X_{CG,RW}$
Engine (wet)	2297.00	75%
Landing Gear (main)	314.37	50%
Systems	1441.50	25%

## Chapter 5

# Fuselage design

For the fuselage design, several aspects must be taken into consideration. First of all, as stated in [3], the correct design of the hull must be based on the concept of a prismatic planing hull. As discussed in the chapter about the matching chart, the geometric parameters of the hull influence both drag and lift generated during planing, and therefore directly affect the required power. It has been observed that keeping the deadrise angle relatively low has a positive effect on the required power. On the other hand, larger deadrise angles ensure greater stability of the aircraft during planing. For an appropriate design, it is also necessary to introduce a step in the fuselage structure. The position of the step, as well as its height and inclination, influence the planing characteristics. In this preliminary design, the center of gravity of the water tank has been considered at 47% of the fuselage length. This allows for a sufficiently large planning surface, capable of supporting the aircraft weight without causing the spray generated by the hull to interfere with the wing aerodynamics. The fuselage design process can be represented using AutoCAD. In particular, a total fuselage length of 20 meters is imposed in order to keep the overall dimensions comparable to those of the CL-415, as previously discussed.

#### 5.0.1 Transversal section considerations

With a water tank capacity of 6000 liters, the Bombardier CL-415 features a fuselage frontal section that can generally be inscribed within a rectangle of dimensions  $2.3 \times 3.0$  meters. With a capacity of 6 cubic meters, assuming rectangular cross-section tanks while maintaining a clearance of 50 centimeters between one tank and another to ensure adequate passage from the forward to the aft fuselage area for maintenance tasks or, potentially, operational purposes, and clearly observing from [?] that the length occupied by the tank is approximately 1.5 meters (estimated by analyzing fuselage sections without windows), we can estimate the fuselage cross-sectional area occupied by the tank and compute a geometric efficiency parameter.

$$Area = \frac{Volume}{Length} = \frac{6 m^3}{1.5 m} = 4 m^2$$
 (5.1)

Having determined that the area occupied by the tank is 4 square meters, and that the section can be inscribed within the previously indicated rectangle, we can calculate the gross geometric efficiency of the fuselage section as the frontal area of the tank divided by the area of the circumscribing rectangle.

The fuselage of the CL-415 is schematically represented in Figure 5.1, where the circumscribing rectangle can also be seen. Using AutoCAD, it is possible to calculate the fuselage cross-section and thus evaluate the average geometric efficiency, defined as the frontal area of the tank divided by the entire fuselage frontal area, conservatively assuming 5 cm thick walls.

If one considers increasing the water-carrying capacity of the aircraft, two solutions emerge: the first is to enlarge the cross-sectional area of the tank, and the second is to increase its length. Both alternatives present advantages and drawbacks.

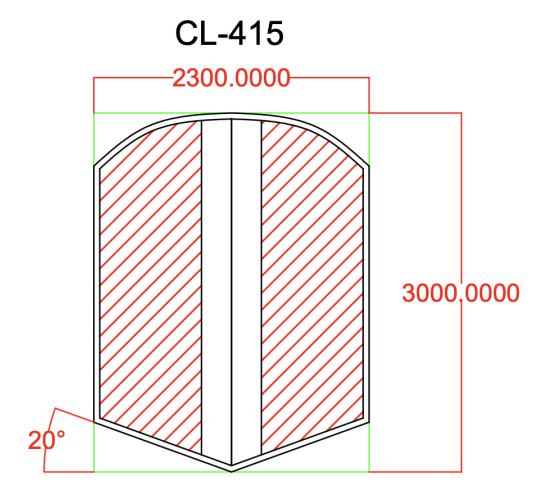


Figure 5.1: Front section CL-415

To increase the cross-sectional area, the fuselage can be made either wider or taller. Widening the fuselage can certainly be effective in increasing tank capacity, but it also leads to the drawback of greater aerodynamic drag generated by the fuselage. At the same time, enlarging the tank laterally produces only a limited effect on the water pressure at the drop outlet. Increasing fuselage height yields the same benefits in terms of water capacity, but due to intrinsic aspects of the box-wing configuration, the space available for the vertical tail is reduced, potentially affecting the aircraft's lateral and directional stability. On the other hand, enlarging the frontal section of the tank results in increased water ejection pressure, an important requirement for obtaining a coherent water column while maintaining a high coverage value.

Regarding tank length, the longitudinal direction offers greater geometric freedom, but attention must be paid to longitudinal stability. A very long tank complicates the task of keeping the payload center of gravity close to the overall aircraft center of gravity. In the case of the CL-415, estimates suggest that the tank is 1.5 meters long in the longitudinal direction, corresponding to about 7% of the aircraft's total length. This value must be taken into account and closely monitored. Since each dimension is critical at its upper limit, a trade-off must be performed, enlarging all dimensions in a balanced manner. A second fuselage concept is shown in Figure 5.2, from which both gross and net efficiencies can be calculated and compared in a table, also allowing for a direct comparison with the CL-415 fuselage, whose circumscribing rectangle is illustrated for clarity.

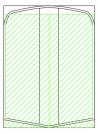


Figure 5.2: Confrontation between CL-415 and the new concept

In Figure ??, only the new concept is shown with its main dimensions. Compared to the

CL-415, the deadrise angle is reduced by 10° in order to improve planing performance.

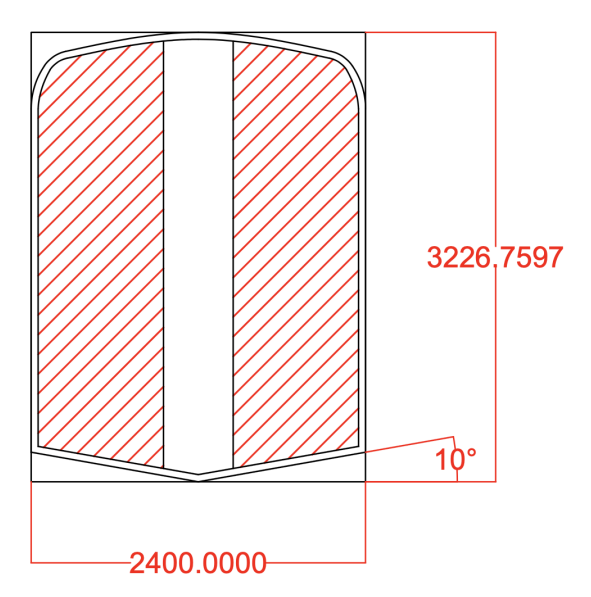


Figure 5.3: Concept fuselage section

	CL-415	Concept	Concept +10%	Concept +10% Height	Concept +10% Width
Rectangle	6.9	7.7	9.4	8.5	8.5
Fuselage section	6.7	7.8	8.2	6.6	7.4
Tank	4.2	5.3	6.4	5.8	6.0
Gross Efficiency	60.9%	68.8%	68.1%	68.2%	70.6%
Net Efficiency	62.7%	67.9%	78.0%	87.9%	81.1%

Table 5.1: Comparison between CL-415, Concept and scaled variants (+10%, +10% Height, +10% Width)

where gross and net efficiencies are defined as follows:

$$GrossEff = \frac{Tank}{Rectangle}$$
 (5.2)

$$NetEff = \frac{Tank}{FuselageSection}$$
 (5.3)

With the efficiencies and cross-sections defined as indicated above, the result shows that the efficiency in terms of utilization of the fuselage cross-sectional area occupied by the tank increases significantly more with an increase in fuselage width than with an increase in fuselage height. This occurs because the inter-tank spacing is fixed at 50 cm and therefore does not grow with fuselage width, whereas increasing the height also increases the cross-sectional area not occupied by the tank.

#### 5.0.2 Rounded fuselage option

Another option in the design of the fuselage cross-section concerns its shape; one possibility would be to adopt a more traditional rounded configuration. After the design of the fuselage section, it is necessary to draw the hull profile. For stability reasons, the bottom of the hull is designed with a deadrise angle of 10°, which helps keep the power requirement low while maintaining adequate lateral stability. Later, the addition of buoyant devices at the wing tips

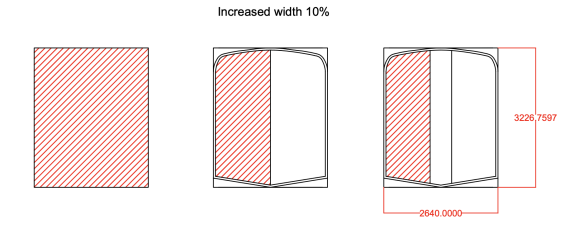


Figure 5.4: Concept Increased Width by 10%

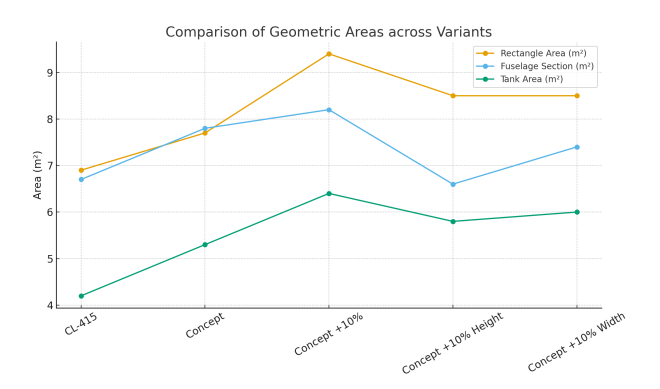


Figure 5.5: Caption

will be discussed; these increase stability during planing and help maintain the correct bank angle on the water. Introducing the hull profile into the fuselage section yields the final fuselage cross-section, which is wider than it is tall-an arrangement consistent with the box-wing lifting system, which requires space for the vertical tail surfaces.

#### 5.0.3 Overall design of the squared fuselage

Since the service ceiling of this aircraft is low enough for the cabin air to remain breathable, fuselage pressurization is not required. The environmental control system, however, must supply clean make-up air with reduced smoke content, which is likely in the aircraft's operational scenario.

Choosing an unpressurized configuration simplifies aspects of the fuselage design. In particular, the cross-section need not be circular: circular sections with rounded windows are typically adopted to mitigate stress concentrations from pressurization loads at corners. For this reason, the following figure illustrates a purposefully "squared" fuselage concept.

A more squared cross-section can improve volumetric efficiency in the bays housing the water tank and, for a given usable volume, can allow a reduction of external width, which may help reduce aerodynamic drag. These choices are enabled by the absence of pressurization loads, which would otherwise penalize non-rounded geometries. In Figure ?? a simplified representation of the fuselage section is provided. Clearly, the fuselage will not have a constant cross-section; the one shown is the largest section of the fuselage. Figure ?? also depicts the forward portion of the hull, which rises toward the nose to prevent it from submerging in the event of an improper maneuver. This design enhances longitudinal stability during the planing phase.

The most challenging task is to determine the appropriate location, shape, and dimensions of the water tank within the fuselage . As a first step, we define the water capacity: for this configuration, a value of  $13000~\rm L~(13\,m^3)$  is selected. Consequently, the fuselage must provide at least  $13\,m^3$  of usable volume. For reference, assuming a constant cross-sectional area of  $5.3\,m^2$ 

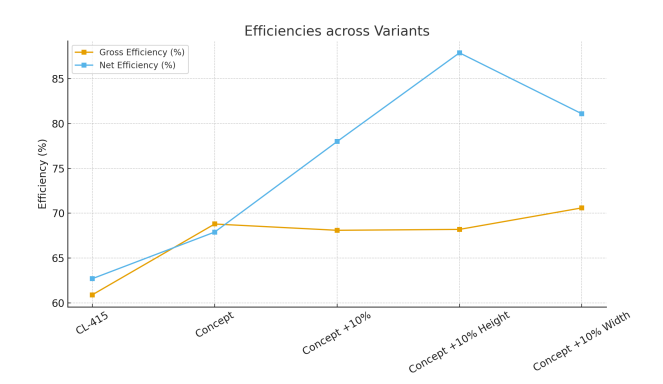


Figure 5.6: Caption

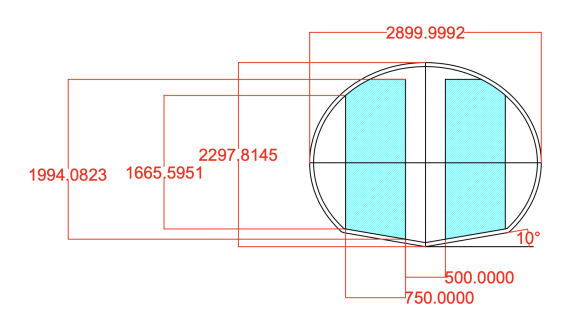


Figure 5.7: Front fuselage section

over a fuselage length of 20 m, the internal volume is approximately 106 m<sup>3</sup>.

From a mass-distribution standpoint, the tank should be placed as close as possible to the aircraft center of gravity (CG). Given that the water load is substantial-exceeding 30% of the aircraft mass-the overall CG will be strongly influenced by the tank position. By selecting the "Concept+10% Width" configuration, a possible tank cross-sectional area of 6 square meters is obtained, which, with a water capacity of 13,000 liters, results in a tank length of 2.166 m. Conversely, if the "Concept" cross-section is adopted, the water tank length becomes 2.4 meters. As previously stated, the shorter the tank, the better it is in general for both the dynamics and statics of the aircraft under different flight conditions. As a first attempt, the "Concept+10% Width" configuration is therefore selected.

In this preliminary configuration, the tank CG is located near the mid-fuselage section, as shown in Figure 5.8.

In this lateral section, an initial position of the forward wing is set to assess the feasible tank capacity. A structural step is retained in the tank geometry to preserve space for the wing carry-through that passes through the fuselage.

The relative position of the hull step and the water intake is critical. The intake must lie on a portion of the hull that remains wetted over a wide range of trim angles. The safest location is typically between the bow and the step, near the mid-hull region: if placed too far forward, the intake may ventilate and emerge from the free surface at higher trim; if placed too close to the step, the incoming flow can be highly disturbed or even separated, degrading refill efficiency. Accordingly, a short duct is routed from the selected intake location to the tank to ensure adequate flow and to minimize refill time. Finally, there is a constraint on the vertical (z) position of the forward wing. In some configurations, the wing may need to be mounted higher above the water to avoid interference with spray.

For this hull, to allow the water intake to properly work, the type of planning hull used is



Figure 5.8: Lateral section of the fuselage with tank

conventional.

This new fuselage section, as noted above, offers the advantages of a reduced width and increased efficiency in the use of inboard space. In Figure 5.9 a detailed view highlights the improved utilization of the sections that house the water tank. The tank capacity remains the same as in the rounded-section configuration, and a clearance of 0.5 m is left along the centerline to provide access to the aft part of the fuselage. In this figure the floor is not shown; however, a floor is provided, and systems can be installed beneath it, ensuring sufficient space for their placement. The rounded ceiling has been retained to help mitigate aerodynamic drag. With respect to figure 5.7 we can compute the improvement in terms of efficiency in space using. For the rounded design

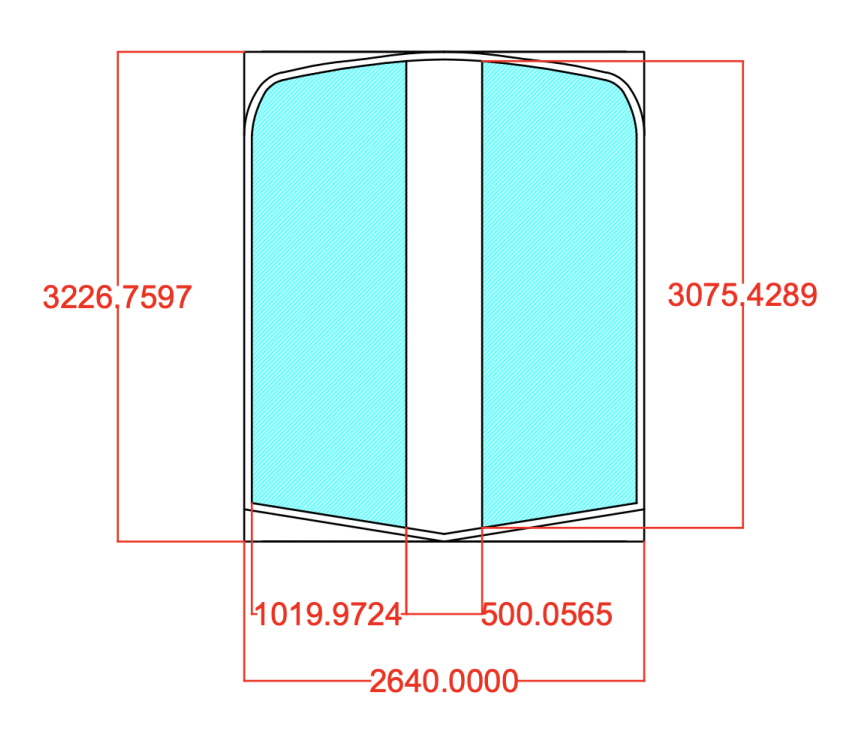


Figure 5.9: Front Section with a focus on tank placement

### 5.1 Design of the front and the rear sections of the fuselage

The front and rear fuselage sections are critical parts of the aircraft. In this case, the main issues are the following:

- The spray generated during refill must not obscure the pilot's visibility; therefore, the hull must be designed with an appropriate bow shape to deflect spray away from the windshield [6].
- The hull bow prevents nose submersion during planing, thereby enhancing spray control and improving the overall hydrodynamic stability of the seaplane
- The nose and the pilot seat must ensure excellent visibility on the ground, on water, and in flight [7].
- The rear section must guarantee adequate clearance from both the ground and the water; since this is a conventional planing hull, a tail contact point is not acceptable.

The fuselage should be as thin as possible to reduce aerodynamic drag and, as discussed in a previous chapter, to minimize hydrodynamic drag as well.

The nose section as said before has to provide good visibility both for land, air and water operation.

The idea is to guarantee visibility at least 3.5 meters ahead of the airplane's nose; therefore, the pilot's head position (and consequently the seat position) must be arranged accordingly.

In the figure 5.10 a possible representation of the seat position with consideration on the visibility. The situation represented in 5.10 is in planning condition with a  $\tau$  selected value of 1°:

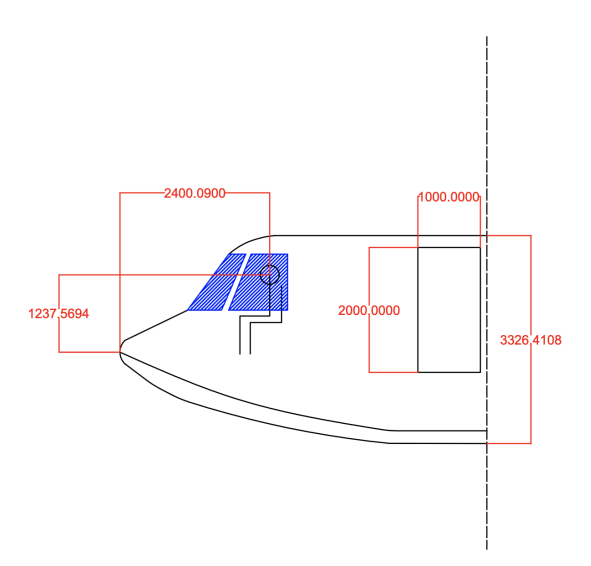


Figure 5.10: Lateral view, visibility of the pilot

On land, the same procedure is used to estimate the landing gear height and is illustrated in Figure 5.11. The figure shows the cockpit visibility when the airplane is on the ground.

When the aircraft is on the ground, the forward visibility distance is 5.787 m, which is greater than on water due to the presence of the landing gear.

With regard to the aft fuselage, the primary concern is to prevent contact with the water during planing and to avoid tail strikes during takeoff and landing on land.

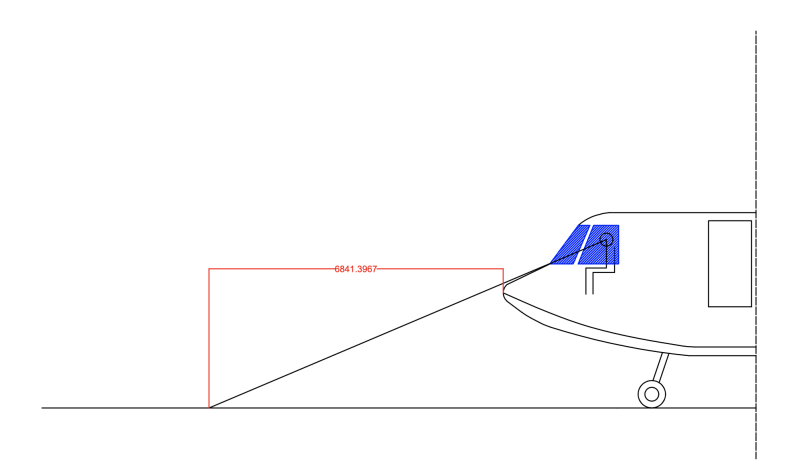


Figure 5.11: Lateral view, visibility of the pilot

In Figure 5.8, the lateral layout of the fuselage is shown. As can be seen, the relative positions of the main landing gear, the water tank, and the hull step are critical. The tank should be located near the aircraft center of mass and, as a first approximation, at mid-fuselage. The front wing is likely positioned ahead of the center of mass; however, as evident in Figure 5.8, its location affects the tank capacity. The main landing gear-which must be retractable cannot be installed in the fuselage bays that house the tank due to lack of space. Since the tank is located near the aircraft center of mass, the main landing gear will, reasonably, be placed aft of the tank but forward of the step, although the structural arrangement will differ and the main landing gear will be longer than in the example shown in Figure 5.12.

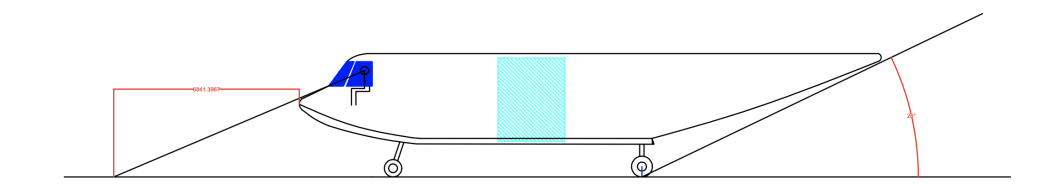


Figure 5.12: Lateral view, tank and landing gear

The landing gear bay will be located within the hull sections of the fuselage. This is a critical area because the hull is submerged during water operations; therefore, the bay must be watertight to protect the landing gear and its associated systems.

The next figure shows the landing gear retraction layout. This layout is indicative rather than precise and should be regarded as an estimate. From the bottom view, it is also possible to see the hull step, which, as noted above, is positioned to optimize its interactions with the other components. As stated in [3], the planform of the hull step is not straight but V-shaped; however, this shape has only a limited impact on the overall hydrodynamic performance of the hull.

The need to install spray chines (spray rails) is clearly stated in [15], which emphasizes that controlling spray is essential; otherwise, significant propeller damage may occur. Spray

chines are specifically designed to deflect the spray downward and away from the propeller (and windshield), thereby reducing ingestion and erosion risks. With these hull dimensions, the refill time is guaranteed to be under 120 seconds at a speed of 50 m/s, ensuring complete filling using the water intake shown in Figure 5.7. Fuselage-wing integration is crucial, both for aerodynamic performance and because the front wing will be located in close proximity to the water tank.

An example of the spray-chine (spray-rail) layout is shown in Figure 5.13. As can be seen, the chines disrupt the water sheet that tends to form on the hull-since water naturally adheres to metal-thereby deflecting the spray in a less damaging direction.

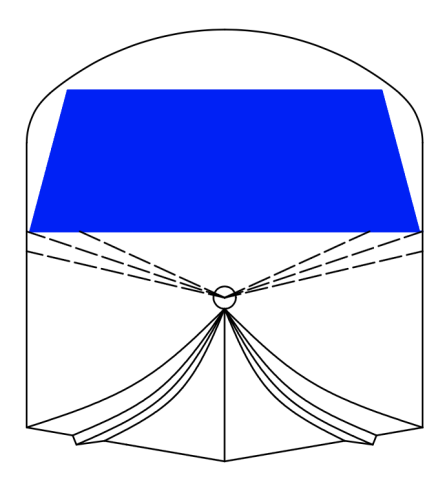


Figure 5.13: Spray chines front view

The cockpit window layout must provide the best possible external visibility while also ensuring easy reach of all controls. The main windshield is large and has a trapezoidal shape to optimize dimensions. Compared with a pressurized aircraft, windows represent a less penalizing design element: in pressurized fuselages, each opening typically requires structural reinforcement that can add several times the mass of the skin material removed. A large windshield improves both forward visibility and lateral field of view, which is particularly important in this context for target recognition and operational safety.

To enhance lateral visibility and the overall field of regard, two additional side windows are provided near the pilots' heads so that, by turning, they can maintain good situational awareness of the operational area. As shown in Figure ??, the windshield layout also accommodates the installation of an overhead control panel, which will be implemented the angle of view of more than 150° for each pilot.

In Figure 5.15, the 60 cm seat width can be appreciated, leaving ample space for the center console that houses the thrust levers and engine controls.

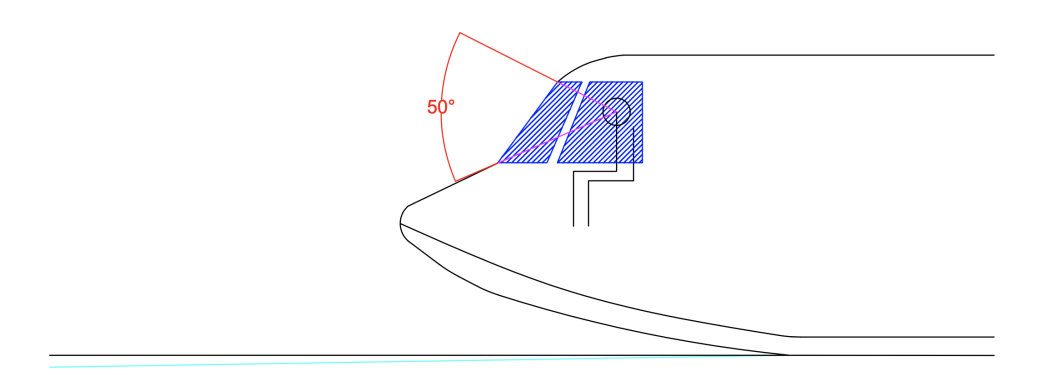


Figure 5.14: Lateral view cockpit window

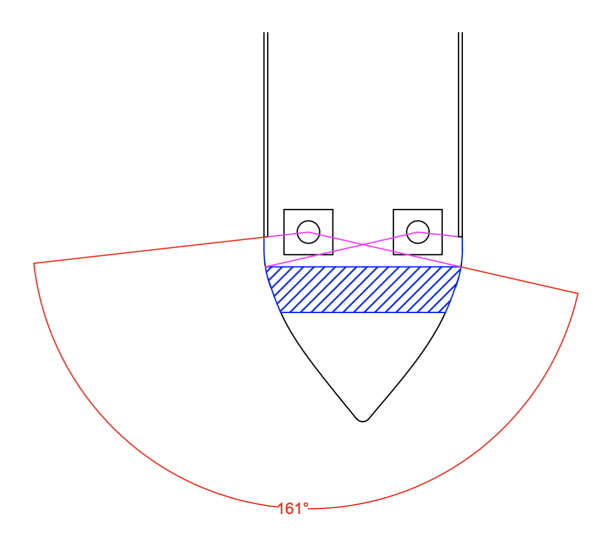


Figure 5.15: Top view cockpit window

## Chapter 6

# Design of the plane and results

The results presented here are the outcome of a design process illustrated in Figure 6.1.

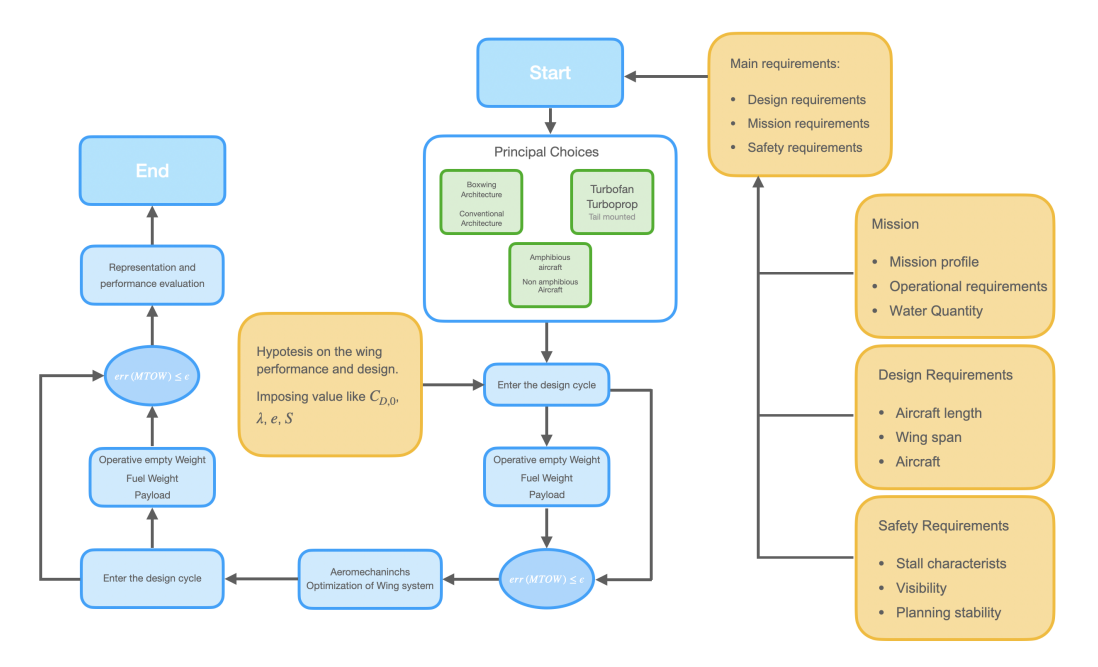


Figure 6.1: Design workflow for this design

Figure 6.1 illustrates the process followed for the aircraft design. The starting point, as is often the case, derives from various types of requirements: some originate from stakeholders' needs, others from regulatory constraints, and others from benchmarking against competitors in the sector, most notably the CL-415. At the starting point, three main categories of requirements can be identified: design requirements, mission requirements, and safety requirements.

Regarding the design requirements, these are mainly derived from comparison with the Bombardier CL-415. As mentioned earlier, this aircraft represents the primary amphibious airplane employed in aerial firefighting. Assuming that operators worldwide are already adapted to this standard, it is advantageous to maintain overall dimensions similar to those of the CL-415, which yields significant logistical benefits. The general dimensions of the CL-415 are a length of about 19-20 meters and a wingspan of 28 meters. These dimensions are therefore retained.

Mission requirements are derived both from comparison with competitor aircraft and from the analysis of wildfire phenomena, which constitute the operational scenario of the aircraft. As for the mission profile, the reference is taken from the profile proposed in [14], where a comparative analysis of various firefighting aircraft is provided. The mission is defined as reported in the table below.

The amount of water carried on board represents a key parameter that strongly influences the

Table 6.1: Mission parameters for the firefighting aircraft (extracted from MATLAB code)

Phase	$z_{\rm start}$ [m]	$z_{\mathrm{end}}$ [m]	ramp [°]	IAS [m/s]	Dur. [s]	type	n	$\varphi$
TAXI	0.0	0.0	0	0.00	600	1	1	0.07
TAKE-OFF	0.0	0.0	0	0.00	60	1	1	_
Climb-1	0.0	1524.0	5	77.17	0	2	1	_
Cruise	1524.0	1524.0	0	77.17	1800	3	1	_
Descent-1	1524.0	457.2	-5	77.17	0	2	1	_
Descent-mission	457.2	0.0	-5	77.17	0	2	1	_
Drop	0.0	0.0	0	36.01	120	3	2	_
Climb-mission	0.0	457.2	5	77.17	0	2	1	_
Cruise-mission	457.2	457.2	0	77.17	480	3	1	_
Tank-Refill	0.0	0.0	0	0.00	120	1	1	1.00
Climb-final	457.2	1524.0	5	77.17	0	2	1	_
Cruise-final	1524.0	1524.0	0	77.17	1800	3	_	_
Descent-final	1524.0	0.0	-5	77.17	0	2	1	_

Note: mission.Cycles = 8 (number of refill/drop cycles). "type": 1 = constant-power phase; 2 = climb/descent (fixed slope, constant IAS); 3 = uniform rectilinear motion (constant IAS and altitude). "n" denotes the number of repetitions of the phase. Undefined fields are indicated with "-".

aircraft's performance. If the same flight capabilities of the CL-415 can be preserved, increasing the transported water volume constitutes a significant improvement in overall performance. However, substantially increasing the water capacity is not a straightforward task, as several limiting factors come into play:

- Structural limitations
- Flight speed limitations
- Aircraft dynamic limitations

Structural limitations refer to the fact that excessive payload requires increased reinforcement of primary structures, which in turn leads to an overall structural weight increase. Flight speed limitations are related to the need to trim the aircraft along the pitch axis. For a given lift coefficient, increasing the aircraft weight raises the wing loading. A higher wing loading requires a higher flight speed to maintain trimmed conditions, as shown in the following equation:

$$\frac{W}{S} = \frac{1}{2}\rho V^2 C_L \tag{6.1}$$

From this equation, it can be seen that an increase in weight requires either a higher lift coefficient-possibly obtained through the adoption of high-lift devices-or an increase in reference wing area. The former approach is limited by stall conditions, since increasing  $C_L$  implies raising the angle of attack, which eventually leads to aerodynamic stall. The latter approach, i.e. increasing wing area, is often adopted by aerodynamic optimization software such as Aerostate. However, as wing area grows, so do form drag and parasite drag, reducing aerodynamic efficiency. Thus, keeping aerodynamic efficiency as the objective function may not be ideal in this context, since the main goal is not maximizing efficiency but ensuring the ability to operate at very low speeds with heavy payloads. Increasing wing area is therefore also subject to an upper bound. An alternative way to maintain trimmed flight is to raise flight speed, but this would move the configuration away from the intended design objective.

As for safety requirements, these are necessarily stringent for this type of aircraft. Regarding stall characteristics, the adoption of a box-wing configuration can be particularly advantageous. Indeed, having two separate wings modifies the stall mechanics compared to a conventional layout, as explained in [?]. In a stable box-wing configuration, the forward wing carries a

higher load than the rear wing, meaning that the forward wing stalls at lower incidence angles. Consequently, when the lift generated by the forward wing collapses, the rear wing still operates in nominal conditions. This naturally generates a nose-down pitching moment, akin to a stall recovery maneuver. As a result, stall characteristics are significantly more favorable in a boxwing layout compared to a conventional one.

Concerning visibility, which must be excellent in this type of aircraft, it primarily depends on fuselage design. The presence of the hull does not inherently provide an advantage, but improvements can be achieved through specific design adjustments. Finally, regarding stability during water landing (planing) phases, it is essential to account for a deadrise angle, hypothetically set around 10-20°. The addition of supplementary planing-stability devices at the wing tips is already foreseen at this stage.

For a solid starting point in the design cycle, it is necessary to make some crucial decisions at the beginning of the work. The three main choices concern:

- Propulsion
- Firefighting typology
- Wing architecture

Regarding propulsion, as highlighted in the chapter dedicated to the matching chart, the difference between the thrust-based and power-based diagrams is evident. In the case of power, it is clear that the phases related to refill and drop are significantly less demanding. Since these occur at low altitude and generally at low speed, propeller-driven configurations prove more suitable. In terms of thrust, however, the refill and drop maneuvers are indeed the most sizing-critical phases of the flight, whereas for an aircraft equipped with turbofan engines the power demand would be excessive. From this perspective, the choice is almost compulsory and directly derives from the mission characteristics.

As for the second choice, concerning the firefighting typology, the decision stems from the discussion presented in Chapter 1 on the state of the art. Amphibious aircraft of the scooper category represent an attractive solution, as they constitute a good trade-off between the other categories of airplanes and the available helicopters. For this reason, the scooper amphibious type is selected.

Finally, regarding the choice of the box-wing architecture, it should be noted that, as previously discussed in relation to aerodynamic performance, it is difficult to envision an aircraft with overall dimensions comparable to those of the CL-415 without adopting a biplane-type configuration. Considering the goal of carrying a significantly larger amount of water, while avoiding an excessive increase in overall dimensions-and thereby maintaining a reasonable compromise between maneuverability and effectiveness, as well as ensuring the feasibility of the necessary drop and refill maneuvers-a biplane configuration such as the box-wing becomes a necessary solution.

The design cycle, as explained in the section on weights, is aimed at determining the crucial value of MTOW (Maximum Take-Off Weight), which characterizes the aircraft. The MTOW is the maximum take-off mass of the aircraft and has fundamental importance because it represents the design reference for several components of the vehicle, as it corresponds to the most critical loading condition.

Within the design cycle, the goal is essentially to achieve convergence of the MTOW value, calculated as:

$$MTOW = OEW + W_{pay} + W_{fuel} (6.2)$$

For the calculation of the OEW value, it is necessary to estimate the structural mass of the wing. To perform this operation, a reasonable wing shape must be assumed in order to carry out the calculation in the most realistic way possible, without having precise knowledge of its final geometric configuration.

In this section, it is necessary to calculate the weights of the components indicated using the models described in the weight chapter, while relying on the matching chart diagram to determine the specific power value to be assigned to the aircraft. This allows the evaluation of the engine weight and, consequently, the weight of the nacelle and propeller if present.

In the future, an integration between a weight estimation method and the Aerostate software should be developed in order to provide updated and consistent estimates within the tool regarding component masses and centers of gravity.

As for the fuel mass, which is a fundamental component of MTOW, it is necessary to perform the mission simulation as described in the corresponding chapter. The fuel mass depends mainly on the mission profile, the engine specific fuel consumption, and of course the aerodynamic characteristics of the aircraft under consideration. To perform this calculation, it is necessary to assume some parameters such as the wing reference area, the Oswald efficiency factor, and the drag coefficient  $C_{D,0}$ . Based on these values, it is possible to calculate the required flight power at each instant and, from this, the corresponding fuel consumption.

The payload in our case is entirely assimilated to the weight of the water carried on board, with no other useful load considered. This value can be set a priori according to the most suitable criterion. One example of determining a reasonable value for this parameter may be based on the wing reference area. For instance, if the CL-415, with a wing area of about  $100 \ m^2$ , carries approximately 6000 liters of water, hypothetically doubling the wing area could allow for doubling the water capacity. If the forward wing were assumed to be similar in size to that of the CL-415 and a rear wing were added, bringing the total wing area to around  $200 \ m^2$ , the water capacity could hypothetically reach about 12000 liters. Since the surface area will not be exactly doubled and not all parameters scale proportionally, further considerations are required. As a first attempt, however, it may be reasonable to set the water quantity to 12000 liters or slightly less to evaluate the results.

After the weight calculation, we obtain a considerable amount of additional information useful for the subsequent steps. As shown in Figure 6.1, the aerodynamic optimization phase essentially consists in performing the operations described in the aerodynamics chapter. In practice, the code, taking as input a plausible assumed wing, the selected design condition, and the defined boundaries and constraints, outputs a new wing that satisfies these parameters and, among all possible configurations, also seeks to maximize efficiency while meeting flight stability and trim requirements.

Once this wing is obtained, thanks to the use of Aerostate, the process continues with the final step, namely the recalculation of the aircraft weights. The variation in wing geometry requires a new weight evaluation which, through the in-house tool for wing weight calculation described in the structures chapter, is able to capture differences with respect to the initial attempt, including twist, dihedral, and overall geometry.

After this weight calculation, a complete mass breakdown of the aircraft is obtained, with all general characteristics defined, making it possible to assess the overall performance.

Regarding the design process, it should be specified that, as previously mentioned, the aerodynamic optimization step should ideally be included within the MTOW determination cycle. However, due to the relatively long computation times of the Aerostate software, which are on the order of hours, in this preliminary phase it is more convenient to maintain the flow as described in Figure 6.1.

### 6.1 First Weight results

In the previous section, an overview of the overall project workflow was presented. The results of the aircraft mass computations are reported below. These values pertain to the initial portion of the code and do not yet include the aerodynamic optimization.

Table 6.2: Aircraft data summary

Parameter	Value	Unit
Constants and standard atmosphere		
g	9.81	$\mathrm{m/s^2}$
$ ho_{SL}$	1.225	$kg/m^3$
$\gamma$	1.4	_
Kinematic viscosity of water	8.9e-7	$\mathrm{m}^2/\mathrm{s}$
Performance / power		
P/W (first guess)	550	W/kg
$k_p \text{ (from 0.282 kg/kWh)}$	7.833e-8	$\mathrm{kg}/\mathrm{J}$
Wing and aerodynamics		
Wing area $S$	150	$\mathrm{m}^2$
Wingspan $b$	28	m
Aspect ratio $AR$	8	_
Oswald factor $e$	1.35	_
$C_{D0}$	0.03	_
Fuselage		
$\operatorname{Length} L$	21.450	$\mathbf{m}$
Mean diameter $D$	2.82	$\mathbf{m}$
Fuselage area $S_f$	141	$\mathrm{m}^2$
Hull		
Hull width $b_{ m hull}$	2.00	m
Immersion/height $d$	0.15	m
Trim $ au$	1	$\deg$
Dead-rise angle $\beta$	10	$\deg$
Water payload		O
Water onboard	12500	kg
Piping/press. volume	189.271	$\Gamma$
Landing gear		
Main gear factor $K_{mp}$	1.126	_
Initial landing weight $W_i$	13000	kg
Number of landings $N_l$	1.5	_
Main gear stroke $L_m$	0.90	m
Main gear wheels $N_{mw}$	2	_
Shock struts $N_{mss}$	1	_
Nose gear factor $K_{np}$	1.1	_
Nose gear stroke $L_n$	2.4	m
Nose gear wheels $N_{nw}$	2	_
Nacelles / pylons		
$K_{nq}$	1.0	_
Nacelle length Nlt	2.0	m
Nacelle width $Nw$	0.5	m
Nacelle area $S_n$	2.60	$\mathrm{m}^2$
	1.5	m
Vertical tail height	1.0	
Vertical tail height Engines / propellers		_
Vertical tail height	2 17	– m

Parameter	Value	$\mathbf{Unit}$
Single engine mass	700	kg
Propeller diameter	4	$\operatorname{ft}$
Avionics / systems / cabin		
Control functions $N_f$	6	_
Mechanical functions $N_m$	2	_
Controlled surface area	3.8	$\mathrm{m}^2$
Lateral inertia $I_y$	1.3e7	${\rm kgm^2}$
Uninstalled APU	100	kg
Avionics factor $K_t$	1.0	_
Instrument panels factor $K_{tp}$	0.793	_
$\text{Crew } N_c$	2	_
Usable fuselage length	11.913	$\mathbf{m}$
Electrical network factor $R_{kvva}$	2.0	_
Wiring length	30	m
Generators $N_{gen}$	2	_
Avionics/utilities	400	lb
Cell weight $W_c$	10000	kg
Pressurized volume $V_{pr}$	141	$\mathrm{ft^3}$
Cargo floor area	200	$\mathrm{ft}^2$

In the case of the MTOW values, these are preliminary estimates that will be updated over the course of the iterative cycle. As noted above, the MTOW is determined iteratively as

$$MTOW = W_{pay} + OEW + W_{fuel} + W_{crew}. (6.3)$$

The computational workflow is illustrated in Fig. 6.2.

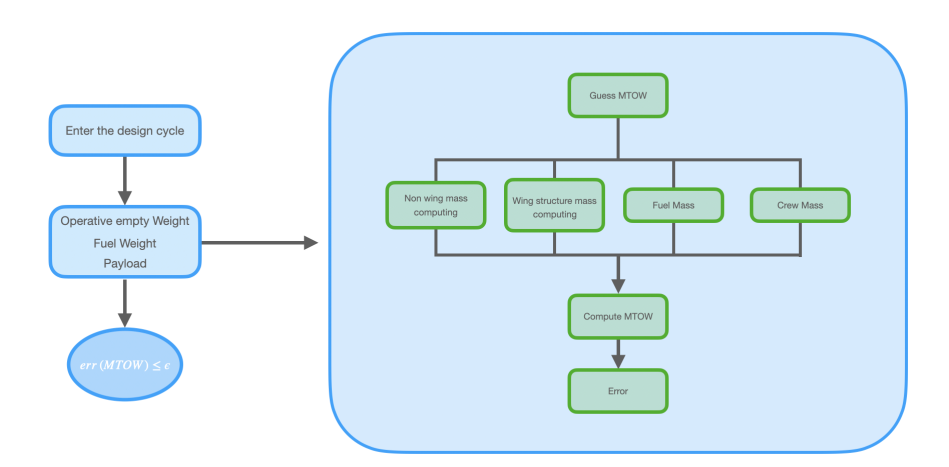


Figure 6.2: MTOW computing flow

The calculation typically converges within at most five or six iterations when a tolerance of 10 kg on MTOW is enforced. Since this is a preliminary study, adopting a tolerance of 100 kg is a reasonable option to accelerate the computation.

The results corresponding to the data reported in the previous table are summarized below.

MTOM [kg] = 28871.3  
Wing weight [kg] = 4681.8  
No-wing weight [kg] = 9109.2  
OEW [kg] = 13791.0  
Fuel mass [kg] = 2280.9  
Water payload [kg] = 12500.0  
Crew mass [kg] = 300.0  

$$M_{\text{fuel}}/\text{MTOM}$$
 [%] = 7.9001  
OEW/MTOM [%] = 47.7672  
Water/MTOM [%] = 43.2956  
Crew/MTOM [%] = 1.0391

A sensitivity analysis with respect to the variable WaterQuantity is now presented. WaterQuantity denotes the amount of water that can be stored on board and is specified as an input. Its lower bound is set by design requirements: reducing it excessively would yield an aircraft with overall firefighting performance comparable to that of the CL-415. Although such a choice is not necessarily undesirable-the adoption of a box-wing would in any case provide higher efficiency-here we choose not to consider values below 8,000 L.

The mass distribution relative to MTOM as a function of the water quantity is shown in Fig. 6.3.

ACQUA [kg]	MTOW [kg]	ALA [kg]	ALTRO [kg]	FUEL [kg]	OEW [kg]
6000	21065	4375	8295	2093	12670
6500	21646	4398	8343	2104	12741
7000	22229	4421	8391	2116	12812
7500	22812	4444	8439	2128	12883
8000	23396	4467	8487	2142	12954
8500	23980	4489	8534	2156	13035
9000	24566	4513	8582	2169	13095
9500	25149	4536	8630	2183	13165
10000	25734	4559	8678	2197	13236
10500	26319	4582	8725	2212	13306
11000	26904	4604	8772	2227	13377
11500	27490	4628	8820	2242	13448
12000	28075	4651	8867	2258	13518
12500	28661	4674	8915	2273	13588

Figure 6.3: Mass distribution vs. Water Quantity

Figure 6.4 and 6.5 depicts the trends of the various masses and their mass fractions as WaterQuantity varies at the design condition.

As evident from Fig. 6.5, MTOM increases with the water quantity, as expected. Consequently, an upper bound on WaterQuantity is imposed: an excessively large MTOW would drive an unduly high design value of W. Nevertheless, WaterQuantity should be kept as high as practicable to maximize firefighting effectiveness.

The fuel mass fraction decreases slightly as the water mass increases, simply because fuel mass grows only modestly whereas MTOW grows more rapidly, thus reducing the fuel percentage. The water fraction relative to MTOM increases with WaterQuantity; in the operating range considered here, the growth of MTOW is slower than that of WaterQuantity, which explains the observed trend. One may hypothesize the existence of a regime-irrelevant in practice because

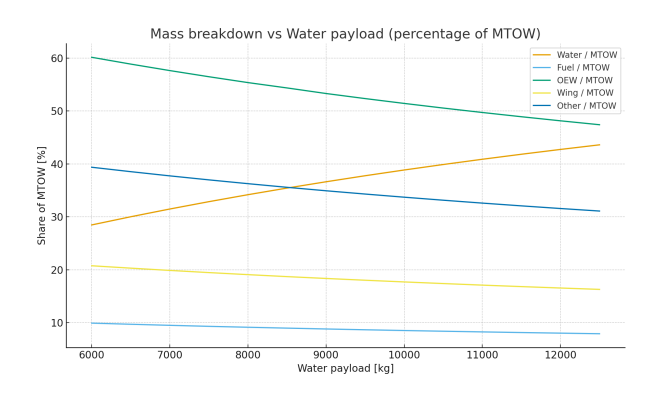


Figure 6.4: Mass distribution percentage vs. Water Quantity

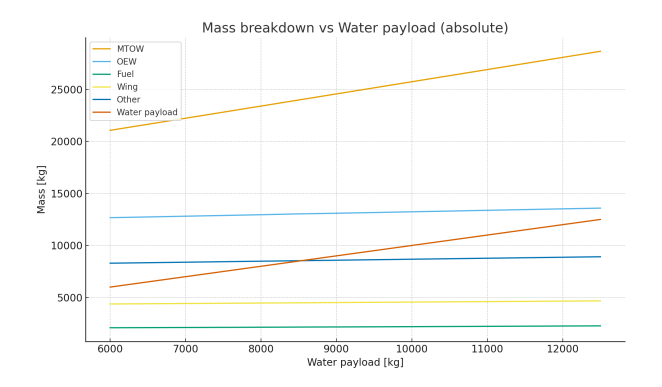


Figure 6.5: Mass distribution vs. Water Quantity

of the aforementioned aeromechanical constraints-in which this curve would attain a horizontal tangent and eventually decrease.

In these regimes, the OEW increases more slowly than the water mass; similarly to MTOW, a horizontal asymptote with a subsequent reversal is expected at sufficiently large values.

Finally, the crew mass fraction relative to MTOM decreases monotonically because the crew mass is fixed at 300 kg while MTOW increases.

Based on the previously presented data, the components of the OEW are distributed as shown in Fig. 6.6. This diagram is important because it illustrates how the weights are apportioned among the various aircraft components, excluding payload and fuel.

These values pertain to the initial stage of the MTOW determination, that is, prior to the aerodynamic optimization process carried out using the Aerostate software. Thanks to this initial assessment of the aircraft mass properties, it is possible to properly initialize the Aerostate software, thereby obtaining meaningful solutions.

In general, the results of this aircraft mass analysis indicate that structural strength does not limit the amount of water carried on board. We are not in a regime where increasing payload mass leads to an uncontrolled growth of total weight; rather, the total weight increases approximately linearly. The true limit on the water quantity is therefore imposed by aerodynamic constraints.

### 6.2 Aerodynamic optimization

To proceed with the design process, it is necessary to perform the aerodynamic optimization of the aircraft wing. As input data, the values derived from the preliminary estimation of the MTOW must be used. The numerical optimization yields several possible wing configurations that can be implemented in the overall aircraft layout. The Aerostate software, being both a

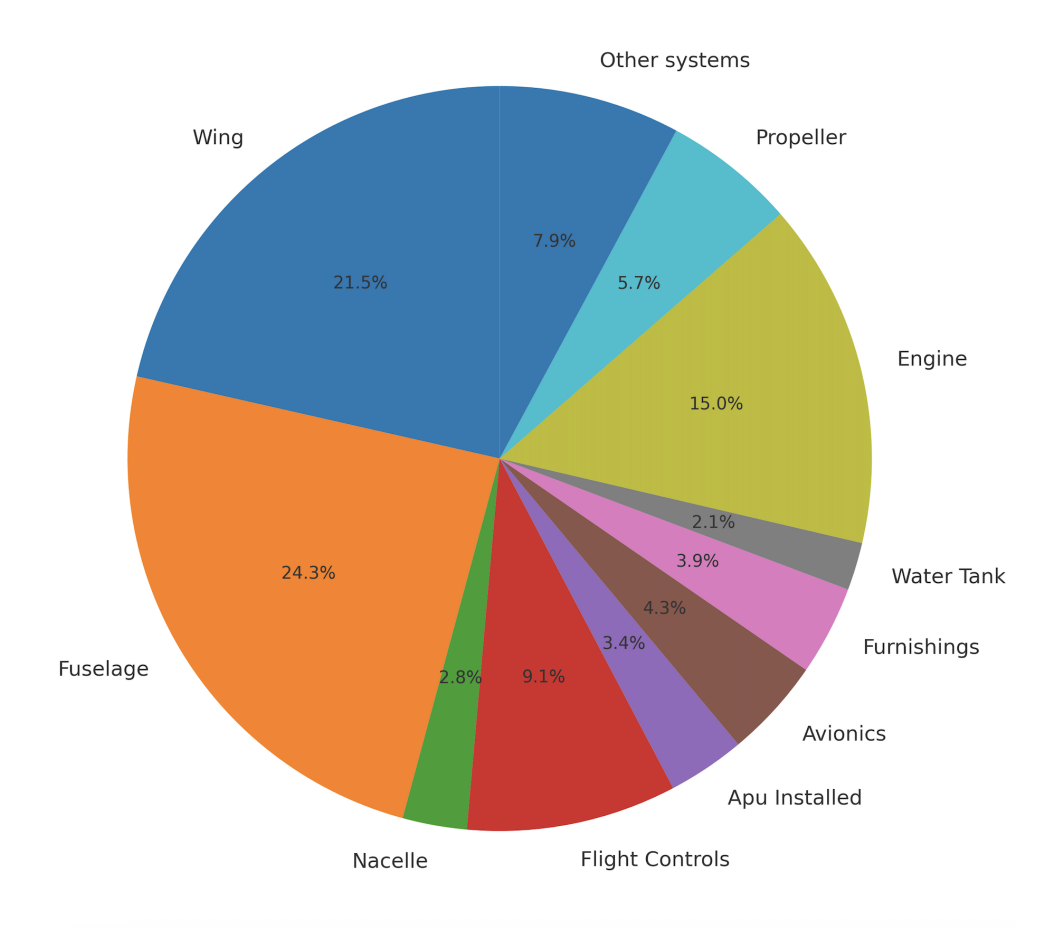


Figure 6.6: Mass Breakdown

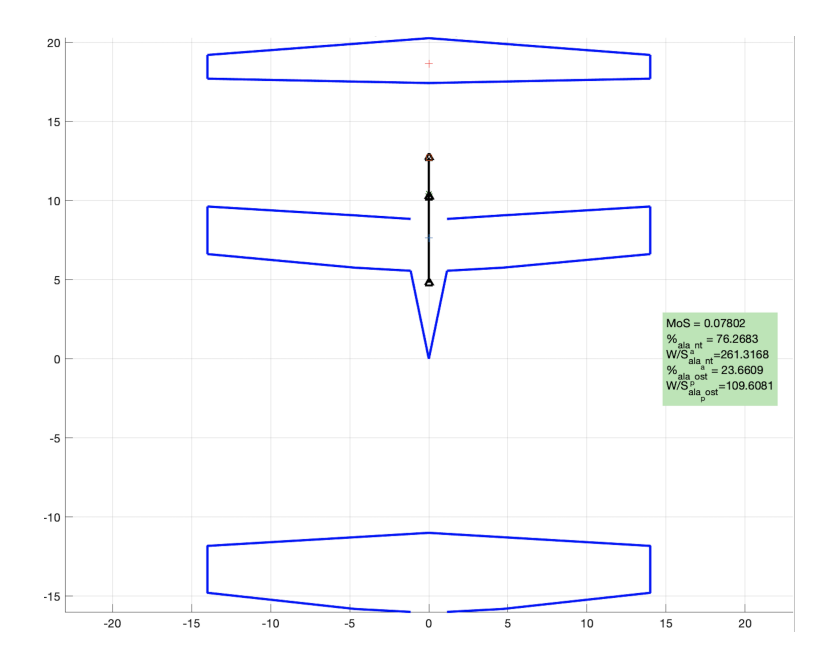
global and local optimizer as previously discussed, explores the local minima of the objective function within the design space to identify the existence and position of a possible global optimum. Among the configurations proposed as output by the software, it is up to the designer to select the most appropriate one based on parameters related to small or large shape variations among the available options.

The criterion adopted in this work was to select the configurations provided by Aerostate according to the following parameters:

- Aerodynamic efficiency value
- Compliance with constraints
- Positivity of the stability margin
- Stability margin value
- Wing loading values of both front and rear wings
- General visual assessment of the planform shape
- Other aerodynamic parameters characterizing the configuration

Based on these parameters, it is possible to analyze the different outputs in order to equip the aircraft with an optimized wing system.

An example of Aerostate output, obtained using the settings defined in the previous chapters, is shown in Figure ??.



Example of wing planform

Quantity	Value
	20.00
Objective $F_{\text{val}}$ Lift to drag $L/D$	-20.92 $20.92$
Constraint level	0.0302
Margin of safety (MoS)	0.0302 $0.078$
% Front Wing	76
W/S - Front Wing	261
% Rear Wing	24
W/S - Rear Wing	110

Figure 6.7: Optimization snapshot. Left: planform and constraint envelopes. Right: numerical indicators transcribed from the original plot.

In Figure 6.8, the mean aerodynamic surface of the wing in three-dimensional space and the corresponding panel discretization used by AVL for aerodynamic computation are shown. Using AVL, it is also possible to obtain an estimation of the aerodynamic derivatives. Based on the data provided by the software, the optimized wing version can be represented, and the calculations can be repeated using the updated information to obtain a definitive mass breakdown of the aircraft.

After the second weight evaluation step with the modified wing, a new weight configuration is obtained compared to the previous iteration.

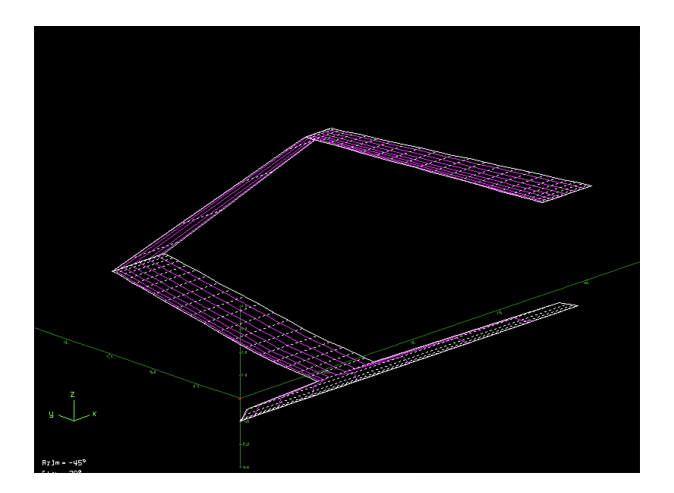


Figure 6.8: 3D view of the mean aerodynamic surface

Thanks to the optimization of the lifting system, a preliminary three-view drawing of the configuration can be obtained, as shown in Figure 6.9.

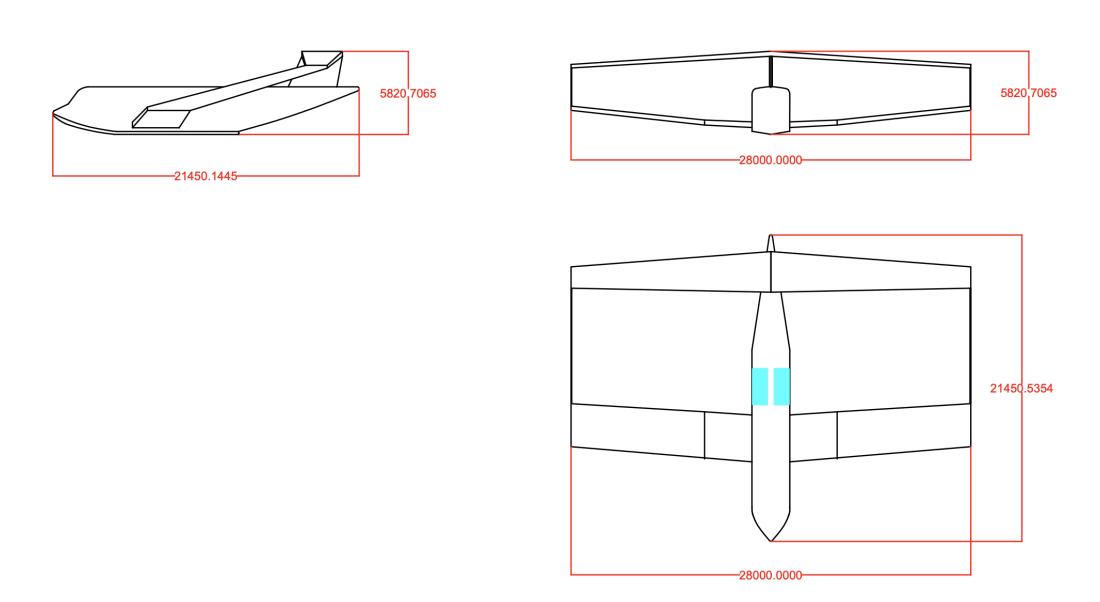


Figure 6.9: Three-view drawing of the configuration

Dopo l'ottimizzazione aerodinamica è possibile fornire un nuovo risultato di masse e distribuzione di masse del velivolo calcolate con la nuova ala e le nuovew prestazioni aerodinamiche.

MTOM [kg] = 27206
Wing weight [kg] = 3802
No-wing weight [kg] = 9017
OEW [kg] = 12819
Fuel mass [kg] = 1460
Water payload [kg] = 12500
Crew mass [kg] = 300.0
$$M_{\text{fuel}}/\text{MTOM}$$
 [%] = 5.73
OEW/MTOM [%] = 47.12
Water/MTOM [%] = 45
Crew/MTOM [%] = 1.1

As can be seen, the mass breakdown does not change much across configurations, which is reassuring from a computational standpoint. Only a few iterations are required to achieve weight convergence, since the variations are already negligible at the first iteration. Additional configurations are generated by the optimizer, and these designs should not be discarded a priori.

### 6.3 Performances

With regard to the calculation of aircraft performance, some considerations must be made in order to evaluate it accurately. A first interesting figure of merit for the new aircraft could be related to the amount of water contained in the retardant tanks. This essentially represents a key function for this type of aircraft, as it directly influences its effectiveness. The number of cycles also affects effectiveness, since completing a load and drop cycle takes less time than performing a refueling on the runway. The mission simulation allows us to compute the total mission time and, of course, the total amount of water released during the entire mission, thus leading to a parameter defined as:

$$E = \frac{Water}{Time} \tag{6.6}$$

where Water is the total amount of water released and Time is the total mission duration. This parameter, which can be calculated, depends essentially on how the mission is designed and on the amount of fuel or water that can be loaded.

To determine which of the configurations produced by the optimizer is superior to the others, aside from geometric features that the designer may evaluate subjectively, we introduce the Water Mission Energy Efficiency (hereafter WMEE). This quantity is analogous to the Payload Range Energy Efficiency (PREE), a useful parameter for evaluating the performance of civil transport aircraft, which quantifies the energy efficiency for transporting each passenger during the chosen design mission. In the present case, since the machine is not strictly a transport aircraft, it is not meaningful to refer to concepts such as range or loiter. Our objective is not to cover as much distance as possible, nor to remain airborne as long as possible, but rather to execute the largest possible number of operation cycles, thereby increasing effectiveness by reducing on runway refueling and turnaround times that drastically limit functionality. The payload range energy efficiency is defined as:

$$\mathbf{PREE} = \frac{W_{\mathbf{pay}} \cdot r}{E_{\mathbf{bf}}} \tag{6.7}$$

where:

•  $W_{pay}$  is the payload mass,

- r is the mission range,
- $E_{\mathbf{bf}}$  is the energy in J, computed as the mass of fuel burned times the energy per unit mass of fuel.

For the present case study, one may reasonably replace the energy used with the mass of fuel burned, since the two quantities are directly proportional. As already noted, the payload weight is essentially the mass of water carried on board, whereas the key modification needed to adapt the parameter concerns the range. The goal of this aircraft is not to travel as far as possible but to perform as many operation cycles as possible. It is therefore natural to replace the range with the number of cycles, a quantity known a priori and suitable for representing performance:

$$\mathbf{WMEE} = \frac{W_{\mathbf{pay}} \cdot n_{\mathbf{cycles}}}{m_{\mathbf{fuel}}} \tag{6.8}$$

If one wishes to exclude the energetic aspect altogether, it may be useful to adopt a simplified parameter that ignores how efficiently fuel is used and captures only the aircraft capability in terms of firefighting operations. Such a parameter can be defined simply as operation cycles times payload mass, which is equivalent to the total amount of water dropped by the aircraft over its mission. This is an informative figure, but it is not fully suitable during wing selection, since the amount of fuel used depends to a large extent on the aerodynamic characteristics of the selected wing configuration and, afterall, the design mission is the same for each configuration presented below:

$$\mathbf{WM} = W_{\mathbf{pay}} \cdot n_{\mathbf{cycles}} \tag{6.9}$$

Another important parameter that could be used as a figure of merit is the stall speed, which clearly has an impact on the effectiveness of the drop maneuver. The lower the stall speed, the better the configuration behavior. In fact, the stall speed can be obtained as follows:

$$V_s = \sqrt{\frac{2\frac{W}{S}}{\rho C_{L,max}}} \tag{6.10}$$

This speed represents the minimum velocity achievable by the aircraft and depends on the maximum lift coefficient, on the wing loading calculated as weight divided by wing area, and on the air density.

[?]

Having structured the mission on the basis of existing CL-415 missions, and having slightly more than doubled the quantity of water carried on board, the aircraft effectiveness level will be approximately doubled. In terms of endurance, it would be theoretically possible to increase mission duration by filling the fuel tanks more fully. What we can state is that a trade-off can be executed between fuel tank filling and effectiveness. This compromise can be achieved by means of mission strategies. For example, one may choose not to fill the entire fuel tank when a short intervention is expected and to exploit the maximum fire suppression capability; conversely, if a longer mission is desired, it is possible to fully fuel the aircraft and then increase the water tank filling as needed, up to the point where the sum does not exceed the maximum weight the aircraft can sustain in glide while maintaining the appropriate speeds. From this standpoint, the box-wing configuration is highly advantageous. For the aircraft under study, since the central bays of the fuselage are largely occupied by the water tank, the useful positions for fuel tanks would be located only in the wing. The aft fuselage could in principle accommodate an auxiliary fuel tank, but because concentrated masses such as fuel should be placed near the aircraft center of gravity to preserve stability, the wing remains the only practical choice. An Airbus A320 has a total wingspan of about 34 m, with a substantial mean aerodynamic chord that, especially in the central wing boxes, allows the installation of large fuel tanks. The aircraft considered here has smaller wings, and the usable space for a hypothetical wing tank is more limited. Hence the

advantage of the box-wing: by adopting two wings, it becomes possible to significantly enlarge the usable volume for fuel, thereby enabling strategies such as those described above.

More detailed studies will be necessary to determine the performance of the aircraft with precision; however, in general, relative to existing scooper aircraft, this conceptual design falls into an interesting higher class, bringing it closer in terms of effectiveness to larger aircraft such as the AC-130 and the B737, which are certainly not capable of performing scooping.

The adoption of a third wing can be considered, but this study does not include it. The design objective is to maximize payload capacity at the lowest possible speed at sea level. A third wing could help maintain adequate wing loading; otherwise, the only solution would be to increase the wing area. Increasing the area may be beneficial, and adding a third wing could help even more. Clearly, adding a third lifting surface would inevitably decrease overall aerodynamic efficiency because of increased drag. Given the abundant installed power on board, this should not be a major issue for the aircraft under consideration, but limitations could arise from other aspects such as controllability and maneuverability. Unlike a freighter, this aircraft does not simply transport payload from point A to point B; it must perform maneuvers that make it closer to other high maneuverability aircraft types. If necessary, a more in depth study should be conducted to assess the trade-off among efficiency, payload capacity, and maneuverability.

Below we show several configurations that could be considered. The configurations shown are outputs from the Aerostate program and are all evaluated using the code developed in this thesis for weight determination. The optimizer parameters are kept constant for all configurations; the values that may vary are the bounds. The configurations are named according to the following convention:

- A\_AF\_Plane\_1\_ indicates the name of the specific run,
- Curr... indicates the identifier of the configuration output by Aerostate.

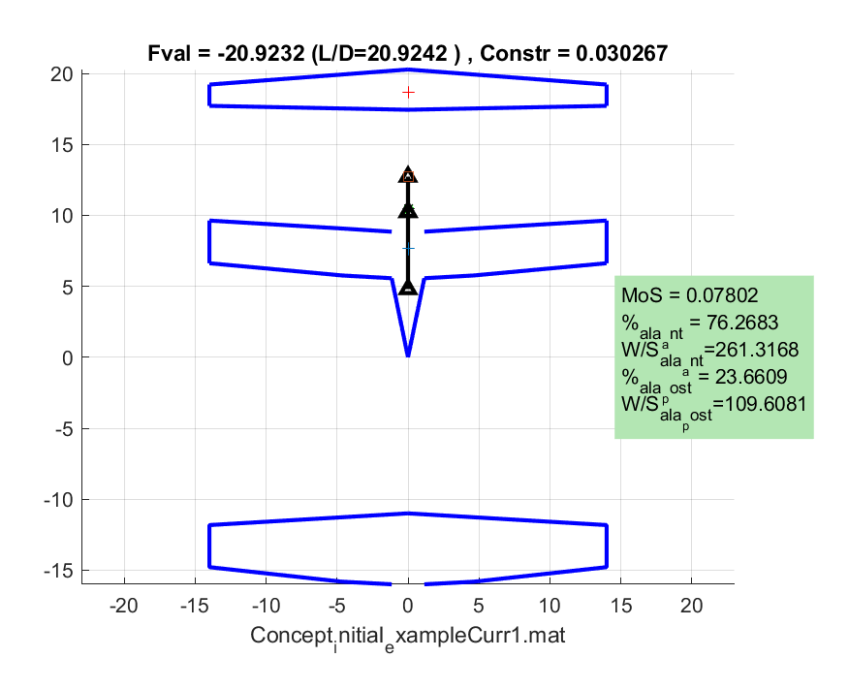


Figure 6.10: A\_AF\_Plane\_1\_4 Curr1

Having identified potential parameters for assessing the performance of a firefighting aircraft, and having used the same mission specification and the same payload to size the aircraft, we can compare the performance of these configurations through the fuel mass and, consequently, through the WMEE value defined earlier. A payload of 12500 kg represents a near limiting case. Some wing configurations do not converge; configurations with poorer aerodynamic performance

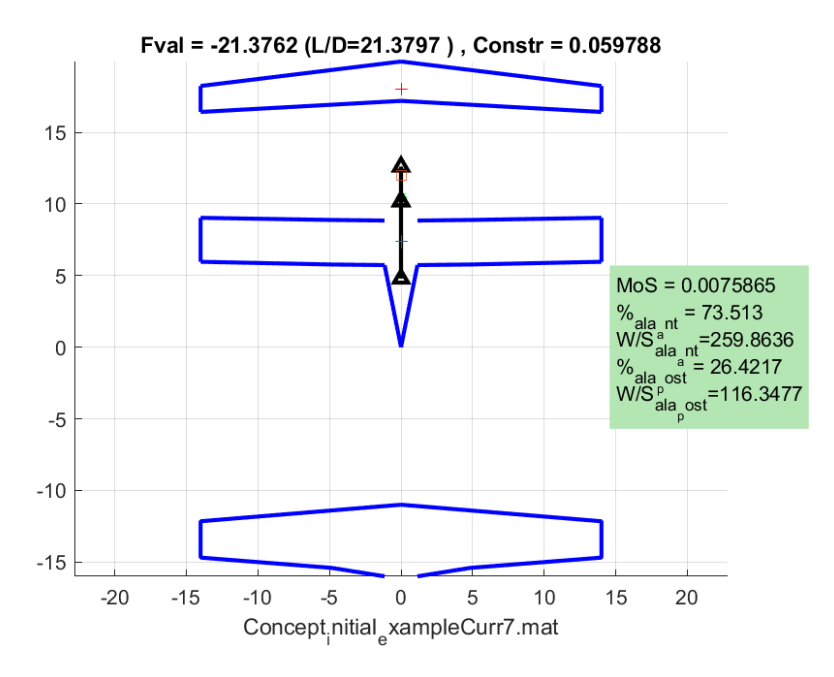


Figure 6.11: A\_AF\_Plane\_1\_6 Curr7

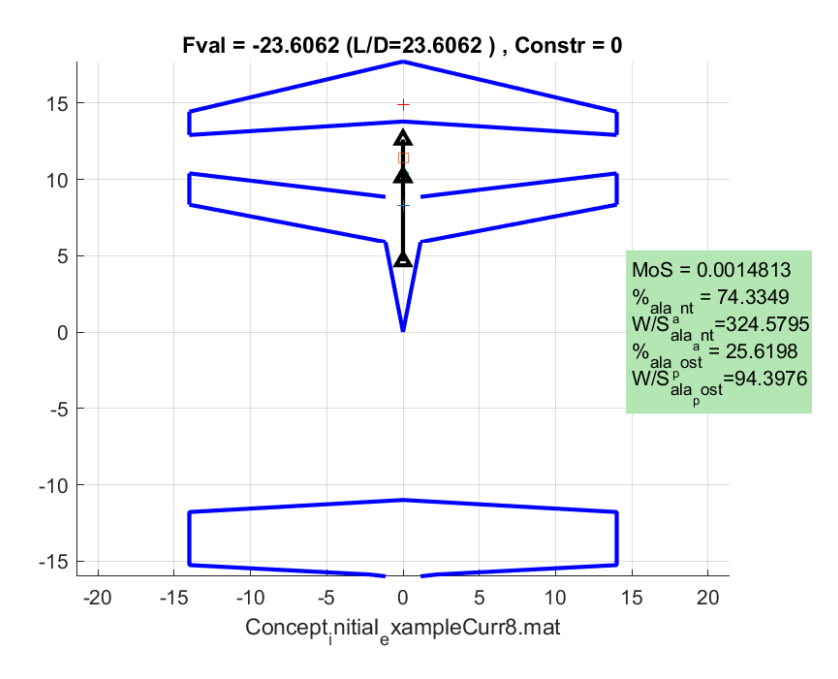


Figure 6.12: A AF Plane 1 7 Curr15

likely fail to converge because the increased fuel mass raises the overall weight, pushing the calculation outside the convergence region. Using WMEE makes it possible to compare these configurations with others that have lower or higher payloads than the 12500 kg used here.

The values are as follows:

As can be seen from the table, the A\_AF\_Plane\_1\_8 Curr8 configuration is the best in terms of fuel efficiency and WMEE, which indicates that it is aerodynamically more efficient. Notably, the best configuration is also the only one that features taper on the front wing. The front wing carries the higher load and therefore operates at a higher lift coefficient than the rear wing, which carries less load and thus operates at a lower lift coefficient. The high lift coefficient on the front wing makes it more prone to induced drag. Taper on the front wing has a beneficial

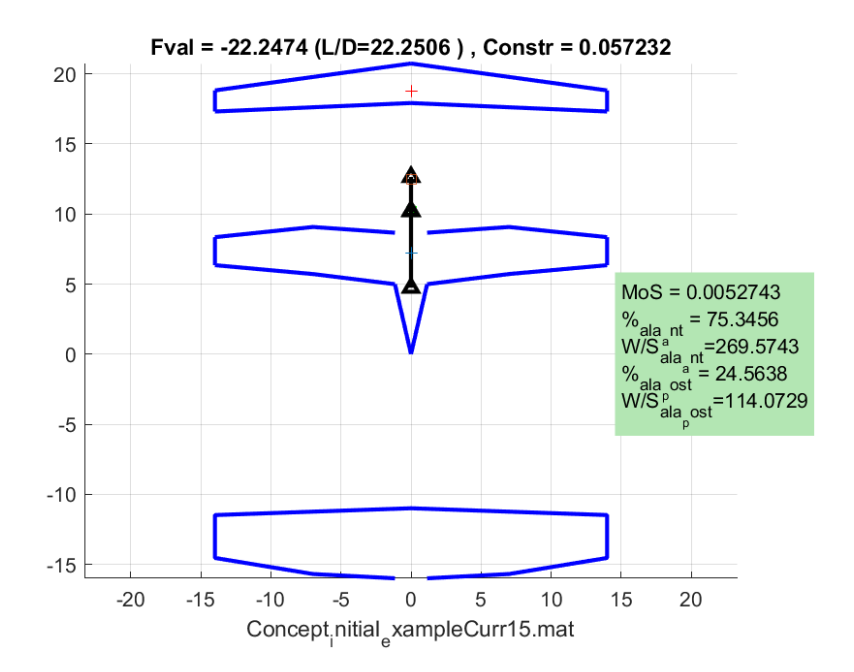


Figure 6.13: A\_AF\_Plane\_1\_8 Curr8

Configuration	WMEE	WM	Mass of Fuel	Mass of Payload	Efficiency
A_AF_Plane_1_4 Curr1	108.63	$1.625 \times 10^{6}$	1495	12500	20.92
A_AF_Plane_1_6 Curr7	130.31	$1.625 \times 10^{6}$	1247	12500	21.37
A_AF_Plane_1_7 Curr15	133.9654	$1.625 \times 10^{6}$	1213	12500	22.25
A_AF_Plane_1_8 Curr8	1138.18	$1.625 \times 10^6$	1170	12500	23.60

Table 6.3: Mass breakdown and efficiency by configuration

effect in reducing the induced drag coefficient and therefore, inevitably, the last configuration turns out to be the best. The Curr8 configuration represents a good compromise in terms of planform. Its high dihedral helps avoid flotation issues. The large dihedral discontinuity of the front wing should be corrected in later stages, as should the pronounced discontinuities in chord and sweep on the front wing. This configuration also exhibits a very limited, albeit positive, stability margin. The rear wing has a good shape characterized by moderate sweep, which is favorable.

The A\_AF\_Plane\_1\_7 Curr15 configuration shows an excellent efficiency value and does not exhibit the geometric discontinuities observed in the previous case. Unfortunately, there is a large difference in planform between the two wings: the rear wing is quite large, and the wing loading values are markedly different. Moreover, the front wing, due to its limited area, exhibits a high wing loading, which may not be ideal for low speed performance, an aspect that has been set aside at this stage.

The A\_AF\_Plane\_1\_6 Curr7 configuration represents an excellent compromise. Its efficiency is high, and its geometry is fairly balanced between the two wings. The complete absence of taper on the front wing is a geometric aspect that does not favor this configuration; on the other hand, the sweep is very small, as would be expected for an aircraft optimized for low speeds. The stability margin is small in absolute terms but still positive, which ensures stability about the longitudinal axis.

The A\_AF\_Plane\_1\_4 Curr1 configuration is also a good compromise. Its efficiency and WMEE are lower than those of the preceding cases. The front wing does not show particular geometric issues, although adding a modest amount of taper would likely be beneficial. The

sweep angles are quite small, which is positive. The dihedral is moderate, does not pose major manufacturing constraints, and helps maintain adequate clearance between the front wing tip and the water surface.

The A\_AF\_Plane\_1\_4 Curr1 configuration is selected for depiction in Figure 6.9 and is shown as a mean surface in three dimensional space in Figure 6.8.

In terms of firefighting performance, the values obtained can be plotted on the same figures presented in Chapter 1 of this work. Some of the parameters shown in those figures cannot be recomputed here because information is missing at this preliminary stage, but other important quantities are computed and inserted into the pre existing plots so that the performance of the new concept, here called AF Plane, can be compared with that of existing firefighters. The performance changes are essentially due to the introduction of the box-wing, which enables a substantial increase in payload.

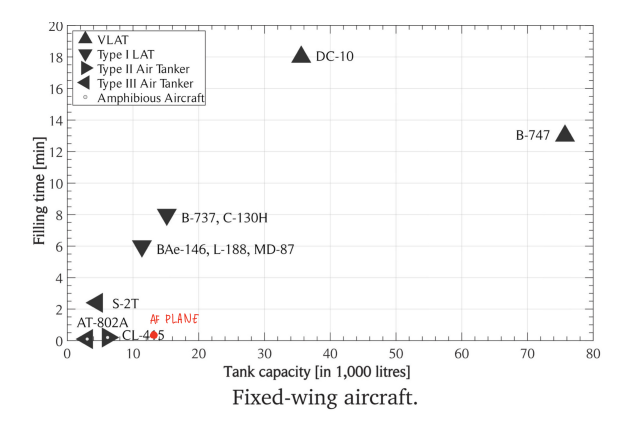


Figure 6.14: Filling time vs tank capacity

Having essentially doubled the water tank capacity and kept the filling time approximately unchanged by using larger intake nozzles relative to the CL-415, the data point in Figure 6.14 shifts essentially along a horizontal line, which is favorable from a performance standpoint.

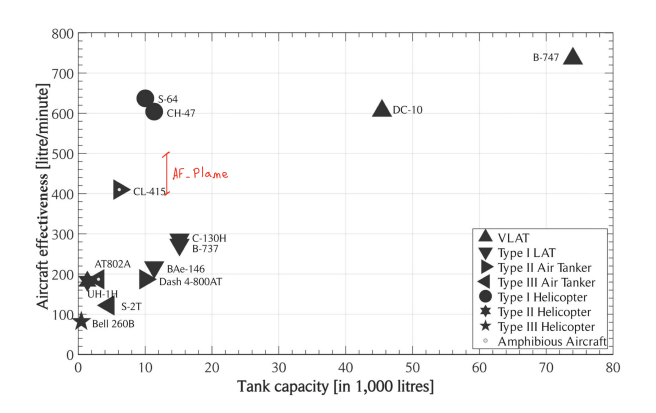


Figure 6.15: Effectiveness vs tank capacity

As clearly visible in Figure 6.15, the aircraft moves to the right with respect to the CL-415. By computing the total mission time and knowing the water tank capacity, one can compute the Effectiveness, which in this case is 423 liters per minute. This value is not directly comparable to that of the CL-415 shown in the figure, because that chart represents the real performance of a specific mission, whereas the mission used here for design purposes was chosen arbitrarily. Nonetheless, the new concept approaches the performance of large bombers such as the B737 and the AC-130 Hercules, while retaining scooping capability, which allows, even with a smaller tank, an increase in effectiveness. At present there are no amphibious aircraft on the market

with the capabilities of the new concept, and this performance can be achieved only with a technology such as the box-wing, which enables much greater payload while maintaining robust aeromechanical performance, unlike a simple biplane that carries several drawbacks.

# Chapter 7

### Conclusion

### 7.1 Conclusions

With climate change, new requirements are emerging across all fields of human activity. The progressive alteration of climate conditions observed in recent years has led to a dangerous increase in the incidence of wildfires. Although natural in origin, these phenomena pose a significant threat to both property and human life, as was dramatically demonstrated, for instance, in Los Angeles (CA) in 2025. Various solutions are currently under investigation worldwide, employing a wide range of approaches. While the hope remains that this problem may one day be entirely eradicated, the present work focuses on one specific strategy: fire suppression. An increasingly effective method for wildfire suppression is represented by the use of aircraft specifically designed for firefighting operations. This study has therefore been devoted to the conceptual design of a firefighting aircraft belonging to the scooper category. This class of aircraft consists of amphibious airplanes capable of skimming over water surfaces to refill their tanks with fire-retardant liquid used in suppression operations. A scooper aircraft is thus equipped with a hull that allows it to glide across the water surface while opening an intake located beneath the fuselage through which water is transferred from the surface into onboard storage tanks. Once refilled, the aircraft must reach the operational area, that is, the wildfire location, and perform a low-altitude, low-speed flight while releasing the entire water load in an effective and precisely targeted manner. The development of the proposed concept followed a methodology that integrated aerodynamic, hydrodynamic, and structural analyses to achieve a coherent and physically consistent design. The aerodynamic study was performed through a numerical optimization process using the Aerostate tool. This software is based on AVL (Athena Vortex Lattice), developed by the Massachusetts Institute of Technology (MIT), which relies on potential flow theory to compute the aerodynamic characteristics of aircraft configurations modeled as a set of lifting surfaces discretized into panels. Through this formulation, the software provides a fast and reliable estimation of aerodynamic performance parameters such as lift, drag, and stability derivatives, making it particularly suitable for conceptual and preliminary design. Starting from an initial geometry, the optimizer defines a design space through variables, boundaries, and constraints that describe the problem and uses an objective function to guide the search toward the best configuration. This process yielded a set of optimized wing geometries corresponding to the selected flight condition. These were analyzed and compared based on parameters such as aerodynamic efficiency, stability, and constraint satisfaction, allowing the identification of the most suitable configuration for the firefighting mission.

To estimate the power requirements associated with the mission, empirical models were implemented to evaluate the hydrodynamic forces acting on the hull during planing on water. The hydrodynamic model adopted is based on the formulation presented in [13], complemented by an additional component accounting for the friction losses produced by the water intake nozzle

during the scooping phase. This latter contribution was modeled through the conservation of linear momentum applied to the mass flow entering the intake system, enabling the evaluation of the additional power needed for water collection. The estimation of aircraft mass properties combined semi-empirical and physics-based approaches. Raymer's method was employed for the general weight breakdown, while a dedicated MATLAB-based finite element model was developed to determine the structural weight of the lifting system. In this model, the wing is represented as a bi-dimensional beam embedded in a three-dimensional space, allowing the calculation of its deformations and stresses. This approach enables a physics-based estimation of the wing mass as a function of the applied loads and the geometric characteristics of the configuration. The model can be adapted to different wing architectures, provided that the aspect ratio is sufficiently high to justify the two-dimensional beam representation without introducing significant errors.

The mission simulation was performed using data derived from literature and applying the Euler method, which introduces relatively strong simplifying assumptions but allows a manageable estimation of a complex mission such as the one considered in this work. The simulated mission includes multiple operational cycles involving water refilling and successive drops over the fire area. Although simplified, this approach makes it possible to obtain a reasonable estimation of the overall fuel consumption required for the complete firefighting operation. The resulting fuel mass contributes directly to the computation of the Maximum Take-Off Weight (MTOW), which depends on both aerodynamic and non-aerodynamic performances of the aircraft, thus linking flight efficiency, payload capacity, and overall mission feasibility.

The lifting system selected for this project, the box wing, represents an innovative architectural choice. This configuration aims to maximize aerodynamic efficiency by reducing the induced drag generated by wingtip vortices, a common limitation of conventional finite-span wings. Moreover, the box wing offers the advantage of nearly doubling the lifting surface for the same wingspan compared to a monoplane configuration, leading to substantial performance benefits. In addition to the improved water tank capacity, the box wing architecture could also lead to enhanced stall resistance, an intrinsic characteristic of this configuration that contributes to safer lowspeed operations typical of firefighting missions. The results obtained show that by maintaining the overall dimensions of the CL-415, the proposed configuration can almost double the water payload capacity, which translates into a significant improvement in firefighting capability. This design therefore provides a solid conceptual foundation for the development of a new-generation scooper aircraft capable of enhanced performance, stability, and operational safety. Although further refinement of the model, for instance through the introduction of stringers and ribs, could improve local accuracy, the current implementation already provides results consistent with existing data and sufficient for conceptual-level design purposes. It allows a physics-based estimation of the wing weight dependent on geometry, aircraft mass, and maximum load factor required for the mission. Through this integrated process, combining aerodynamic optimization, structural modeling, hydrodynamic estimation, and mission simulation, it has been possible to define a coherent concept of a box-wing firefighting aircraft. The characteristics of the proposed configuration demonstrate a marked improvement over existing solutions, achieving approximately twice the tank capacity of current scoopers and ensuring superior overall performance in aerial firefighting operations

# List of Figures

1.1	Image taken from [1]	8
1.2	Image taken from [?]	9
1.3	Image taken from [1]	9
1.4	DC-10 SuperTanker	9
1.5		9
1.6	AC-130 Tanker	0
1.7	CL-415	1
1.8	Grumann s2T	1
1.9	Sikorsky s64 Tanker	2
1.10	1	2
1.11		3
1.12	1	4
2.1	Forces layout for a generic Aircraft	
2.2	TOD vs TOP	
2.3	Force diagram on during refilling	
2.4	Plane surface planning	
2.5	Model of prismatic Hull Lateral View	
2.6	Model of prismatic Hull Front View	
2.7	Model of prismatic Hull Bottom view	
2.8	Water intake model	
2.9	Control Volume	
2.10	Specific Power Matching Chart	
2.11	Specific Thrust Matching Chart	9
2.12		0
2.13		0
2.14		1
2.15	3	2
2.16		3
0.1	D 171 /	_
3.1	Beam Element	
3.2	au vector	
3.3	Construction of the stiffness matrix	
3.4	Deformation along the axis line	
3.5	Displacement out of the axis line	
3.6	Wing Box	
3.7	Equivalent Panel Model	
3.8	Representation of the iterative procedure	
3.9	Airbus a320 wing planform and twist distribution	
3.10	Mass breakdown standard for CSR-01	
3.11	One Wing weight	7

3.12	Wing weight variation with the Sweep Angle		 	 48
	Variation of the front sweep			
3.14	Variation of the rear sweep		 	 51
3.15	Variation of the front dihedral		 	 51
3.16	Variation of the rear dihedral		 	 51
3.17	Dihedral for the front and the rear wing		 	 52
3.18	Mission		 	 56
3.19	Forces equilibrium		 	 57
3.20	Mission profile		 	 60
3.21	Weight of the aircraft		 	 60
3.22	Lift coefficient as a function of mission time		 	 61
4.1	Biot-Savart problem		 	 64
4.2	Horseshoe vortex and panel modeling		 	 65
4.3	Starting point of the optimization process		 	 72
4.4	"geo.ala_ant.var" structure			 73
5.1	Front section CL-415		 	 78
5.2	Confrontation between CL-415 and the new concept		 	 78
5.3	Concept fuselage section		 	 79
5.4	Concept Increased Width by 10%		 	 80
5.5	Caption		 	 80
5.6	Caption			
5.7	Front fuselage section		 	 81
5.8	Lateral section of the fuselage with tank		 	 82
5.9	Front Section with a focus on tank placement		 	 82
5.10	Lateral view, visibility of the pilot		 	 83
5.11	Lateral view, visibility of the pilot		 	 84
	Lateral view, tank and landing gear			
5.13	Spray chines front view		 	 85
	Lateral view cockpit window			
5.15	Top view cockpit window			 86
6.1	Design workflow for this design		 	 87
6.2	MTOW computing flow		 	 92
6.3	Mass distribution vs. Water Quantity		 	 93
6.4	Mass distribution percentage vs. Water Quantity		 	 94
6.5	Mass distribution vs. Water Quantity		 	 94
6.6	Mass Breakdown		 	 95
6.7	Optimization snapshot. Left: planform and constraint envelopes.	_		0.0
	ical indicators transcribed from the original plot			96
6.8	3D view of the mean aerodynamic surface			
6.9	Three-view drawing of the configuration			97
6.10				100
	A_AF_Plane_1_6 Curr7			
	A_AF_Plane_1_7 Curr15			
	A_AF_Plane_1_8 Curr8			
	Filling time vs tank capacity			
0.15	Effectiveness vs tank capacity			 103

# Bibliography

- [1] Central reference aircraft data system.
- [2] https://web.mit.edu/drela/public/web/avl/.
- [3] F. Olivieroa M. Lucchesi T. Lippi S. Luci A. Frediania, V. Cipollab. A new ultralight amphibious prandtlplane: preliminary cfd design of the hull. *Aerotecnica Missili Spazio*, *The Journal of Aerospace Science*, *Technology and Systems*, 2021.
- [4] Maria Richetta Antonio Gloria, Roberto Montanari and Alessandra Varone. Alloys for aeronautic applications: State of the art and perspectives. *metals*, 2019.
- [5] Giovanni Bovio, Marco Marchetti, Luca Tonarelli, Michele Salis, Giorgio Vacchiano, Raffaella Lovreglio, Mario Elia, Paolo Fiorucci, and Davide Ascoli. Forest fires are changing: let's change the fire management strategy. Forest@ Journal of Silviculture and Forest Ecology, Volume 14, Pages 202-205, 2017.
- [6] A Fast Optimization Method of Water-Dropping Scheme for Fixed-Wing Firefighting Aircraft.
- [7] PART 25—AIRWORTHINESS STANDARDS: TRANSPORT CATEGORY AIRPLANES.
- [8] Aldo Frediani Karim Abu Salem, Giuseppe Palaia. From theory to flight: the box-wing configuration implications for the next-generation aircraft. 34th congress of the International Council of the Aeronautical Sciences, 2013.
- [9] Cipolla Vittorio Binante Vincenzo Zanetti Davide Karim Abu Salem, Palaia Giuseppe and Chiarelli Mario. Tools and methodologies for box-wing aircraft conceptual aerodynamic design and aeromechanic analysis. *Mechanics Industry*, 2021.
- [10] Enrico Panettierib Marco Picchi Scardaonia, Marco Montemurrob. Prandtlplane wing-box least-weight design: A multi-scale optimisation approach. Aerospace Science and Technology, 2020.
- [11] L. Prandtl. Induced drag of multiplanes. NACA Techni- cal Note, no. 182, 1924, 1924.
- [12] Daniel P. Raymer. Aircraft design: A conceptual approach. 2024.
- [13] Daniel Savitsky. Hydrodynamic design of planning hull. TODO, 1964.
- [14] A. Struminska and A. Filippone. Flight performance analysis of aerial fire fighting. *Royal Aeronautical Society*, 2024.
- [15] Flight test division. *Hydrodinamic Manual*. Naval Air Test Center, Patuxent River, Maryland, 1967.
- [16] Yongliang Tian Zikun Chen Zhiyong Cai Xiyu Wang, Hu Liu. A fast optimization method of water-dropping scheme for fixed-wing firefighting aircraft. *IEEE*, 2021.